

UNIVERSITY OF BIRMINGHAM

NAD^+ and the metabolism of cellular glucocorticoids in Endoplasmic Reticulum

By

Ali Yahya Kabli

A thesis submitted to The University of Birmingham

for the degree of

DOCTOR OF PHILOSOPHY

Institute of Metabolism and Systems Research

College of Medical and Dental Sciences

University of Birmingham

May 2023

UNIVERSITY OF
BIRMINGHAM

University of Birmingham Research Archive

e-theses repository

This unpublished thesis/dissertation is copyright of the author and/or third parties. The intellectual property rights of the author or third parties in respect of this work are as defined by The Copyright Designs and Patents Act 1988 or as modified by any successor legislation.

Any use made of information contained in this thesis/dissertation must be in accordance with that legislation and must be properly acknowledged. Further distribution or reproduction in any format is prohibited without the permission of the copyright holder.

Dedicated to my mother, my wife and

my son

Acknowledgment

I would like to thank my supervisor Prof. Gareth Lavery for his tremendous guidance and support throughout my study period. He is a great teacher and scientist who always encouraged me to improve during my academic research. I also would like to thank my second supervisor Prof. David Hodson for his support and advice on my project. Words cannot express my gratitude to my group members who offered endless help and support through my Ph.D. journey (Yasir, David, Dean, Peter, Lucy, Silke, Sam, Stuart, Olivia, Caitlin, Antje, and Rachel). I was so lucky to meet you all and share a good time with you. I also want to express my profound appreciation and special thanks to Silke, Sam, Stuart, and Yasir for their immense guidance and assistance in the lap and manuscript. I also would like to thank Dr. Rowan Hardy and his group members (Ana, Claire, and Michael) for offering us reagents and allowing us to use a fluorescence microscope. Finally, I am grateful to my family for their love and support through my Ph.D. study. They stood by me and supported me to achieve my goals and finish this project.

Conferences and memberships:

1- **Attended The Endoplasmic Reticulum (ER) Conference: Structure, Function, and Disease provided by Federation Of American Societies For Experimental Biology (FASEB). 22-24 June 2021.**

2- **Poster Presentation at the ENDO conference. Atlanta, Georgia, USA. 11-14 June 2022.**
(Targeting NAD^+ availability modulate 11β- Hydroxysteroid dehydrogenase 1 activity in mouse and human cells)

3- **Poster presentation at SfE, BES annual meeting. Harrogate, UK. 14-16 November 2022.**
(Depleting NAD^+ pools specifically in the endoplasmic reticulum lumen impairs 11β-HSD1 activity).

4- **Member of Endocrine Society. 03/04/2022.**

5- **Member of society of Endocrinology. 15/08/2022.**

Abstract

Nicotinamide Adenine Dinucleotide (NAD^+) has a primary role in cellular metabolism and energy production as a cofactor for a set of enzymatic reactions. The endoplasmic reticulum (ER) lumen enzyme 11β-hydroxysteroid dehydrogenase type 1 (11β-HSD1) obtains NADPH from hexose-6-phosphate dehydrogenase to reduce cortisone to the active glucocorticoid cortisol. Cells depleted in NAD^+ (parent molecule of NADPH) have impaired 11β-HSD1 activity, which can be rapidly rescued with supplementation of the NAD^+ precursor nicotinamide riboside (NR). This suggests the existence of an ER-specific pathway to NAD(P)(H). Here we depleted cellular NAD^+ using FK866 (NAMPT inhibitor) and poly-ADP-ribose assisted protein localization assay to study ER-specific NAD^+ metabolism using 11β-HSD1 as a readout. To assess the generalizability of our results, we examined the enzyme activity in multiple cell types such as liver, muscle, dermal fibroblast, and human kidney. Results show preliminary evidence that depleting ER NAD^+ can impair NADPH-dependent 11β-HSD1 activity. Repleting NAD^+ availability with NR treatment significantly rescued the enzyme activity. Further experiments are required to thoroughly evaluate the potential of a dynamic NAD(P)(H) pathway in the ER compartment.

Table of Contents

CHAPTER 1 ..... ***22***

General introduction ***22***

1.1. Nicotinamide Adenine Dinucleotide (NAD) **23**

1.2. NAD Biosynthesis pathway **27**

1.2.1. Preiss-Handler pathway 27

1.2.2. De novo pathway 27

1.2.3. Salvage pathway by NAD^+ precursor (NAM) 30

1.2.4. salvage pathway by NAD^+ precursor (NR) 33

1.2.5. NAD kinase 31

1.3. NAD consuming enzymes **35**

1.3.1. Sirtuins 36

1.3.2. Poly ADP-ribose polymerase 36

1.3.3. Cyclic ADP-ribose Synthase 38

1.4. NAD^+ compartmentalization **40**

1.5. PAR as a biosensor of subcellular NAD^+ pool **42**

1.6. Glucocorticoids **43**

1.6.1. Hypothalamic pituitary adrenal axis (HPA) 44

1.6.2. 11 β-hydroxysteroid dehydrogenase (11 βHSD) 45

1.6.2.1. 11 β-HSD Tissue expression 46

1.6.3. Clinical implication of glucocorticoid and 11 β-HSD1 dysregulation 47

1.7. Endoplasmic reticulum (ER) **48**

1.8. Hexose-6-phosphate dehydrogenase (H6PDH) 52

1.9. Thesis rationale 54

1.10. Hypothesis 54

1.11. Aim 54

Chapter 2 55

General methodology 55

2.1. Cell culture 56

2.1.1. C2C12 56

2.1.1.1. Proliferation 56

2.1.1.2. Freezing down 58

2.1.2. primary mouse myotubes 59

2.1.3. Dermal fibroblast 61

2.1.4. HepG2 62

2.1.5. HEK293 63

2.2. Modulation of NAD with FK866 and NR 65

2.3. NAD^+/NADH assay 65

2.4. Cell viability assay (AlamarBlue) 68

2.5. Protein extraction and determination 69

2.6. Western blotting 70

2.7. Bacterial transformation 73

2.8. RNA extraction 74

2.9. RNA quantification 75

2.10. Reverse transcription (RT) and polymerase chain reaction (PCR) 75

2.11. Real-Time PCR 76

2.12. Gel electrophoresis……..……73

2.13. 11β-Hydroxysteroid dehydrogenase 1 (11βHSD1) activity 77

2.13.1. Production of 3H-11DHC. 80

2.14. Transfection of HepG2 and C2C12 81

2.15. statistical analysis..…….……78

Chapter 3 88

Targeting NAD^+ metabolism to modulate 11β-Hydroxysteroid dehydrogenase type1 activity in the ER of mouse and human cells 88

3.1 Introduction 89

3.2. Results 91

3.2.1. NAD^+ /NADH manipulation by FK866 and NR in C2C12 mouse myotubes. 91

3.2.2. The effect of NAD^+/NADH manipulation on 11β-HSD1 enzymes activity in C2C12 myotubes. 93

3.2.3. Time course of 11β-HSD1 oxo-reductase activity in response to NAD^+ 94

manipulation by FK866 and NR in C2C12 myotubes.....94

3.2.4. 11β-HSD1 oxo-reductase activity in WT mouse myotubes in response to FK866 and NR. 96

3.2.5. 11β-HSD1 dehydrogenase activity in H6PDH mouse myotubes. 97

3.2.6. The effect of NAD^+ manipulation by FK866 and NR on the liver's 11β-HSD oxo-reductase and dehydrogenase activity. 99

3.2.7. The effect of NAD^+ manipulation by FK866 and NR on 11β-HSD oxo-reductase in dermal fibroblast (HDFn).....102

3.2.8. The effect of NAD^+ manipulation by FK866 and NR on 11β-HSD2 dehydrogenase activity in the kidney.....104

3.3. Discussion..... 106

Chapter 4..... 110

Optimization of HepG2 and C2C12 transfection to examine Poly-ADP-Ribose Formation as a Biosensor for NAD^+ pools in the Endoplasmic Reticulum..... 110

4.1. Introduction 111

4.2. Results 113

4.2.1. Plasmid DNA quality after Restriction/Digest with (XabI and EcoRI) 113

4.2.2. Transfection of HepG2 cells with vectors encoding ER-PARP1cd, ER-EGFP, Mitochondrial PARP1cd and Mitochondrial-EGFP 114

4.2.2.1. Optimization of lipofectamine for HepG2 transfection 114

4.2.2.2. Transfection efficiency of different ER-PARP plasmids 116

4.2.2.3. Transfection of HepG2 at a density of 2.2*10^5 cells/well 118

4.2.2.4. Transfection of HepG2 at a density of 1.1 *10^5 cells/well 120

4.2.2.5. Transfection of HepG2 at a density of 1.5 *10^5 cells/well 122

4.2.2.6. Transfection of HepG2 at a confluence of 2.5 *10^5 cells/well 123

4.2.2.7. Increasing DNA concentration to improve transfection efficiency 125

4.2.3. Transfection of C2C12 cells with vectors encoding ER-PARPcd and ER-EGFP. 127

4.2.3.1. Transfection of C2C12 at a density of 1.1*10^5 cells/well 127

4.2.3.2. Transfection of C2C12 at a density of 2.2*10^5 cells/well. 129

4.2.3.3. Transfection of C2C12 at a density of 1.5*10^5 cells/well 131

CHAPTER 5 136

11β- Hydroxysteroid dehydrogenase1 activity as a read-out of NAD^+ depletion in a cell models of Poly-ADP Ribose polymerase overexpression 136

5.1. Introduction 137

5.2. Results 139

5.2.1. ER-cytosol crosstalk in HepG2 overexpressing ER-PARP 139

5.2.1.1. NAD^+ precursor (NR) increased PAR formation 139

5.2.1.2. 11β-HSD1 activity as a read-out of ER NAD^+ bioavailability in ER-PARP1cd overexpression cell model. 141

5.2.1.3. ER stress genes expression in response to transfection with ER-PARP1cd and ER-EGFP constructs. 143

5.2.2. Examining ER-cytosol crosstalk in C2C12 overexpressing ER-PARP1cd. 146

5.2.2.1. The effect of NR treatment on the formation of PAR protein. 146

5.2.2.2. Time-point of 11 β-HSD1 oxo-reductase activity in C2C12 myoblast. 148

5.2.2.3. 11β-HSD1 activity as a read-out of ER NAD^+ bioavailability in ER-PARP1cd overexpression. 150

5.2.2.4. ER stress genes expression in response to transfection with ER-PARP1cd and ER-EGFP constructs. 152

5.3. Discussion 155

CHAPTER 6 157

Final discussion and future direction 157

References 164

List of Figures

Figure 1.1 Molecular structure of NAD+. 25

Figure 1.2. NAD as a redox molecule through its reduced and oxidized forms. 26

Figure 1.3. Schematic illustration of NAD+ biosynthesis pathway in the cell cytoplasm. 29

Figure 1.4. NAD+ biosynthesis via NAMPT salvage pathway. 32

Figure 1.5. NR as a biosynthesis precursor of NAD+. 34

Figure 1.6. Schematic illustration of NAD+ consuming enzymes. 39

Figure 1.7. Mechanism of subcellular NAD+ pool, with the distribution of NAD+ dependent enzymes and salvage pathway. 41

Figure 1.8. Schematic diagram representing the metabolic effect of cortisol and HPA axis. 44

Figure 1.9. The conversion reaction catalysed by 11B-HSD enzymes. 46

Figure 1.10. The endoplasmic reticulum structure. 51

Figure 1.11. Regulation of cellular GCs generation by 11 B-HSD1. 53

Figure 2.1 Mouse skeletal muscle myotubes cell line (C2C12). 58

Figure 2.2 Mouse primary skeletal muscle cells. 60

Figure 2.3. Neonatal human dermal fibroblast (HDFn). 61

Figure 2.4. human hepatocellular carcinoma cell line (HepG2). 62

Figure 2.5. Human kidney cell line (HEK293). 63

Figure 2.6. Example of standard NADH curve for analysis of NAD^+/NADH Quantitation. 66

Figure 2.7. NAD^+ quantification assay. 68

Figure 2.8. cell Viability assay (AlamarBlue). 69

Figure 2.9. Illustrative Bioscan traces of 11β-HSD1 oxo-reductase activity in (A) mouse cell line (c2c12) and (B) human cell lines (HEPG2, Dermal fibroblasts, and HEK293). 80

Figure 2.10. Steps of thin layer chromatography. 78

Figure 2.11. ER-PARP plasmid……..……..82

Figure 2.12. EF-EGFP plasmid…...……..83

Figure 2.13. Mito-EGFP plasmid…….84

Figure 2.14. Mito-PARP plasmid……..85

Figure 3.1. NAD^+ manipulation with FK866 and NR in differentiated C2C12 myotubes. 92

Figure 3.2. 11β-HSD1 activity in C2C12 myotubes in response to nucleotides manipulation by FK866 and NR. **93**

Figure 3.3. Time course of 11β-HSD1 oxo-reductase activity in response to NAD+ manipulation by FK866 and NR in C2C12 myotubes. **95**

Figure 3.4.The effect of NAD+ manipulation by FK866 and NR on 11β-HSD oxo-reductase activity in WT mouse myotubes. **96**

Figure 3.5. 11β-HSD1 dehydrogenase activity in H6PDH mouse myotubes. 98

Figure 3.6. The effect of NAD^+ manipulation by FK866 and NR on 11β-HSD oxo-reductase and dehydrogenase activity in the liver (HepG2 cell line).... 101

Figure 3.7. The effect of NAD^+ manipulation by FK866 and NR on 11β-HSD oxo-reductase after enzyme boosting by TNFα in dermal fibroblast. 103

Figure 3.8. The effect of NAD^+ manipulation by FK866 and NR on 11β-HSD2 dehydrogenase activity in the human kidney cell line (HEK293). 105

Figure 4.1. Gel electrophoresis of the plasmids DNA after restriction/digestion with xbal and EcoRI. 113

Figure 4.2. Transfection of HepG2 cells with vectors encoding ER-PARP1cd, ER-EGFP, Mitochondrial PARP1cd and Mitochondrial-EGFP. 115

Figure 4.3. Transfection of HepG2 with vectors encoding ER-PARP1cd (four plasmid preparations), ER-GFP, Mitochondrial PARP1cd and Mitochondrial-eGFP. 117

Figure 4.4. Transfection of HepG2 at a density of 2.2 *10^5 cells/well with vectors encoding ER-PARPcd, ER-EGFP Mitochondrial PARPcd and Mitochondrial-EGFP. 119

Figure 4.5 Immunofluorescence and western blotting images of transfected HepG2 48h after transfection (at a confluence of 1.1* 10^5 cells/well). 121

Figure 4.6. Transfection of HepG2 at a density of 1.5 *10^5 cells/well with vectors encoding ER-PARP1cd, ER-EGFP. 122

Figure 4.7. Transfection of HepG2 at a density of 2.5 *10^5 cells/well with vectors encoding ER-PARPcd, ER-EGFP. 124

Figure 4.8. Transfection of HepG2 at a density of 2.2 *10^5 cells/well with vectors encoding ER-PARPcd, ER-EGFP with double DNA concentration (1000ng). 126

Figure 4.9. Transfection of C2C12 at a density of 1.1 *10^5 cells/well with vectors encoding ER-PARPcd, ER-EGFP. 128

Figure 4.10. Transfection of C2C12 at a density of 2.2 *10^5 cells/well with vectors encoding ER-PARPcd, ER-EGFP. 130

Figure 4.11. Transfection of C2C12 at density of 1.5 *10^5 cells/well with vectors encoding ER-PARPcd, ER-EGFP. 132

Figure 5.1. The effect of NR on PAR formation in HepG2. 140

Figure 5.2. 11β-HSD1 oxo-reductase activity in transfected HepG2. 142

Figure 5.3. The effect of HepG2 transfection on genes involved in ER stress. 144

Figure 5.4. The effect of NR on PAR formation in C2C12. 147

Figure 5.5. Optimization of 11 β-HSD1 oxo-reductase activity in non-transfected C2C12 myoblast. 149

Figure 5.6. 11β-HSD1 oxo-reductase activity in transfected C2C12 myotubes. 151

Figure 5.7. The effect of C2C12 transfection on genes involved in ER stress. 153

Figure 6.1. Schematic figure illustrating the results generated in this thesis……. ....……....……..155

List of tables

Table 1.1. 11 β HSD expression in different cell types……..47

Table 2.1. Cell types used to study 11 B-HSD1 enzyme activity showing the cell source, seeding density, media used, type of well plate, passage number, and the incubation time of inactive cortisol…….……65

Table 2.2. Concentrations of the reagents used to prepare:

A. separation Gel……...71

B. stacking gels…. 72

Table 2.3 List of primary and secondary antibody used to detect protein expression.

A: Primary antibodies……..

Table 2.4. Concentrations of the reagents used to prepare LB medium….. 73

Table 2.5. Reagents and concentration used for revere transcription reaction. 75

Table 2.6. Lipofectamine protocol for cell transfection in 6 well plates…….82

Table 5.1. ∆Ct values of genes involved in ER stress response in transfected HepG2……....145

Table 5.2. ∆Ct values of genes involved in ER stress response in transfected C2C12.....……..154

Abbreviations

3D	3-Dimensional
4Ds	Dermatitis, Dementia, Diarrhea, and Death
5'-NTs	5'-nucleotidases
6 PGL	6-phosphogluconolactone
11 β-HSD	11 β-hydroxysteroid dehydrogenase
11 DHC	11 Dihydro-corticosterone
ACTH	Adrenocorticotropic hormone
ADP	Adenosine diphosphate
ADPR	ADP-ribose
AMP	Adenine monophosphate
AMPK	AMP-activated protein kinase
ANOVA	Analysis of Variance
ATP	Adenosine triphosphate
BSA	Bovine serum albumin
Ca^{2+}	Calcium
cADP	Cyclic-ADP
cDNA	Complementary DNA
CEE	Chicken embryo extract
CRH	Corticotropin-releasing hormone
DM	Differentiation medium
DMEM	Dulbecco's Modified Eagle's Medium

eNAMPT	Extracellular nicotinamide phosphoribosyl transferase
EM	Electron microscope
ER	Endoplasmic reticulum
ER-PM	Endoplasmic reticulum-plasma membrane contact site
FBS	Foetal bovine serum
G3P	Glycerol-3-phosphate
G6P	Glucose-6-phosphate
GCs	Glucocorticoids
GM	Growth media
GR	Glucocorticoid receptor
H6PDH	Hexose-6-phosphate dehydrogenase
HDFn	Human dermal fibroblasts (neonatal)
HPA	Hypothalamic pituitary-adrenal axis
HRP	Horse-raddish peroxidase
HS	Horse serum
iNAMPT	Intracellular nicotinamide phosphoribosyl transferase
LB	Luria Broth
MCs	Membrane contact sites
NA	Nicotinic acid
NAADP	Nicotinic acid adenine dinucleotide phosphate
NAD(H)	Nicotinamide adenine dinucleotide
NADP(H)	Nicotinamide adenine dinucleotide phosphate
NADS	Nicotinamide adenine dinucleotide synthase

NAFLD	Non-alcoholic fatty liver disease
NAM	Nicotinamide
NaMN	Nicotinic acid mononucleotide
NAMNAT	Nicotinic acid mononucleotide transferase
NAMPT	Nicotinamide phosphoribosyl transferase
NaPT	Nicotinic acid phosphoribosyl transferase
NaR	Nicotinic acid riboside
NFW	Nuclease free water
NMN	Nicotinamide mononucleotide
NMNAT	Nicotinamide mononucleotide adenylyl transferase
Nmrk1	Nicotinamide riboside kinase 1 (gene)
Nmrk2	Nicotinamide riboside kinase 2 (gene)
NR	Nicotinamide riboside
NRK1	Nicotinamide riboside kinase 1 (protein)
NRK2	Nicotinamide riboside kinase 2 (protein)
P/S	Penicillin/Streptomycin
PAR	Poly-ADP-ribose
PARPs	Poly-ADP-ribose polymerases
PPi	Inorganic pyrophosphate
PPP	Pentose phosphate pathway
PRPP	Phosphoribosyl pyrophosphate
PTMs	Post-translational modifications
QA	Quinolinic acid

QAPRT	Quinolinic acid phosphoribosyltransferase
qPCR	Real-time Polymerase Chain Reaction
QS	Quinolinate synthase
RER	Rough endoplasmic reticulum
RNA	Ribonucleic acid
ROS	Reactive oxygen species
SDS	Sodium dodecyl sulfate
SDS-PAGE	SDS – polyacrylamide gel electrophoresis
SER	Smooth endoplasmic reticulum
SIRT1	Sirtuin-1
SLE	Systemic lupus erythematosus
TAG	Triacylglycerol
TBST	Tris-buffered saline with tween
TCA cycle	Tricarboxylic acid cycle
TEMED	Tetramethylethylenediamine
tNAD	Total NAD; NAD^+ & NADH
Trp	Tryptophan
v/v	Volume/volume

CHAPTER 1

General introduction

This chapter will discuss the general overview of Nicotinamide Adenine Dinucleotide (NAD) metabolism and its importance as a central cofactor in cellular metabolic functions. In addition, we will discuss the significance of glucocorticoids and how their metabolism is regulated at the cellular level. Finally, we will focus on the functions of the Endoplasmic reticulum and how NAD^+ is maintained in this compartment and its relation with cellular glucocorticoid metabolism.

1.1. Nicotinamide Adenine Dinucleotide (NAD)

Nicotinamide Adenine Dinucleotide (NAD) was first discovered in boiled yeast extract by Sir Arthur Harden in 1904, who described it as a low molecular weight coenzyme essential for sugar fermentation (Harden and Young, 1906). In the late 1920s, Hans von Euler-Chelpin isolated NAD and described its structure as two compositions, adenine monophosphate (AMP) and nicotinamide mononucleotide (NMN) (Berger et al., 2004) (**Figure 1.1).** At this time, pellagra, a disease characterised by "4 D's" Dermatitis, Dementia, Diarrhea, and Death, was an endemic disease in the United States with an unknown cause (Bollet, 1992, Hegyi et al., 2004). Joseph Goldberger was the first scientist who proposed that dietary deficiency was the main cause of this disease when he observed health improvement among dogs with pellagra fed with Brewer's yeast extract (Rajakumar, 2000). In 1937, Conrad Elvehjem and his colleagues described the link between pellagra and niacin (Vitamine B3) deficiency, and that nicotinic acid (NA), an NAD^+ precursor, is the main element in the treatment and prevention of the disease (Koehn Jr and Elvehjem, 1937).

In 1936, Otto Warburg discovered the properties of NAD^+ as a hydrogen-transferring molecule through his experiments on alcohol fermentation (Berger et al., 2004). Electron transfer from a molecule to NAD^+ to produce NADH and the oxidized molecule is catalysed by a specific group of enzymes known as oxidoreductases (Warburg et al., 1935). In dehydrogenase reactions, the electron transfer from an electron donor to NAD^+ produces reduced NADH used in catabolic reactions to generate energy, such as the citric acid cycle and glycolysis.

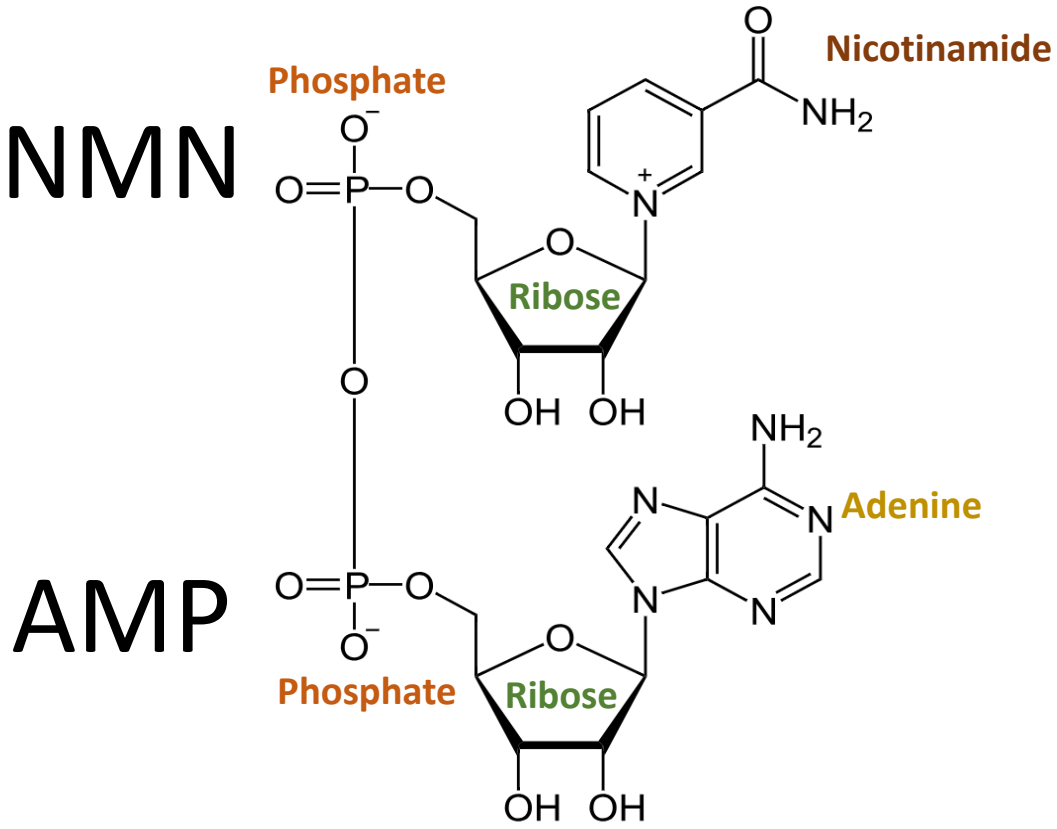


Figure 1.1 Molecular structure of NAD+.

NAD comprises two different nucleosides attached together by the phosphate group. The first molecule is nicotinamide mononucleotide **(NMN)** which has a nicotinamide base attached to the ribose, and the second molecule is adenine monophosphate **(AMP)** with an adenine base attached to the ribose group.

NAD is a cofactor found in all living cells and plays a central role in cellular metabolism and energy production (Magni et al., 2004, Ruggieri et al., 2015). In cellular respiration, NAD and both its reduced and phosphorylated forms (NADH, NADPH, and $NADP^+$) act as cofactors for a series of reactions that produce energy in the form of ATP (Houtkooper et al., 2010, Belenky et al., 2007) (**Figure 1.2**). In cell metabolism, NAD^+ is most commonly

involved in the catabolic reactions to generate energy, while NADPH functions in anabolic reactions encompassing the synthesis of cholesterol and fatty acids. The level of NAD^+ has been shown to decline with aging and medical conditions, such as diabetes and obesity (Imai and Guarente, 2014), possibly due to cellular processes involving oxidative stress and DNA damage. This highlights the importance of studying NAD as a substrate for metabolism and energy homeostasis.

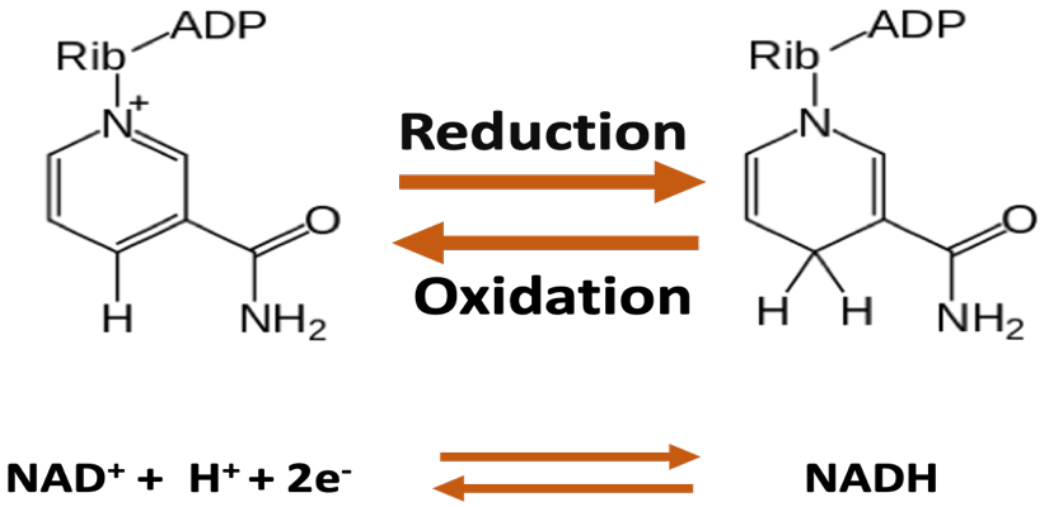


Figure 1.2. NAD as a redox molecule through its reduced and oxidized forms.

NAD^+ is reduced to NADH by accepting two electrons and one hydride ion. In reverse, NADH is oxidized to NAD^+ by donating the electrons. These reactions are essential for cellular energy production in the form of ATP in the electron transport chain reaction by generating the mitochondrial membrane proton gradient.

1.2. NAD Biosynthesis pathway

Maintaining adequate NAD^+ regeneration is critical for cell function and survival. NAD^+ can be synthesized through three different pathways; Preiss-Handler, *de novo* synthesis, and the salvage pathway via nicotinamide (NAM) and nicotinamide ribose (NR) (de Figueiredo et al., 2011) (**Figure 1.3**).

1.2.1. Preiss-Handler pathway

In the Preiss-Handler pathway, NAD^+ is synthesized by utilizing dietary supplements of NAD^+ precursor nicotinic acid (NA) and nicotinic acid phosphoribosyl transferase (NaPT) enzyme to produce nicotinic acid mononucleotide (NAMN) using phosphoribosyl pyrophosphate (PRPP) as a cofactor. NAMN transferase (NAMNAT) enzyme catalyses the transformation of NAMN to nicotinic acid adenine dinucleotide (NAAD), which is then converted to NAD^+ by NAD synthase (the rate-limiting step in the Preiss-Handler and *de novo* pathways) (Houtkooper et al. 2010). This NAD^+ biosynthesis pathway predominantly occurs in tissues where NaPT is highly expressed, such as kidney, heart, and red blood cells (RBCs) (Di Stefano and Conforti, 2013).

1.2.2. *De novo* pathway

NAD^+ can be synthesized *de novo* from the essential amino acid L-tryptophan (Trp), which can be present in the diet (egg, milk, and meat). Trp is converted to quinolinic acid (QA) through the kynurenine pathway which is converted by the quinolinic acid phosphoribosyl-transferase (QAPRT) enzyme using PRPP as a cofactor to generate NAMN (Nishizuka and Hayaishi, 1963, Dolle et al., 2013). (**Figure 1.3**)**.** NAMN is then converted via NMNAT

to NAAD, which is further converted to NAD^+ via the NAD synthase enzyme (Magni et al., 2004).

The generation of QA from Trp mainly occurs in the liver, as the expression of the QAPRT enzyme is relatively higher compared to other tissues (Dölle et al., 2013). It has been suggested that the kynurenine pathway is not the primary source of NAD biosynthesis. A study found that the absence of the kynurenine pathway did not affect normal functional development in QAPRT knock-out mice (Terakata et al., 2012). The role of the kynurenine pathway is thought to be related to energy production in immunological responses as an important immune system regulator (Savitz, 2020). Additionally, it was shown that Trp could not support the required NAD^+ to support cellular functions, as 1 mg of niacin can provide the same level of NAD^+ as 60 mg of Trp (Nikiforov et al., 2011) (Bogan and Brenner, 2008).

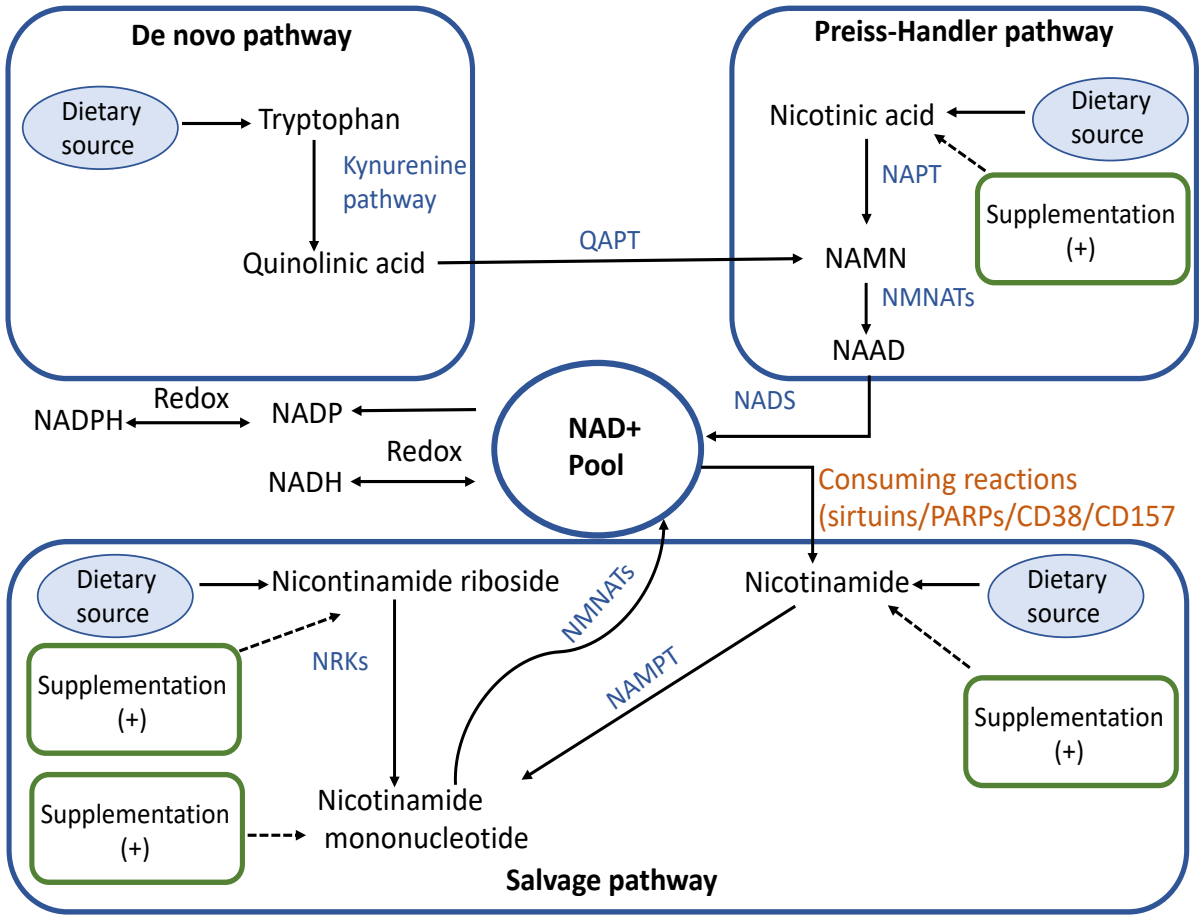


Figure 1.3. Schematic illustration of NAD+ biosynthesis pathways in the cytoplasm.

The three entry points for NAD^+ synthesis are the *de novo* pathway by tryptophan (Trp), Preiss-Handler pathway by nicotinic acid (NA), and the salvage pathway through Nicotinamide riboside (NR). NAD is consumed by C38, CD157, PARP, and sirtuins, and the result of NAD^+ breakdown is nicotinamide (NAM) which is converted to nicotinamide mononucleotide (NMN) to enter the NAD^+ synthesis pathway. NAAD, nicotinic acid adenine dinucleotide; NaPT, nicotinic acid phosphoribosyl-transferase; NADS, NAD^+ synthase; NMNAT, nicotinamide mononucleotide adenylyl-transferase; QAPT, quinolinic acid phosphoribosyl-transferase. *The conversion of NA to NMN through nicotinamide phosphoribosyl transferase (NAMPT) is the rate-limiting step in NAD^+ biosynthesis.

1.2.3. Salvage pathway by NAD^+ precursor (NAM)

NAD^+ can be synthesized by recycling NAD^+ precursor NAM in several enzymatic reactions. Firstly, NAM is converted to NMN in a PRPP- and ATP-dependent reaction via NAMPT, and then NMNAT catalyses the conversion of NMN to NAD^+ (Garten et al., 2009) (**Figure 1.4)**. The source of NAM can be acquired from the diet (meat and eggs) or as an end product of NAD^+ dependent enzymatic reactions (Fricker et al., 2018, Garten et al., 2009). This pathway, known as the NAMPT salvage pathway, has a critical role in metabolic homeostasis and development as determined using NAMPT knock-out mice (Revollo et al., 2007, Di Stefano and Conforti, 2013).

The NAMPT-mediated NAD^+ biosynthesis is regulated by the circadian pattern of NAMPT gene expression, which can impact the activity of NAD-dependent enzymes (Nakahata et al., 2009, Ramsey et al., 2009). NAMPT was initially known as 'pre-B-cell colony enhancing factor (PBEF)' which was later described according to its location as intracellular (iNAMPT) and extracellular (eNAMPT) (Tan et al., 2013, Di Stefano and Conforti, 2013). Although NAMPT expression is essential to preserve cellular NAD^+ levels, a study showed that NAMPT knock-out in mice had only a minor effect on mitochondrial NAD^+ levels in the liver cell compared to other cellular compartments (Dall et al., 2019).

Although an increase in NAMPT is accompanied by cellular benefits such as improved mitochondrial biogenesis (Kim et al., 2014) and regulation of blood glucose (Kieswich et al., 2016), it was shown that NAMPT protein was overexpressed in oncogenic cells (Wang et al., 2011). Pharmacological inhibition of NAMPT by FK866 (competitive, highly specific NAMPT inhibitor) has been shown to deplete NAD^+ through binding to the NAMPT

nicotinamide binding pocket. A large number of studies highlighted the benefit of FK866 as a potential therapeutic target for cancer, such as prostate cancer (Moore et al., 2015), gastric cancer (Lee et al., 2018), and hepatocellular carcinoma (Schuster et al., 2015). The role of NAMPT as an NAD^+ regulator indicates its significance for controlling NAD^+-dependent enzyme activity and cellular homeostasis (Garten et al., 2015).

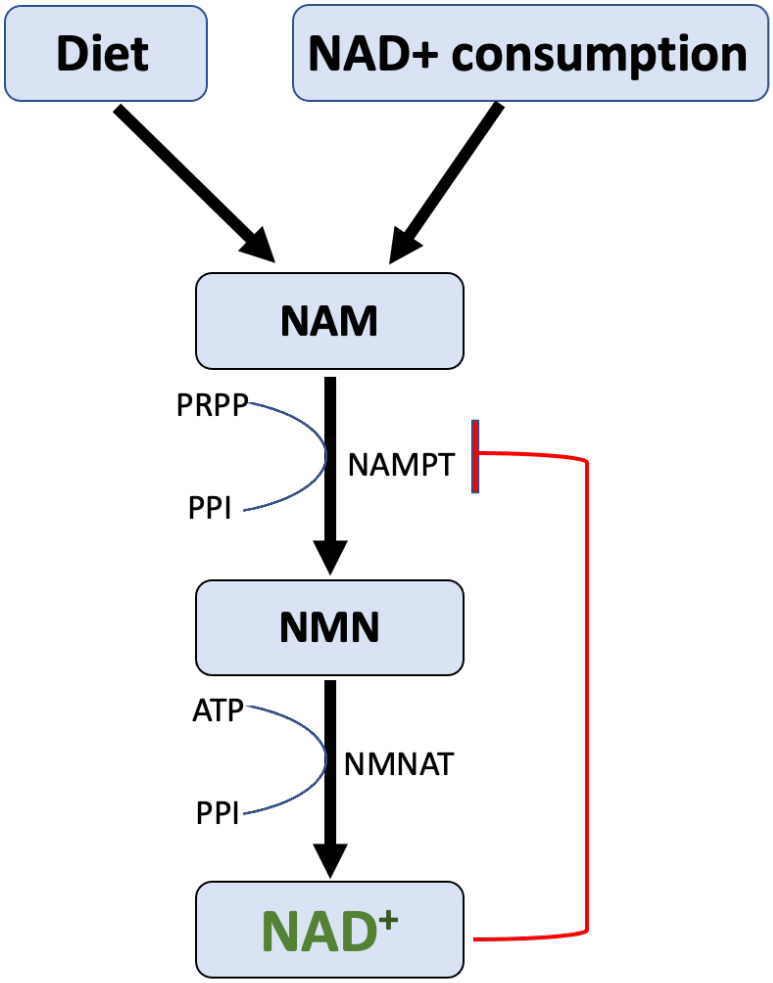


Figure 1.4. NAD+ biosynthesis via NAMPT salvage pathway.

NAM can be directly acquired from the diet or produced as an end product of NAD^+ metabolism. NAD^+ recycling through NAMPT and NMNAT is the rate-limiting step in cellular NAD^+ synthesis. High concentrations of NAD^+ inhibit the NAMPT salvage pathway through a feedback mechanism to control NAD^+ levels.

1.2.4. Salvage pathway by NAD^+ precursor nicotinamide ribose

Nicotinamide ribose (NR) is known as a form of vitamin B3, which was discovered as an essential NAD^+ precursor found in cow's milk (Bieganowski and Brenner, 2004). The cytosolic nicotinamide ribose kinase (NRK) enzymes phosphorylate NR to NMN using ATP as a cofactor which is then converted by NMNAT1 to produce NAD^+ (Bieganowski and Brenner, 2004, Garten et al., 2009) (**Figure 1.5)**. NR has long been known as an NAD^+ precursor in bacterial strains lacking the enzymes for NAD^+ biosynthesis pathways (Gingrich and Schlenk, 1944). In 2004, NR and its phosphorylating enzymes (NRK1, NRK2) were identified as an essential source of NAD^+ in mammals (Bieganowski and Brenner, 2004). As an NAD^+ precursor, exogenous NR has been studied as a possible therapeutic target for aging by extending yeast lifespan through boosting SIRT2 signaling, which sparked intense interest in the NR and NRK enzymes as a potential anti-aging therapy (Belenky et al., 2007). The importance of NAD^+ salvage by NR was shown in cells where NAM salvage was inhibited and revealed that administration of NR can restore depleted NAD^+ levels (Fletcher et al., 2017, Ratajczak et al., 2016).

The capacity to boost NAD^+ by exogenous NR has been shown to be more efficient than other NAD^+ precursors (NAM, NA) in multiple tissues (Fletcher et al., 2017). Chronic administration of NR enhanced oxidative metabolism in mice by boosting NAD^+ levels in the liver, skeletal muscle, and brown adipose tissue, increasing SIRT enzyme activity. This outcome also prevented insulin resistance, weight gain induced by a high-fat diet (Cantó et al., 2012), type 2 diabetes mellitus (Trammell et al., 2016b), and non-alcoholic fatty liver disease (NAFLD) (Zhou et al., 2016). In humans, NR supplementation is

available as an oral capsule which was shown to be well-tolerated in middle aged and older adults (Trammell et al., 2016a, Martens et al., 2018). Many researchers highlight the potential health benefit of NR treatment in normalizing blood pressure (Martens et al., 2018), reducing liver fat (Dollerup et al., 2018), and age-related cognitive decline (Braidy et al., 2019). A recent report indicated that acute administration of NR improved redox homeostasis and exercise activity among the aging population (Dolopikou et al., 2020). Further research is needed to investigate the potential benefit of NAD^+ and its precursors (NR, NMN) in human diseases.

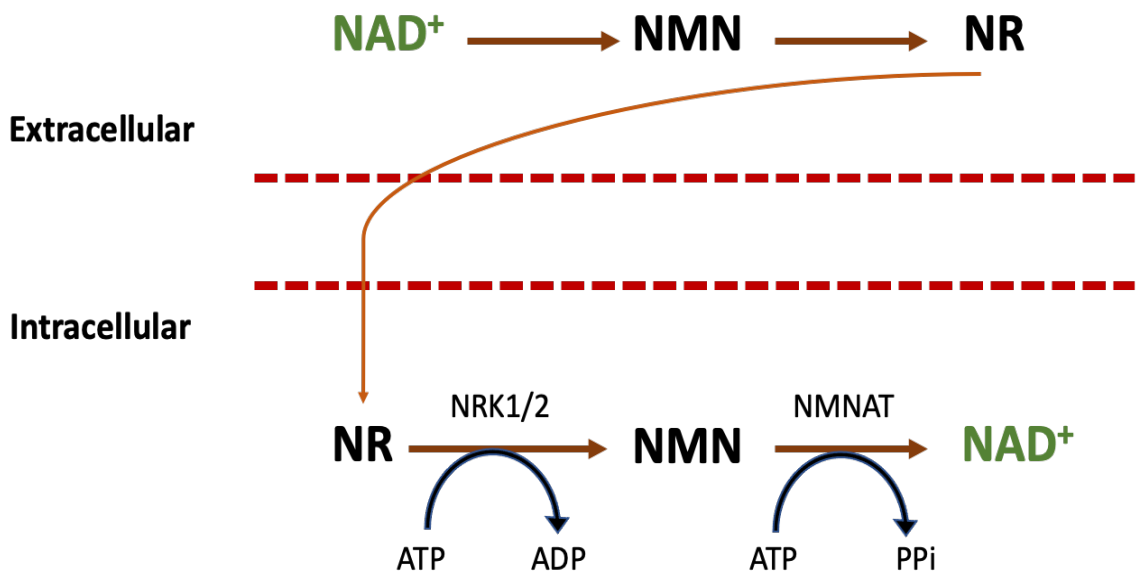


Figure 1.5. NR as a precursor of NAD+.

The cell membrane is impermeable to the direct entry of NAD^+; therefore, NAD^+ needs to be converted to NR by 5'nucleotidases (5'-NTs). NR is converted to NMN via the NRK enzymes inside the cell before it is metabolized into NAD^+ through the NMNAT enzyme.

1.2.5. NAD Kinase

NAD kinase is a key enzyme in NAD metabolism and plays a pivotal role in maintaining the cellular balance of NAD and NADP. This enzyme found in eukaryotic and prokaryotic cells catalyses the phosphorylation of NAD to produce NADP (Gao and Xu, 2012). This reaction is fundamental for maintaining the NAD/NADP balance within the cell. By modulating the level of NADP, NAD kinase contributes to cellular redox homeostasis and overall maintenance of cellular health, making it a critical component for cell function and survival.

1.3. NAD consuming enzymes

Recently, an essential function of NAD^+ has been shown in posttranslational modifications (PTMs), as a rate-limiting substrate for several enzymatic reactions (Belenky et al., 2007, Houtkooper et al., 2010). These NAD-consuming enzymes play a central role in cellular metabolic signaling, which can be classified into three categories: poly(ADP-ribose) polymerases (PARPs), sirtuins (SIRTs), and cADP-ribose synthases (CD157 and CD38) (**Figure 1.6**).

PARP proteins are found in the cell nucleus and facilitate DNA repair by initiating cellular reactions in response to a chemical or metabolism-induced DNA damage (Herceg and Wang, 2001). Sirtuins have many roles in energy metabolism, cellular stress responses, DNA repair, and regulation of circadian rhythm (Chang and Guarente, 2014). Due to the regulatory roles in cell metabolism, these NAD-dependent reactions are essential for cellular energy homeostasis. Therefore, the cellular availability of NAD^+ is vital to control the activity of these consuming enzymes in metabolism and signaling processes.

1.3.1. Sirtuins

The sirtuin enzymes are a group of NAD-dependent deacetylases that regulate the cellular metabolic profile (Houtkooper et al., 2012, Imai et al., 2000). Sirtuins consume NAD^+ and release deacetylated protein, O acetyl ADP ribose, and nicotinamide (NAM) (Sauve et al., 2006) (**Figure 1.6(C)**). Seven sirtuin homologs exist in mammalian cells with different functions, targets, and subcellular locations (Imai et al., 2000). SIRT 1,6 and 7 are primarily located in the nucleus (Vaziri et al., 2001, Michishita et al., 2005), SIRT 2 is a cytosolic protein (Wang et al., 2007), and SIRT 3, 4, and 5 predominantly appear in the mitochondria (Michishita et al., 2005, Onyango et al., 2002). A number of researchers have shown the crucial function of sirtuins as a metabolic sensor of the mammalian cell's energy homeostasis as NAD^+ consuming enzyme (Li, 2013, Cantó et al., 2009).

The role of SIRT1 was seen in regulating glucose production in the liver at a transcriptional level through promoting gluconeogenesis during fasting (Erion et al., 2009), while metformin suppresses gluconeogenesis by inducing SIRT1 (Cuyàs et al., 2018, Caton et al., 2010). Sirtuin1 can also increase insulin sensitivity in beta cells protecting against obesity and type 2 diabetes (Banks et al., 2008). The expression of SIRT1 and NAD^+ biosynthetic enzymes was reduced in obesity, which indicates that cellular NAD^+ homeostasis is crucial to maintain SIRT's metabolic functions (Jukarainen et al., 2016).

1.3.2. Poly ADP-ribose polymerase

Poly ADP-ribose polymerases (PARPs) are a group of NAD^+ consuming enzymes first described in the 1960s (Chambon et al., 1963). They exist in mammals in 17 different isoforms, with the most studied being PARP1 and PARP2 (Cantó et al., 2015). PARPs

use NAD^+ as a substrate to produce adenosine diphosphate ribose (ADPRs) to be transferred to the targeted protein and form a chain of poly-ADP ribose (PAR), which can reach up to 200 ADPR units (Alvarez-Gonzalez and Jacobson, 1987, Juarez-Salinas et al., 1982) (**Figure 1.6(B)**). PARP1 is mainly located in the cell nucleus, while reports also indicate the presence of PARP1 and other poly-ADP ribosyl-transferases in the mitochondria (Smith, 2001, Du et al., 2003).

1.4.2.1. The role of PARP in the cell and its relation to NAD+/NADP

The primary functions of PARPs are related to cellular genomic stability through their role in DNA repair (Javle and Curtin, 2011). They are recruited by DNA damage and genotoxic stress to the site of DNA strand breaks (Koh et al., 2004). Additionally, they are involved in modulating transcription, chromatin structure, cellular proliferation, and apoptosis (Morales et al., 2014). PAR is rapidly generated, which can help to recruit proteins to the site of DNA damage (Krietsch et al., 2013).

PARP enzymes are NAD^+ dependent, which means they need a continuous source of NAD^+, and therefore, to establish DNA repair, they utilize NAD^+ biosynthetic enzymes at the site of DNA damage (Zhang et al., 2012). The activity of PARP enzymes is the main consumer of NAD^+ during the cellular stress response. However, it is essential to note that significant cross-talk exists between PARPs and other NAD^+-consuming enzymes. Therefore, reduced NAD^+ level and higher sirtuin activity can have an impact on PARP activity resulting in an increase in NAM and, consequently PARP inhibition (Park et al., 1983).

PARP activity is thought to increase with age due to higher DNA damage accumulation leading to diminished NAD^+ availability. This will lead to decreased SIRT activity, exacerbated by PARP's higher affinity for NAD^+ (Guarente, 2014, Massudi et al., 2012, Cantó et al., 2015). Research on PARP inhibition in skeletal muscle and other tissues has found that it has a protecting cellular metabolic effect by reducing excessive NAD^+ consumption by PARP activity and, therefore, stimulating SIRT activity (Bai et al., 2011, Rajamohan et al., 2009). Nevertheless, considering PARP inhibition to target metabolic disorders is not applicable as this can induce genomic instability via the lack of PARP's central role in DNA damage repair (Ito et al., 2016, Guarente, 2014).

1.4.4 Cyclic ADP-ribose Synthase

cADP-ribose synthases (CD38, CD157) are a group of enzymes that consume NAD^+ to produce cADP-ribose which can be hydrolyzed to ADPR (**Figure 1.6(A)**). Under acidic conditions, these enzymes utilize NADP+ to generate nicotinic acid adenine dinucleotide phosphate (NAADP) (Lee, 2006, Howard et al., 1993). These molecules are essential to regulate calcium mobilization and influx as intracellular second messenger (Okamoto, 1999, Guse et al., 1999).

The role of CD38 in regulating NAD^+ levels was seen in a CD38 knock-out mouse model. The level of NAD^+ was increased 20 fold compared to wild type mice, which led to enhanced SIRT activities (Aksoy et al., 2006b, Aksoy et al., 2006a). This relation explains the significance of NAD^+ as the primary regulator of these enzyme functions (Quarona et al., 2013).

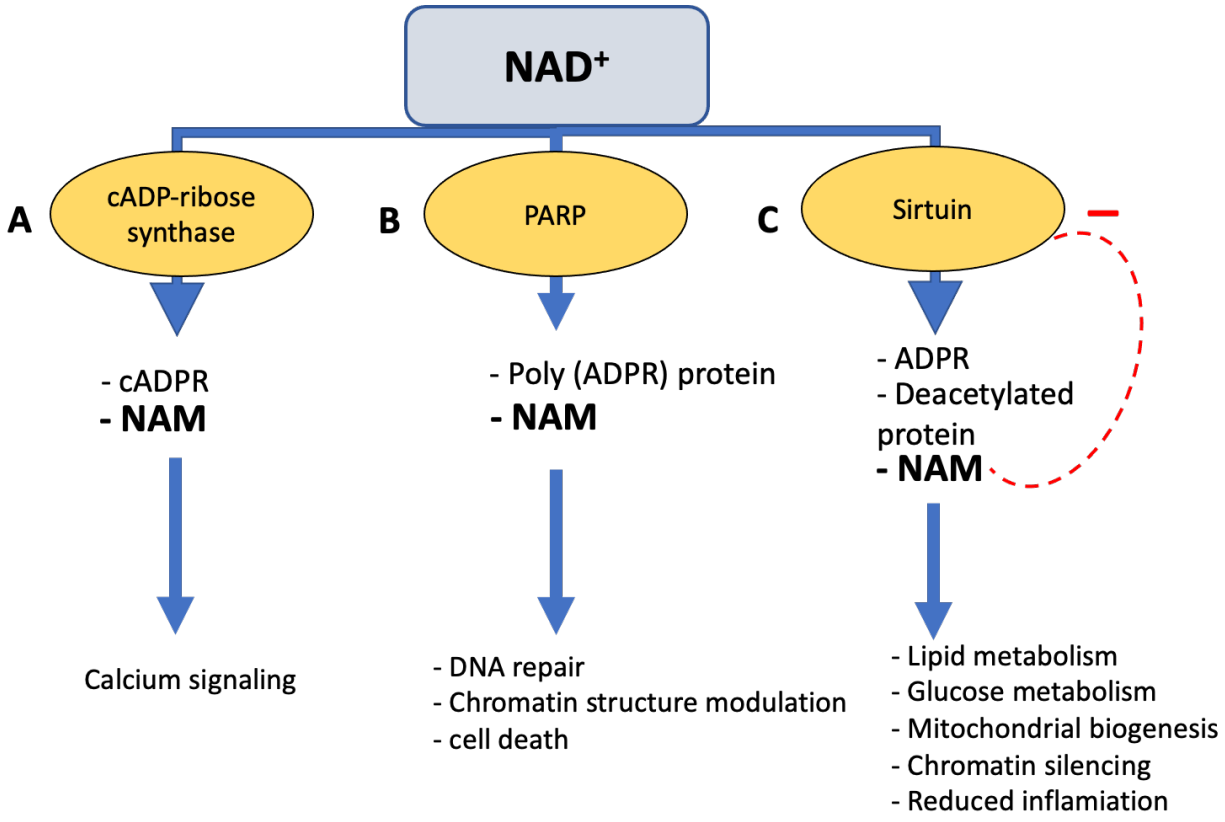
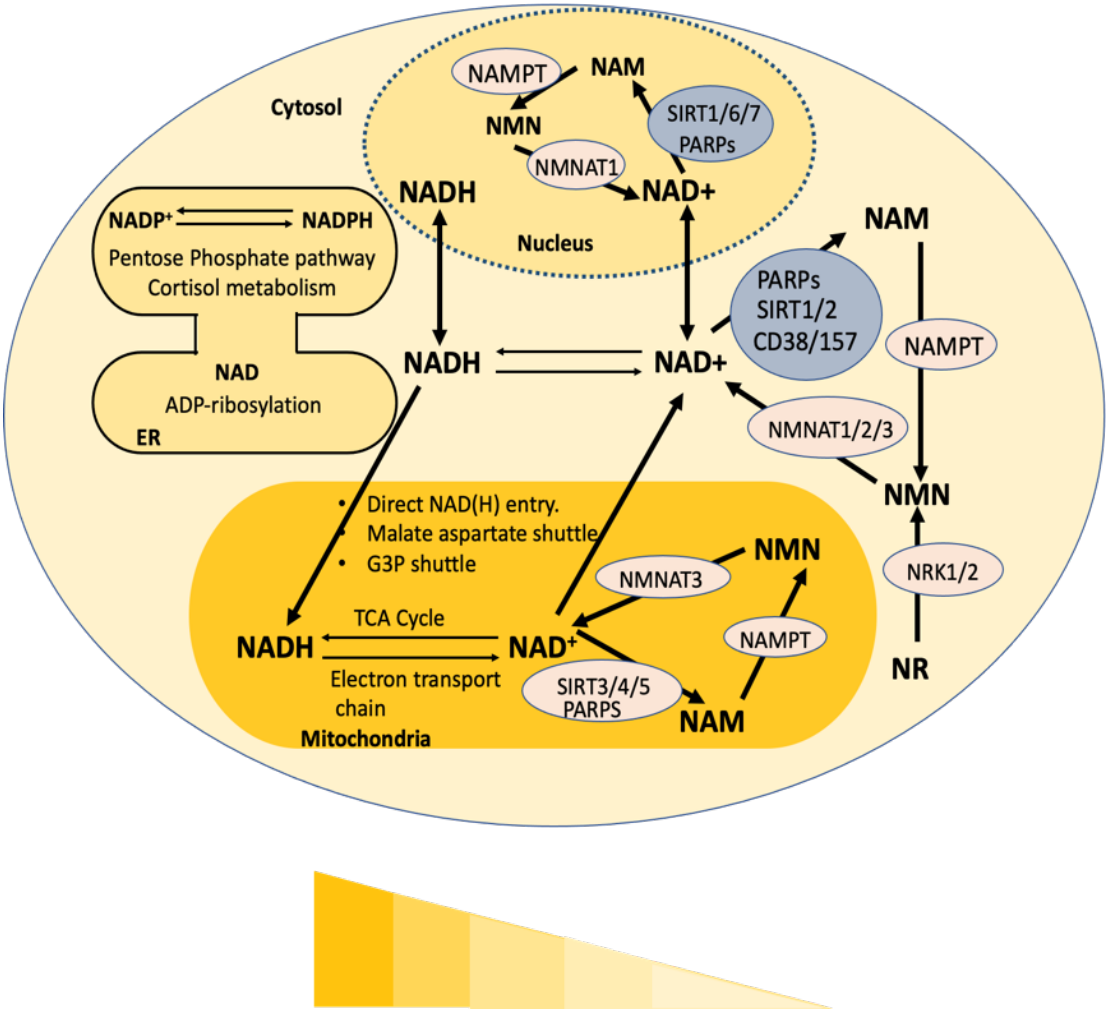


Figure 1.6. Schematic illustration of NAD+ consuming enzymes.

A. cADP-ribose synthase consumes NAD^+ to produce cADPR responsible for calcium signaling. Its primary role is the activation of Ca^{2+} release from the endoplasmic reticulum. **B.** PARPs are mainly involved in DNA repair through catalyzing ADP-ribose release from NAD^+ and transferring it to itself and to target proteins. **C.** Sirtuins play a role in cellular energy metabolism through their role in protein deacetylation. Sirtuins are inhibited by NAM.

1.4. NAD^+ compartmentalization

Regulation of subcellular NAD^+ availability is essential to maintain cellular energy homeostasis and signaling pathways. However, the intracellular NAD^+ pool is separated by cellular compartments and is not equally distributed between subcellular organelles (Cambronne and Kraus, 2020). This relative variation in the NAD^+ pool reflects the necessity of the subcellular organelles to utilize NAD^+ as a cofactor for redox and signaling reactions. It is assumed that NAD^+ can freely move between the cytosol and the nucleus without any diffusion barriers, given that the majority of NAD^+ biosynthesis enzymes and NAD+-dependent reactions occur in the cytosol or the nucleus (Nikiforov et al., 2015) (**Figure 1.7**.) In the mitochondria, there is no evidence to suggest passive NAD^+ exchange between mitochondria and cytosol. However, instead, the malate-aspartate NADH shuttle is known as a source of NADH in the mitochondria (Satrústegui et al., 2007). In the endoplasmic reticulum (ER), there is still a debate about the mechanisms that allow molecules to transport NAD across the ER membrane. Several observations suggested that the ER membrane is separated from cytosolic components by a barrier that allows the transport of selective cytosolic molecules (Lomax et al., 2002, Heritage and Wonderlin, 2001, Csala et al., 2006). On the other hand, a study on rat liver microsomes reported an increase in the activity of 11 beta-hydroxysteroid dehydrogenase type 1 (11β-HSD1), an NADPH-dependent enzyme located in the ER lumen, when incubated with NADPH (McCormick et al., 2006). This might indicate that the ER membrane is not entirely separated from the cytosolic component, and there might be a possible ER-cytosol communication in terms of the NAD^+ pool **(Figure 1.7**).



The relative concentration of NAD$^+$

Figure 1.7. Regulation of subcellular NAD+ pools, with the distribution of NAD+ dependent enzymes and salvage pathways.

The nuclear pores allow free diffusion of NAD$^+$ and NADH molecules into the nucleus. In the mitochondria, the NAD$^+$ pool is maintained via NAD$^+$/NADH shuttle (glycerol 3-phosphate and malate aspartate shuttle) and by direct entry of NAD$^+$. Although it is identified that NAD(P)(H) is produced in the ER by the pentose phosphate pathway (PPP), it is unknown whether there is a mechanism that allows for NAD entry into the ER.

1.5. PAR as a biosensor of the subcellular NAD^+ pool

Historically, the distribution of organellar NAD^+ had only been determined by cell disruption and fractionation, followed by extraction of nucleotides (Simpson and Pepperkok, 2006). This technique measured nucleotide contents in cytosol/nucleus and mitochondria, while the amount of NAD^+ in other cellular compartments has not been determined. Recently, visualization of subcellular NAD+ pools has been studied based on the overexpression of catalytically active PARP as NAD^+ consumer enzyme that cleaves the NAD nicotinamide-glycosidic bond to generate polymers of ADP ribose (ADPr), a process known as PARylation (Dölle et al., 2010). Both GFP and a peptide tag are fused to the catalytically active PARP. The detection of both via fluorescence or immunofluorescence is used to visualize the subcellular localization of catalytically active PARP. This method was used to investigate PAR formation in mitochondria and ER. It revealed a specific intra-organellar presence of PARylated protein linked to NAD^+ availability and PARP activity.

Detection of poly-ADP-ribose polymers by specific antibodies reflects changes in the subcellular pool of free NAD^+. Experimental evidence revealed a significant decrease in PARP enzymatic activity 4 hours after the start of adipocyte differentiation (Luo et al., 2017). This reduction in PARylation is considered to be linked to a decrease in nuclear-free NAD^+ (Ryu et al., 2018). Furthermore, treating the cells with NAD^+ precursor (NMN) increased free NAD^+ in the nucleus and restored PARP enzymatic activity (Luo et al., 2017). Therefore, the subcellular NAD^+ pool can be examined based on converting nucleotides to immunochemically detectable PAR polymers.

1.6. Glucocorticoids

Glucocorticoids (GCs) are a class of steroid hormones secreted by the adrenal cortex. Cortisol (corticosterone in rodents) is the main active GC that has a significant role in maintaining whole-body energy homeostasis and the capacity to tolerate environmental changes. The widespread effects of glucocorticoids involve cardiovascular, immunological, body fluid homeostasis, and metabolic effects (Rhen and Cidlowski, 2005). Glucocorticoids are released in response to stress conditions and exert important physiological actions in various tissues. These effects vary depending on the glucocorticoid receptor (GR) expression in the tissues (Parker, 1986, RABBITT et al., 2002). One of the most common effects of GCs is associated with immunosuppression through binding to GR and activating specific transcription factors involved in the upregulation of anti-inflammatory mechanisms (Bamberger et al., 1996).

In metabolism, GCs tend to increase glucose concentration by enhancing gluconeogenesis in the liver and the output of glucose during fasting (Kraus-Friedmann, 1984). Also, GCs interfere with protein synthesis and promote protein degradation in skeletal muscle leading to peripheral muscle myopathy (Long et al., 2001). In adipose tissue, GCs increase central obesity through enhancing adipogenesis and the accumulation of triacylglycerol (TAG) and increase circulatory fatty acids due to the lipolysis effect (Peckett et al., 2011).

1.6.1. Hypothalamic pituitary adrenal axis (HPA)

Systemic glucocorticoid levels are under the regulation of the hypothalamic-pituitary-adrenal (HPA) axis system (Lightman and Conway-Campbell, 2010). In the hypothalamus, corticotropin-releasing hormone (CRH) is secreted in response to stress ('fight or flight' response) which activates the release of the adrenocorticotrophic hormone (ACTH) by the anterior pituitary gland. This subsequently activates the release of glucocorticoids from the adrenal cortex (Grossman et al., 1982). Conversely, a negative feedback mechanism is activated at a high cortisol level, inhibiting the release of ACTH and CRH (Munck and Naray-Fejes-Toth, 1992) (**Figure 1.8**).

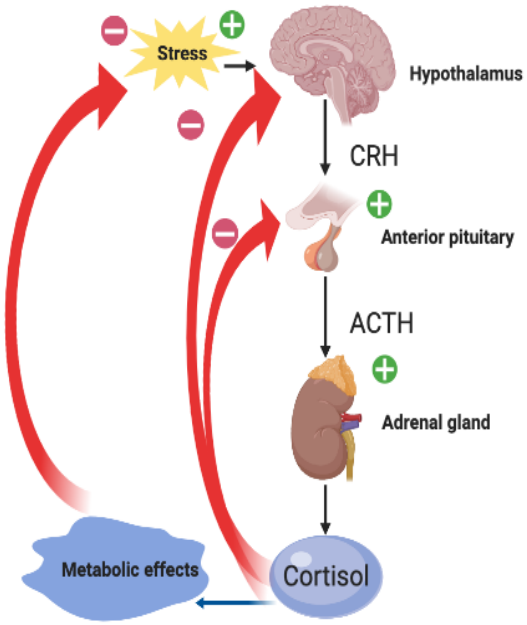


Figure 1.8. Schematic diagram representing the hypothalamic pituitary adrenal (HPA) axis and metabolic effect of cortisol.

(CRH) corticotropin-releasing hormone, (ACTH) adrenocorticotrophic hormone.

1.6.2. 11 β-hydroxysteroid dehydrogenase (11 β-HSD)

Despite the systemic regulation of cortisol levels by the HPA, an enzyme named 11 β-HSD regulates cortisol availability at the tissue level. There are two isoforms of the enzyme, 11 β-HSD1 (catalyzes the activation of inactive cortisone to active cortisol in the oxo-reductase reaction) and 11 β-HSD2 (catalyzes the inactivation of cortisol to cortisone in the dehydrogenase reaction) (**Figure 1.9**)**.** The 11 β-HSD1 enzyme is located in the endoplasmic reticulum lumen, and its oxo-reductase activity depends on NADPH availability inside the ER (Lavery et al., 2006). The role of 11 β-HSD1 in regulating metabolism has been studied in transgenic animal models. In adipose tissue, 11 β-HSD1 overexpression in mice was associated with the development of insulin resistance, visceral obesity, hypertension and dyslipidemia (Masuzaki et al., 2001, Masuzaki et al., 2003). A similar outcome of insulin resistance and hypertension was shown in liver-specific 11 β-HSD1 overexpressing mice (Paterson et al., 2004). In all of the previous models, the systemic corticosteroid level was not elevated, suggesting a role of 11 β-HSD1 in the observed phenotype through increasing intracellular availability of cortisol. Therefore, the loss of 11 β-HSD1 enzyme activity in peripheral tissue can reduce the cortisol effect and increase its metabolic clearance.

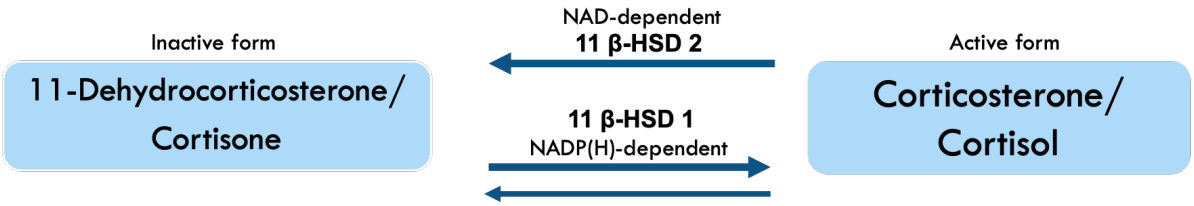


Figure 1.9. The conversion reaction catalyzed by 11 β-HSD enzymes.

The activation reaction of cortisone to cortisol is carried out by 11 β-HSD1 and requires NADPH as a cofactor. The inactivation of cortisol to cortisone is a reductase reaction that requires NAD as a cofactor and is carried out by 11 β-HSD2. In animal studies, cortisone is referred to as 11 Dehydro-corticosterone (11DHC), and cortisol is referred to as corticosterone.

1.6.2.1. 11 β-HSD tissue expression

11 β-HSD1 is expressed in the metabolically active tissues, such as skeletal muscle, liver, and adipose tissue, where it converts inactive cortisone to active cortisol to increase the availability of substrates needed for energy production (Morgan et al., 2014, Seckl and Walker, 2001). The expression of 11 β-HSD1 was also assessed in fibroblasts derived from different tissues, which showed expression in all fibroblasts derived from bone marrow, synovium, and skin, but with higher enzymatic activity and mRNA levels in dermal and synovial fibroblasts (Hardy et al., 2006a), **Table 1.1** shows the expression of 11 β-HSD1 in different tissues. In contrast, 11β-HSD2 is predominantly found in mineralocorticoid target tissue, such as the kidney, placenta, colon, and salivary glands.

Table 1.1. 11 β-HSD expression in different cell types.

Cell type	Expression	Reference
Adipocyte/3T3-L1 cell line	+	(Paulmyer-Lacroix et al., 2002, Napolitano et al., 1998, Morton et al., 2004)
Dermal Fibroblast	+	(Hammami and Siiteri, 1991, Terao et al., 2014)
Primary myotube/ C2C12 cell line	+	(Whorwood et al., 2002, Morgan et al., 2009, Aubry and Odermatt, 2009)
Hepatocyte/HepG2	+	(Ricketts et al., 1998b, Ricketts et al., 1998a, Tannin et al., 1991)
Adrenal cortex	+	(Ricketts et al., 1998b)
Osteoblast and osteosarcoma (MG-63)	+ –	(Cooper et al., 2000, Bland et al., 1999)

1.6.3. Clinical implication of glucocorticoid and 11 β-HSD1 dysregulation

Due to the role of glucocorticoid as an effective anti-inflammatory drug, glucocorticoid synthetics have been considered the most prescribed drugs worldwide, such as cortisone, dexamethasone and prednisolone. These drugs are effective for the treatment of many autoimmune and anti-inflammatory diseases, such as systemic lupus erythematosus

(SLE), asthma, multiple sclerosis, and inflammatory bowel syndrome (Ramamoorthy and Cidlowski, 2016). However, high doses and long-term use of glucocorticoids can lead to many side effects, such as osteoporosis, muscle myopathy, fat accumulation, weight gain, increased insulin resistance, and type 2 diabetes (Schacke et al., 2002, Gathercole et al., 2013).

One of the most common syndromes associated with corticosteroid dysregulation is Cushing syndrome. It is caused by long-time exposure to a high cortisol level as a result of adenoma or corticosteroid medications. The classical phenotypes include hypertension, central obesity, abdominal striae, and proximal myopathy. In a case study of a 20 years old female patient with chronic elevation of cortisol levels, the absence of typical Cushingoid symptoms was reported, which was shown to be associated with a defect in the activity and expression of 11 β-HSD1 (Tomlinson et al., 2002). Moreover, previous observations on mice showed an association between increased 11 β-HSD1 activity and the phenotype of type 2 diabetes and obesity through the activation of gluconeogenesis and insulin resistance (Mariniello et al., 2006).

1.7. Endoplasmic reticulum (ER)

The ER (or sarcoplasmic reticulum SR in muscle cells) is a membranous organelle that makes a continuation with the outer membrane of the nucleus and acts as a separate subcellular compartment executing multiple cellular functions (Csala et al., 2006) (**Figure 1.10**). The primary function of the ER is the synthesis, modification, and release of folded proteins, encoded by specific signal sequences and transported in cooperation with the

Golgi body to the cytosol or outside the cell (Hotamisligil, 2010). In addition, the SR controls the storage and release of calcium ions (Ca^{2+}) required for muscle contractions. There are two sub-organellar structures of ER, rough ER (RER) and smooth ER (SER). RER is a sheet-like structure featuring the presence of a macromolecular complex called ribosome that is responsible for protein biosynthesis. At the same time, SER is a tube-like shape associated with the production and storage of steroids and lipids which do not have ribosomes bound to it (Chen et al., 2013).

ER can interact with other subcellular organelles including mitochondria, lysosomes, peroxisomes, Golgi, and plasma membranes by forming membrane contact sites (MCSs). These sites are created by two opposing membranes when they come closer (around 30nm), but are not fully fused. Forming direct communication with other compartments is essential to maintain cellular homeostasis and stability (Friedman and Voeltz, 2011). In the mitochondrial contact site, ER regulates lipid synthesis and Ca^{2+} signaling which is critical for energy production and regulation of apoptosis. In addition, ER communicates with the plasma membrane (ER-PM) to regulate lipid synthesis, cell signaling, and ion dynamics in response to internal or external stimuli (Li et al., 2021). A previous study demonstrating ER 3D-structure in yeast using electron microscopy (EM) and tomography showed that ~20-45% of the plasma membrane is covered by interconnected ER tubules (West et al., 2011). ER-PM contact sites are also critical for controlling phosphatidyl inositol metabolic pathways and can directly transfer sterols with no vesicle formation required (Schulz and Prinz, 2007, Stefan et al., 2011).

The composition of ions and small molecules in the ER lumen is thought to be different from the cytosol. This observation was made concerning the concentration of oxidized glutathione (Margittai et al., 2015), and calcium ions (Meldolesi and Pozzan, 1998). Despite this, the ER membrane is thought to be more permeable than other subcellular organelles, due to the low cholesterol content and translocon pores (Heritage and Wonderlin, 2001). Analyzing pH levels in subcellular compartments revealed no differences in pH between the ER and the cytosol. At the same time, the Golgi showed a lower pH value than that of the cytosol (Kim et al., 1998, Kneen et al., 1998, Wu et al., 2000). It was shown that ER membranes have a unique mechanism that allows the passage of molecules. For example, glutathione can cross the ER in an energy-dependent reaction resulting in an alteration of ER redox status (Bánhegyi et al., 1999). In general, the permeability of the ER membrane and cross-talk with the cytosol is not clearly understood and requires further investigation.

The ER lumen is the area bounded by the ER which is separated from the cytosol by the ER membrane. It is a metabolically active area representing approximately 10% of total cell volume and is the main site of protein folding and modification (Palade, 1956). It was shown that the ER lumen displays an oxidative environment which is optimal for protein folding and modification by forming of disulphide bonds (Hudson et al., 2015, Hwang et al., 1992). The ER lumen's oxidizing nature is determined by the availability and activity of redox cofactors, i.e. thiol/disulfate redox system, $NADP^+$/NADPH, and glutathione redox system (Margittai et al., 2015, Gansemer et al., 2020). Dysregulation in the NAD/NADP+ pool can activate the ER stress response, resulting in disturbances in redox status and enzymatic activity (Mandl et al., 2009). Dysregulation of enzyme activities in the ER can

affect vital cellular metabolic reactions such as the regulation of glucose homeostasis and can lead to insulin resistance and the development of metabolic diseases, such as obesity and type 2 diabetes (Özcan et al., 2004). In addition, ER stress is indicated by the presence of ER stress markers, such as binding immunoglobulin protein **(BIP**), which is located in the ER lumen maintaining newly synthesized proteins in a competent state for protein folding, and CCAAT/enhancer binding protein homologous protein (CHOP), which is involved in the induction of apoptosis in response to ER stress.

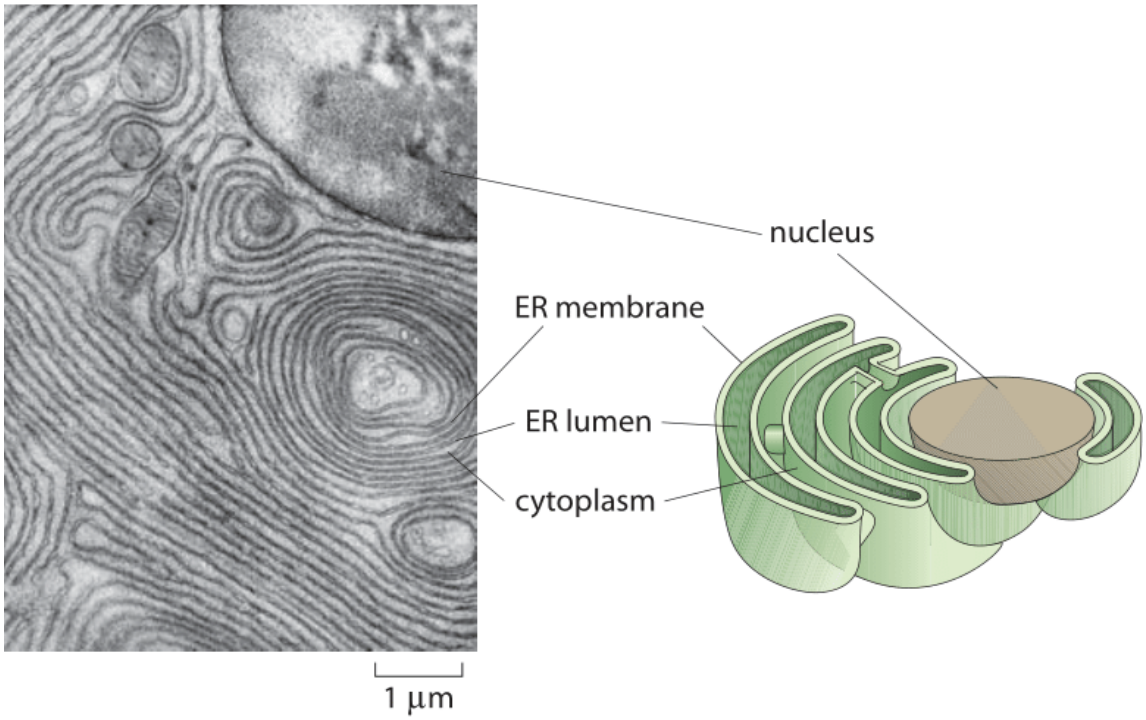


Figure 1.10. The structure of the endoplasmic reticulum.

An electron micrograph shows the area surrounding the nucleus in cells extracted from bat pancreatic cells (Fawcett, 1966).

1.8. Hexose-6-phosphate dehydrogenase (H6PDH)

In the ER, H6PDH catalyses the conversion of glucose-6-phosphate (G6P) to 6-phospho-gluconolactone (6-PGL), the end product of the first two steps of the pentose phosphate pathway, with the production of NADPH that serves as an electron donor for 11 β-HSD1 reductase activity (Collard et al., 1999, Banhegyi et al., 2004, Morgan et al., 2016). H6PDH promotes the oxo-reductase reaction of 11 β-HSD1 by generating NADPH as a cofactor in the pentose phosphate pathway. The link between H6PDH and the activity of 11 β-HSD1 has been investigated using an H6PDH knock-out mouse model. The oxo-reductase activity of 11 β-HSD was depleted by H6PDH gene knock-out, and the metabolite of 11-DHC was only seen in the urine analysis (Lavery et al., 2006). Mice lacking H6PDH were unable to convert 11-DHC to Corticosterone and instead adopted a dehydrogenase activity, inactivating CORT to 11-DHC. These findings suggest the role of H6PDH as a regulator of the 11 β-HSD1 oxo-reductase activity in the ER/SR (**Figure 1.11**).

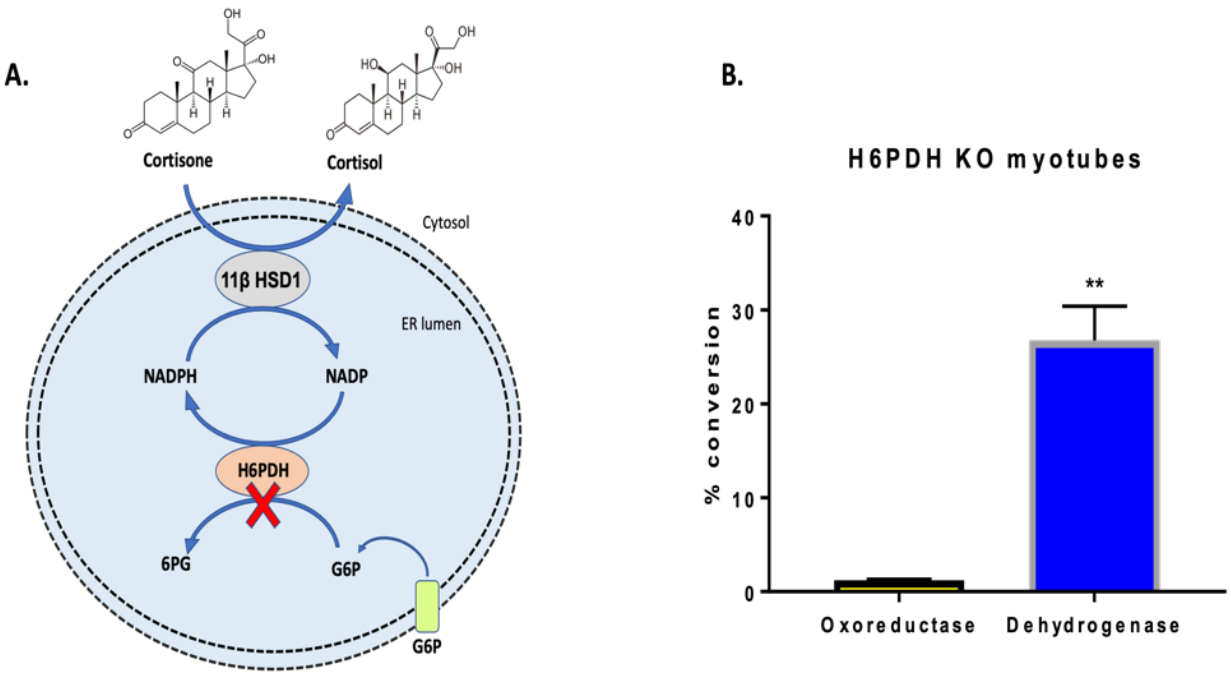


Figure 1.11 Regulation of cellular GC generation by 11 β-HSD1.

A. Oxo-reductase activity of 11β-HSD1 is NADPH dependent and maintained by the activity of H6PDH enzyme in the pentose phosphate pathway. **B.** 11β-HSD1 shift to dehydrogenase activity (inactivation of H^3 corticosterone to H^3 11-DHC in H6PDH KO mouse myotubes (Lavery et al., 2006).

1.9. Thesis rationale

Pathways that control the interaction between cytosolic and ER substances are complex. To our knowledge, it is unknown whether NAD^+ passively crosses the ER membrane, or if there is a unique transporter system that mediates its diffusion (for example a system similar to the shuttle system present in mitochondria) (Satrústegui et al., 2007). Understanding the mechanism of ER NAD^+ homeostasis can improve our knowledge of metabolic diseases induced by the ER stress response.

1.10. Hypothesis

- ER-PARP overexpression consumes NAD^+ which can be established as a genetic model of ER NAD^+ depletion**.**
- 11β-HSD1 activity is determined by the availability of NAD(P)(H) in the ER.

1.11. Aim

- Investigate the cytosolic/ER NAD^+ cross-talk by manipulating cytosolic availability of NAD+ and using the activity of the ER NADPH-dependent enzyme 11β-HSD1 as a readout.
- Examine the generalizability of cytosolic/ER NAD^+ cross-talk in multiple cell types (skeletal muscle, liver, dermal fibroblast, and kidney).
- Establish a model of ER NAD^+ depletion by transfecting cells with catalytically active ER-PARP in mouse skeletal muscle and human liver cells.
- Examine cytosolic/ER NAD^+ cross-talk in the cells overexpressing catalytically active PARP as a genetic model of NAD^+ depletion.

Chapter 2

General methodology

2.1. Cell culture

All cell culturing procedures were conducted using a laminar flow hood in an aseptic environment, and all materials used in the hood were sterilized with ethanol 70% (v/v).

2.1.1. C2C12

The mouse skeletal muscle myotubes (C2C12) cell line was purchased from the European Collection of Cell Cultures (Salisbury, UK). This cell line is derived from mouse myoblasts and has been used as a model of skeletal muscle differentiation and proliferation. It was initially produced by serial passage of myoblasts cultivated from C2H mice's thigh muscles 70 hours after a crush injury (Yaffe and Saxel, 1977). A sub-clone of these myoblasts was chosen because of its capacity to grow rapidly and express distinctive muscle proteins (Blau et al., 1985). In addition, C2C12 is established as a good model for investigating cellular metabolic conditions such as insulin resistance and oxidative stress (Wong et al., 2020).

2.1.1.1. Proliferation

C2C12 cells were grown in 75 cm^2 tissue culture flasks (Corning, Surrey, UK) in growth media (GM) - Dulbecco's modified Eagle's medium (DMEM) (GibcoTM, UK) supplemented with 10% (v/v) foetal calf serum (FCS), 1% (v/v) penicillin/streptomycin (P/S), 2 mM L-glutamine, and 4.5 g/L glucose at 37°C under a 5% CO2 atmosphere. Cells were grown with a low passage number (<22) to avoid any changes in the myoblast/myotubes functions and morphology (Pronsato et al., 2013).

At 60-70 % confluence, cells were split by removing the media and washing with sterile phosphate-buffered saline (PBS). To detach the cells, 3 ml of TrypLE^{TM} Express trypsin

enzyme (GibcoTM, UK) was added to the flask and incubated at 37°C. After 5-7 min incubation, 7 ml of fresh DMEM was added and transferred to a 10 ml falcon tube and centrifuged at 1300 rpm for 5 min. The pellet was resuspended with 10 ml of media and reseeded into new flasks. To prepare well plates for experiments, cells were counted using a hemocytometer and seeded at the desired density into 6 or 12-well plates (Corning, Surrey, UK), and the media were replaced every 48 hours with fresh proliferation media.

2.1.1.2. Differentiation

To initiate myotube formation, proliferation media were replaced with DMEM supplemented with 5% (v/v) horse serum (HS), and 1% (v/v) penicillin/streptomycin (P/S). Once myoblasts reached 60-70% confluence, media were replaced every other day until myotubes had fused and formed multinucleated myotubes (6-8 days) (**Figure 2.1**).

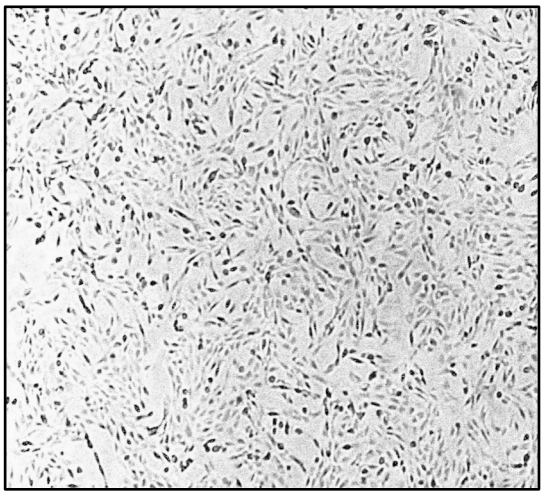


Figure 2.1 Mouse skeletal muscle myotubes cell line (C2C12).

Cells were cultured for 6-8 days in Dulbecco's modified Eagle's medium (DMEM) supplemented with 5% (v/v) horse serum (HS), and 1% (v/v) penicillin/streptomycin (P/S). Cells were treated when they started to form multinucleated myotubes.

2.1.1.2. Freezing down

Freezing down C2C12 cells allowed for long-term storage and kept the cells at low passage numbers for further use. At 60-70% confluence, cells were trypsinized and resuspended in 9 ml of proliferation media supplemented with 10% FCS, and 1% P/S and then centrifuged at 1300 rpm for 5min. The cell pellet was resuspended in 3 mL of FCS supplemented with 10% DMSO. The cells were aliquoted into 1 ml cryotubes (Nalgene, Hereford, UK), pre-cooled overnight in a Mr. Frosty^{TM} freezing container (Sigma, UK), and transferred to liquid nitrogen at -180°C for long-term storage.

To start a new culture of C2C12, the cryopreserved cells were thawed in a water bath at 37°C and transferred to a new 10ml falcon tube with 10 ml DMEM. Cells were centrifuged and the pellet was resuspended and transferred to new T75 flasks.

2.1.2. Primary mouse myotubes

A primary mouse myoblast culture represents a better reflection of muscle cell characteristics than C2C12 cells. Primary cells were collected from the gastrocnemius muscle of mice (C57/B6N) and washed with DMEM for 1 hour supplemented with 1% P/S. To stimulate the proliferation of satellite cells, media containing 0.5% chicken embryo extract (CEE), 10% HS, and 1% P/S was added to the plate and left in the incubator for 24 hours. Medium was replaced with differentiation DMEM medium supplemented with 10% HS, 0.5% CEE, and 1% P/S. At this stage, the medium was replaced every 48 hours until the cells differentiated to form myotubes (approximately 7 days) (**Figure 2.2**).



Figure 2.2 Mouse primary skeletal muscle cells.

Cells were extracted from the gastrocnemius muscle of mice (C57/B6N) and cultured in Dulbecco's modified Eagle's medium (DMEM) supplemented with 2% (v/v) HS, 0.5% (v/v) chicken embryo extract (CEE), and 1% (v/v) P/S for 7 days to differentiate and form multinucleated myotubes.

2.1.3. Human dermal fibroblasts

Human dermal fibroblasts, a neonatal (HDFn) primary cell culture isolated from the neonatal foreskin, was purchased from Thermo Fisher, NY, USA. The fibroblasts were cultured between passage number two and eight in DMEM high glucose media supplemented with 2 mmol/l L-glutamine, 10% (v/v) FBS, 1% (v/v) P/S at 37°C under a 5% CO_2 atmosphere.

Upon arrival, cells were recovered from the cryopreserved vial in a 75-cm^2 flask at a density of 5×10^5 cells. At 60-70 % confluence, cells were trypsinized as described above and incubated at room temperature for 5 min. Cells were seeded into 6 or 12-well plates at a density of 2.5×10^3 cells/cm^2 according to manufacturer's instructions (Thermo Fisher, USA) (**Figure 2.3**).



Figure 2.3. Neonatal human dermal fibroblasts (HDFn).
Cells were cultured for 3-5 days in Dulbecco's modified Eagle's medium (DMEM) supplemented with 10% (v/v) FBS, and 1% (v/v) P/S.

2.1.4. HepG2

HepG2 (Thermo Fisher, NY, USA) is a human hepatocellular carcinoma cell line isolated from a 15-year-old white male with liver cancer. Cells were cultured in Eagle's Minimum Essential Medium (EMEM) supplemented with 10% (v/v) FBS, and 1% (v/v) P/S between passage number 10 and 22. At 60-80% confluence, cells were trypsinized as described above and incubated at 37°C under a 5% CO_2 atmosphere. A day before the experiment, cells were seeded at a density of 2.2×10^5 cells in 2 ml of growth media per well of a 6-well plate (**Figure 2.4**).

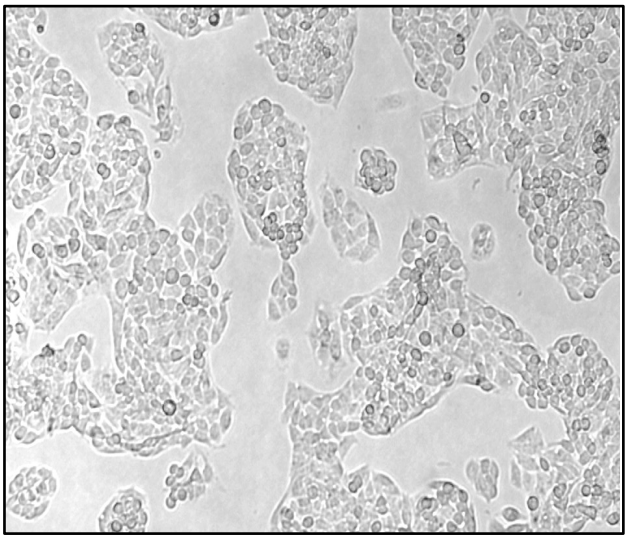


Figure 2.4. Human hepatocellular carcinoma cell line (HepG2).

Cells were cultured for 48 hours in Eagle's Minimum Essential Medium (EMEM) supplemented with 10% (v/v) FBS, and 1% (v/v) P/S.

2.1.5. HEK293

HEK293 (Thermo Fisher, NY, USA) is a human kidney cell line isolated from the kidney of a human embryo. Cells were cultured in Dulbecco's modified Eagle's medium (DMEM) supplemented with 10% (v/v) FBS, and 1% (v/v) P/S between passage number 8 and 12. At 60-80% confluence, cells were trypsinized as described above and incubated at 37°C under a 5% CO^2 atmosphere. A day before the experiment, cells were seeded at a density of 2.2 × 10^5 cells in 2 ml of growth media per a single well of a 6-well plate (**Figure 2.5**). The list of all cell types used is shown in **Table 2.1.**

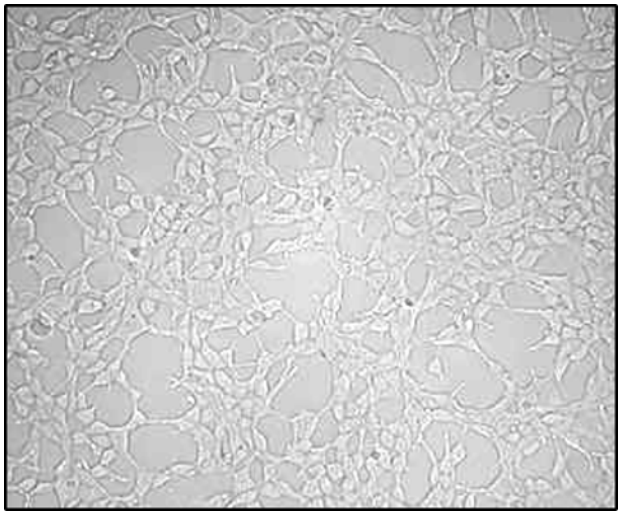


Figure 2.5. Human kidney cell line (HEK293).

Cells were cultured for 2-4 days in Dulbecco's modified Eagle's medium (DMEM) supplemented with 10% (v/v) FBS, and 1% (v/v) P/S.

Table 2.1. Cell types used to study 11β-HSD1 enzyme activity showing the cell source, seeding density, media used, type of well plate, passage number, and the incubation time of inactive cortisol.

Cell type	Source	Seeding density	Culture media	Culture Plates	Passage number	Time of incubation
C2C12	Mouse myoblast	1 x 10^5	**Proliferation media:** DMEM high glucose + 10% fetal bovine serum + P/S. **Differentiation media:** DMEM high glucose + 10% horse serum + P/S	12 well Plate	16-20	20 minutes
U2OS	Human Osteosarcoma cell line	1 x 10^5	DMEM high glucose +10% FBS + P/S.	12 well Plate	8-14	3,5,7 hours
HEK293	Human embryonic kidney	1 x 10^5	Minimum Essential Media (MEM) with Earl's salts + 10% FBS + P/S + glutamine	12 well Plate	7-12	3,5,7 hours
HepG2	Hepatocellular carcinoma cell line	5 x 10^4	Minimum Essential Media (MEM) with Earl's salts + 10% FBS + P/S + glutamine	12 well Plate	14-20	14,24 hours
HDFn	Human dermal fibroblast	1 x 10^5	DMEM high glucose +10% FBS + P/S.	6 well Plate	2-8	12 hours

2.2. Modulation of NAD with FK866 and NR

Twenty-four hours after plating (HepG2, HEK293, and HDFn) cells and after 6-7 days of C2C12 myotubes differentiation, cells were left as a control (PBS only) or treated with FK866 (Nampt inhibitor; Sigma-Aldrich, UK) at concentrations of 100 nM for 48 hours. This concentration was adequate to deplete NAD^+ as indicated by the dose-response curve published by (Tan et al., 2015). NR (Chromadex, US) was prepared by adding 28mg of NR powder to 1 ml of H2O (dd) and sterile-filtered. 5 ul of NR was added to the cell for a final concentration of 0.5 mM. This concentration was proven to elevate NAD^+ levels in the cells (Cantó et al., 2012). Dr. Rachel Fletcher in our group showed that the viability of C2C12 myotubes was intact in response to treatment with FK866 (100 nM; 24 hours) and NR (0.5 mM; 24 hours) (Fletcher, 2017).

2.3. NAD^+/NADH assay

NAD^+/NADH concentrations were determined using a colorimetric NAD^+/NADH quantification kit (Bio Vision, California, USA). The assay works on the principle of a cycling enzyme that catalyses the conversion of NAD^+ to NADH before measuring NADH levels. After adding the NADH developer reagent, sample colour intensity is directly proportional to the total NADH available (**Figure 2.6)**. To determine total NAD^+/NADH levels, a cycling enzyme was added to unmodified samples. In contrast, NADH levels are determined by heating the samples to 60 °C for 30 minutes before cycling, to destroy all NAD^+, while NADH remains intact. NAD^+ levels are subsequently measured by subtracting the NADH value from the total NAD^+/NADH value.

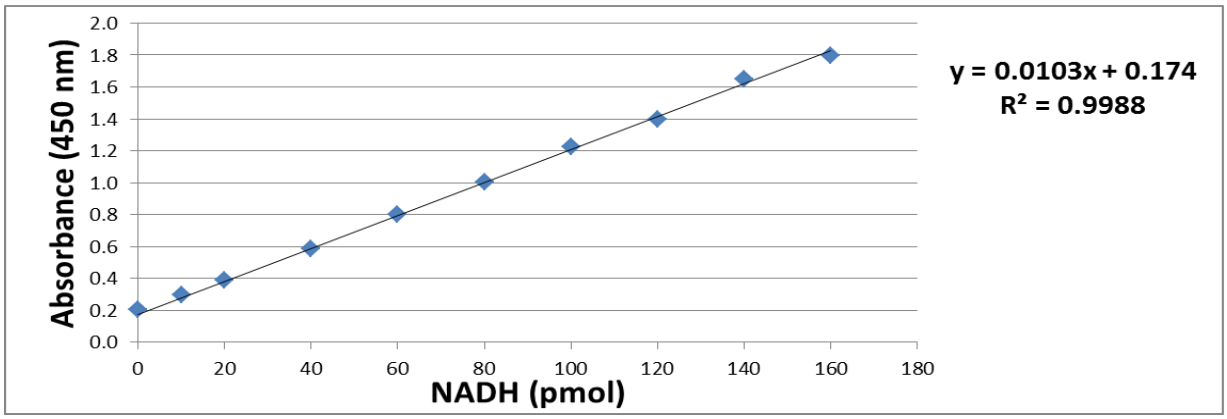


Figure 2.6. Example of standard NADH curve for NAD^+/NADH quantification.

In 6 well culture plates, cells were washed with PBS, then 400 µl of NAD^+/NADH extraction buffer was added and the cells were scraped and transferred to a new microcentrifuge tube. Samples were freeze-thawed twice on dry ice to confirm lysis before being vortexed for 5 seconds and centrifuged at 13, 000 rpm for 5 minutes at 4 °C. The supernatant was then transferred to a new microcentrifuge tube and used to measure the total NAD, and 200 µl was used to measure NADH concentration. To decompose the NAD within the sample, the NADH samples were heated for 30 minutes at 60 °C. 50 µl of total NAD and NADH for each sample in duplicate was loaded onto a clear bottomed 96 well plate, along with a known concentration of NADH standards from which the standard curve was calculated.

The NAD^+ cycling enzyme was reconstituted and 98 µl cycling buffer and 2 µl enzyme were loaded per sample. Before the addition of 10 µl NADH developer per well, the plate was incubated at room temperature for 10 minutes to allow NAD^+ fully cycle to NADH.

Data was calculated according to the slope of the NADH standard curve from the known standard samples. The concentrations of the unknown samples were indicated from the standard curve using their absorbance. The value for NAD^+ was measured by subtracting NADH measurement from the total NAD(H) concentration and then the NAD^+/NADH ratio was calculated. The visualization of the colored probe was read at 450 nm using Victor3 1420 multi-label counter (PerkinElmer, UK). (**Figure 2.7**)**.** illustrates the measurement of NAD^+/NADH using the colorimetric quantification kit. All data were normalized to the protein concentration calculated using a Bio-Rad protein assay **(as described in section 2.5).**

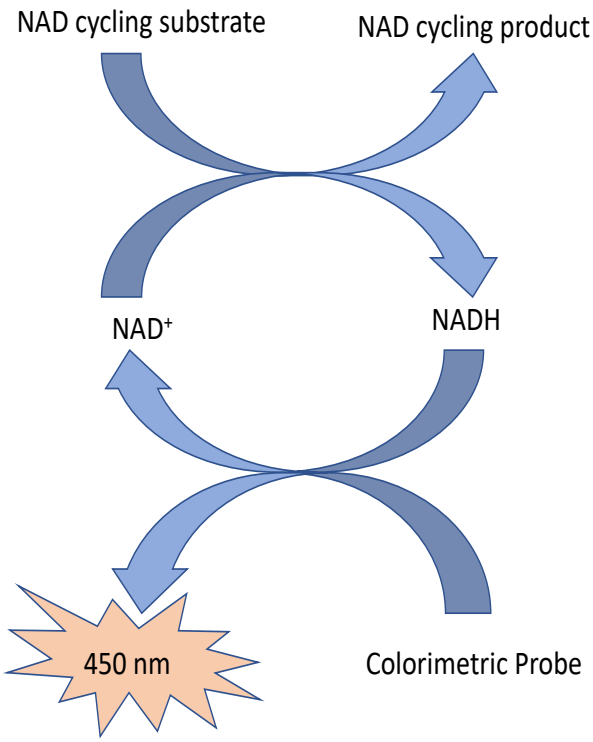


Figure 2.7. NAD⁺ quantification assay.

NAD and NADH were quantified using the NAD⁺ cycling assay kit through the colorimetric detection of the conversion of NAD⁺ to NADH. The visualization of the colored probe was read at 450 nm.

2.4. Cell viability assay (AlamarBlue) The AlamarBlue cell viability assay utilizes resazurin as a cell-permeable, blue dye indicator of cell viability. It was described by (O'Brien et al., 2000) as an alternative to the MTT viability assay (3-(4,5-dimethylthiazol-2-yl)-2,5-diphenyl-tetrazolium bromide) as it is a non-toxic reagent. The AlamarBlue assay provides a quantitative measurement of cell viability. In contrast, cells are metabolically active, and the cytotoxic effects of reagents used for cell treatment and cell transfection with plasmid DNA can be assessed. AlamarBlue were added to cells seeded 4 h on a 96

well plate and incubated for 1-4 h in the appropriate condition (37 °C, 5 % CO_2). The number of living cells indicates the intensity of the pink fluorescence produced by the viable cells measured at Ex 530-560- Em 590 as shown in **Figure 2.8.**

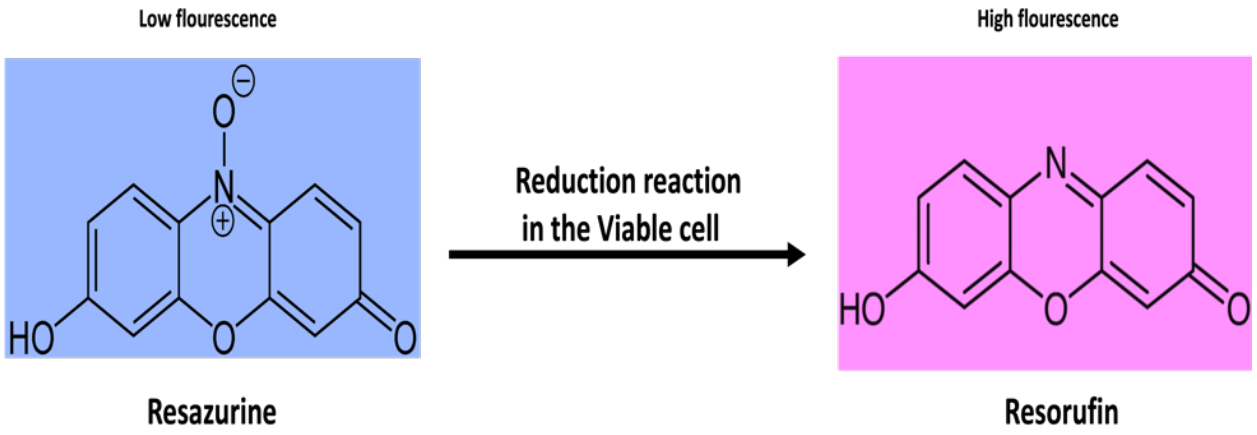


Figure 2.8. Cell viability assay (AlamarBlue).

Viable cells can reduce the low fluorescence resazurin to higher intensity pink fluorescence measured at Ex 530-560- Em 590 by Victor3 1420 multi-label counter (PerkinElmer, UK).

2.5. Protein extraction and determination

Quantification of protein concentration was calculated using the DC™ protein assay kit (BioRAD, UK). For 6 well plates, cells were washed with cold PBS and 60 µl of RIPA buffer (1 mM EDTA, 150 mM NaCl, 0.25% SDS, 1% NP40, 50 mM Tris pH 7.4) was added to each well and the cells were scraped using a cell scraper. The cell lysate was then transferred into fresh microcentrifuge tubes and centrifuged at 14, 000g for 15 minutes at

4°C. The soluble protein supernatant was transferred to new microcentrifuge tubes and stored at -80°C for further protein analysis.

Protein concentration was assessed according to the manufacturer protocol (BioRad, UK) in a 96-well plate. Bovine serum albumin (BSA) was used as a standard (0-2 mg/ml of protein) in the same buffer used for the protein extraction. 25 ml of solution A (alkaline copper tartrate) (with 20 µl of solution S per ml of solution A) was added followed by 200 µl of solution B (Folin reagent). After the solutions and the samples were added, the plate was incubated at room temperature for 30 minutes and the absorbance read at 562 nm on a Victor3 1420 multi-label counter (PerkinElmer, UK). Subsequently, the protein concentration was calculated from the slope of the standard curve.

2.6. Western blotting

To start making the gel for western blotting, 7.5% acrylamide was prepared using an SDS-PAGE kit (BioRad, UK) using precision plus protein as a standard (BioRad, UK) **Tables 2.2 A, B**. Protein samples were made up to 60 ug and mixed with the appropriate volume of 4x Laemmli buffer and denatured by heating at 90°C for 5 minutes. Samples were loaded in the gel and ran at 100 V for 60 minutes and then transferred onto nitrocellulose membranes using the iBlot (Invitrogen, UK) for 7 minutes. In the wet transfer technique, the membranes were placed in the tank with transferring buffer and run at 140 mA for 90 minutes. To check for the efficiency of protein transfer, membranes were incubated with Ponceau staining solution and gently agitated for 2 minutes, and then washed with water to visualize the protein bands. The membranes were then blocked in 10 mL of blocking buffer containing 1 g BSA in 20 ml of TBST and gently agitated at room temperature for 1

hour. Then, membranes were rinsed 3 times with washing buffer for 10 min and incubated overnight in the primary antibody at 4°C. On the following day, membranes were washed 3 times for 10 minutes and incubated with the secondary antibody for 2 hours at room temperature, followed by washing 3 times for 10 minutes. The list of primary and secondary antibodies used are shown in **Tables 2.3 A, B**. To detect antigen-antibody complexes, enhanced chemiluminescence reagent (Immobilon® Western, USA) was used with a ratio of 50:50 of substance A (luminol reagent) and substance B (peroxide solution) and agitated for 1 minute. Finally, images were taken using a ChemiDoc MP imager (Bio-Rad, UK) and the exposure time was automated by the machine.

Table 2.2. Concentrations of the reagents used to prepare separation and stacking gels.

Separation Gel: A

Reagent	**concentration**
Final acrylamide %	**7.5%**
H_2O (mL)	4.9
4X Tris-SDS pH 8.8 (mL)	2.5
30% Acrylamide solution (mL) (fridge)	2.5
10% APS (µL)	100
TEMED (µL) (lab)	10-16

Stacking gel: B

Reagent	concentration
Final acrylamide %	**5%**
H_2O (mL)	4.67
4X Tris-SDS pH 6.8 (mL)	2
30% Acrylamide solution (mL)	1.33
10% APS (µL)	65
TEMED (µL)	12

Table 2.3 List of primary and secondary antibody used to detect protein expression.

A: Primary antibodies.

NAME	Primary antibody	Dilution	supplier
Myc	Rabbit monoclonal antibody	1:4000	Santa Cruz Biotech, (USA)
PAR	Anti-PAR antibody Clone 10H	1;5000	Sigma Aldrich, (USA).
Tubulin	mouse monoclonal antibody	1:1000	Santa Cruz Biotech, (USA)

B: Secondary antibodies.

Secondary Antibody	Dilution	Supplier
Anti-Rabbit HRP	1:10000	Dako (Denmark)
Anti-mouse HRP	1:10000	Dako (Denmark)

2.7. Bacterial transformation

Competent *E.coli* DH5α (Invitrogen, UK) were thawed on ice for 20 mins to maintain the cell membrane permeability for efficient plasmid uptake. 50 ul of competent *E.coli* were mixed with 5 µl of plasmid DNA in a microcentrifuge tube and mixed gently by flicking the tube then incubated on ice for 20 minutes. The mix was then placed at 42˚C for 45 seconds (heat shock) to allow DNA entry through the cell membrane and then placed back on the ice for 2 minutes. The mixture was then spread on a 10 cm LB agar plate containing Ampicillin using a sterile inoculation loop and incubated at 37˚overnight. After 24-48h incubation, a single colony was picked using a sterile pipette tip and dropped in a 5 ml falcon tube with LB media+Ampicillin and incubated at 37˚C for 8 hours in a shaking incubator at 200-250 rpm. After incubation, bacterial growth was confirmed by checking the cloudy haze appearance of the media, and 5 ml of culture media was added to 50 ml of LB media in a sterile conical flask and incubated at 37˚C in a shaking incubator at 200-250 rpm overnight. The reagents used to make LB medium is listed in **Table 2.4.**

Table 2.4. Concentrations of the reagents used to prepare LB medium.

Reagent	concentration
NaCL	4 g
Tryptone	4 g
Yeast extract)	2 g
ddH_2O	400 ml

2.8. RNA extraction

TRIzol reagent (Sigma- Aldrich, UK) was used for RNA extraction because it effectively denatures proteins while maintaining RNA integrity. Cells were washed with PBS on ice after removing all culture media. In 6 well plates, 500 ul of TRIzol reagent was added per well, and cells were incubated for 5 minutes at room temperature (RT). The cell lysates were then scraped and transferred into a fresh microcentrifuge tube and 100ml of chloroform was added and shaken for 15 seconds at RT, following which they were incubated at RT for 15 minutes. The tubes were then centrifuged at 4^{o}C at 12,000g for 10 minutes. The aqueous phase containing the nucleic acid was then transferred to a new microcentrifuge tube for precipitation. 250ul of isopropanol per ml of TRIzol was added and tubes were mixed by inverting 3-5 times and placed at -20^{o}C 1-2 hours. After spinning the tubes at 12,000g at 4^{o}C for 10 minutes, the supernatant was removed carefully not to disturb the pellet. 500 µl of 75 % ethanol/ml of TRIzol reagent was added to wash the pellet and centrifuged at 12,000g at 4^{o}C for 5 minutes. The ethanol supernatant was

removed and the RNA pellet was left to dry for 10 minutes and then re-suspended in 30 ul of Nuclease-free water and put on a heating block at 55^{o}C to allow the pellet to dissolve.

2.9. RNA quantification

The RNA was measured using NanoDrop Spectrophotometer (ThermoFisher Scientific, UK). To start the quantification, 1 µl of nuclease-free water (NFW) was added to the Nanodrop arm and then 1 µl of samples was measured and the arm was cleaned in between the samples. The absorbance of 1.5 µl of RNA at 260nm and 280nm was considered a good RNA quality for use. RNA was diluted to give a final concentration of 1 µg in 10 µl of NFW.

2.10. Reverse transcription (RT) and polymerase chain reaction (PCR)

To produce a complementary strand of DNA (cDNA), the RNA undergoes RT and PCR using a High Capacity cDNA Reverse Transcription Kit (Applied Biosystems, USA). To generate a 2x RT master mix the following reagents were mixed in a microcentrifuge tube per sample **Table 2.5.**

Table 2.5. Reagents and concentration used for reverse transcription reaction.

Reagent	Volume per sample
RT Buffer	2 µl
10X Random Primer	2 µl
Multiscribe Reverse Transcriptase	1 µl
dNTP mix	0.8 µl
Nuclease-free H2O	2.3 µl

10µl of 2x RT master mix was added to 1 µg of RNA in 10 µl of NFW giving a final volume of 20µl. The 20µl samples were loaded onto a PCR thermal cycler (Applied Biosystems, UK), and the program ran as follows: 25 ºC for 10 mins, 37 ºC for 120 mins, 85 ºC for 5 mins. Samples were then stored in a -80 ºC freezer.

2.11. Real-Time PCR

All reactions were run in duplicate in 384 well plates by adding: 5 µL of 2x Master Mix, 100 ng of cDNA, 0.5µL of either gene of interest or housekeeping gene (GAPDH), and

NFW to a final volume of 10 µL per well. Plates were sealed with Oxygen Ultra Clear Sealing Film (Corning, UK) and finally run on a 7500 real-time PCR system (Life Technologies, UK). The final data was expressed as Ct values and utilized to calculate ∆Ct values (Ct of the gene of interest – Ct of housekeeping gene). All the ΔCt values were converted to arbitrary units by this equation (AU = 1000x2-ΔCt).

2.12. Gel electrophoresis.

The quality of the RNA was assessed by gel electrophoresis on a 1% agarose gel with GelRed Nucleic acid Gel Stain. The gel was visualised under a UV light in a G:Box gel documentation system (Syngene, UK). RNA separates in the gel according to its molecular mass and the resultant bands were visualised under UV light.

2.13. 11β-Hydroxysteroid dehydrogenase 1 (11β-HSD1) activity

11β-HSD1 activity was measured using thin layer chromatography (TLC). This technique is based on a separation principle to isolate nonvolatile mixtures on a sheet of aluminum foil coated with a thin layer of adsorbent material. The separation depends on the affinity of compounds that move in the mobile phase to the surface of the stationary phase. At the end of separation, the individual compounds show as a spot on the TLC plate at variable locations.

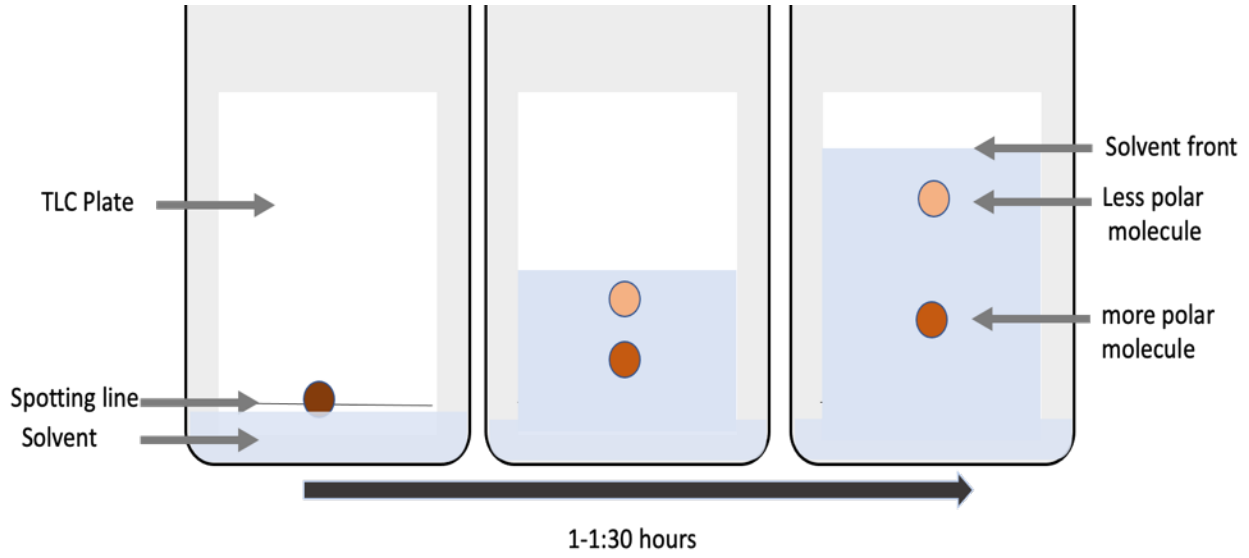


Figure 2.9. Steps of thin layer chromatography.

The TLC plate was placed in a glass beaker with the solvent (chloroform 92% and ethanol 8%) to separate the compounds based on their relative affinity in a mobile phase.

At the desired confluence, cells were washed once with PBS and a mix of 1 ml of serum-free media + 2 ul (100 nM) 20000 cpm/reaction of radioactive cortisone (or ^{3}H -11DHC in rodents cell line) + 1 ul of non-radiolabeled cortisone/11DHC (GE Healthcare, BUCKS, UK) was added to each well of 6 well plates. The plates were incubated at 37ºC under a 5% CO^{2} atmosphere for different times depending on each cell enzyme activity **(Figure 2.9)**. At the end of the incubation time, the mix's media was transferred to the corresponding glass tubes, and the plates were stored at -20 ^{0}C for further protein analysis. To extract steroids from the samples, 5ml of dichloromethane was added to each glass tube and rocked gently on a rocking machine for at least 5 minutes. Then, the tubes were centrifuged at room temperature at 1000 g for 15 minutes to separate the aqueous phase from the organic phase. The top layer (aqueous layer) and the protein layer were

aspirated using suction in the fume hood. Tubes with the bottom layer (organic) were placed under the air-blowing concentrator (Techne, New Jersey, US) set at 55ºC for 1 hour to allow the evaporation of dichloromethane. The precipitated steroids were re-suspended by adding 70ul of dichloromethane and vortexed for 15 seconds to get all steroids in the glass tube. Silica-coated thin layer chromatography (TLC) plates (Thermofisher, UK) were labelled by a pencil as follows; 1.5 cm apart horizontally and 5 cm from the bottoms. Using a glass Pasteur pipette, each steroid sample was spotted onto a corresponding spot of silica plate. In each spot, was added 1ul of cold E (cortisone) and F (cortisol) (in case of human cell lines; HepG2, HDFn, HEK293, and U2OS) or cold A (11-DHC) and B (corticosterone) (in rodent cells; C2C12) to determine the positions of non-radioactive steroids under UV light. Silica plates were then placed in the TLC tank prepared with 200ml of chloroform and absolute ethanol (92:8) as a mobile phase for 1.5 hours to separate steroids. Radioactivity of the corresponding compound was measured using Bioscan 200, imaging scanner (Lap Logic, Sheffield, UK) to scan the plates at a reading of 45 minutes per spot. The activity of 11 β-HSD1 was assessed by measuring the conversion percentage of E to F (or A to B in rodents cell lines) using individual peak counts (**Figure 2.10**)**.** 11β-HSD 1 activity was expressed as follows:

(B) area count / (A+B) area counts *100 per mg of protein per hour (pmol/mg/h) or (E) area count /(E+F) area count *100 per mg of protein per hour (pmol/mg/h).

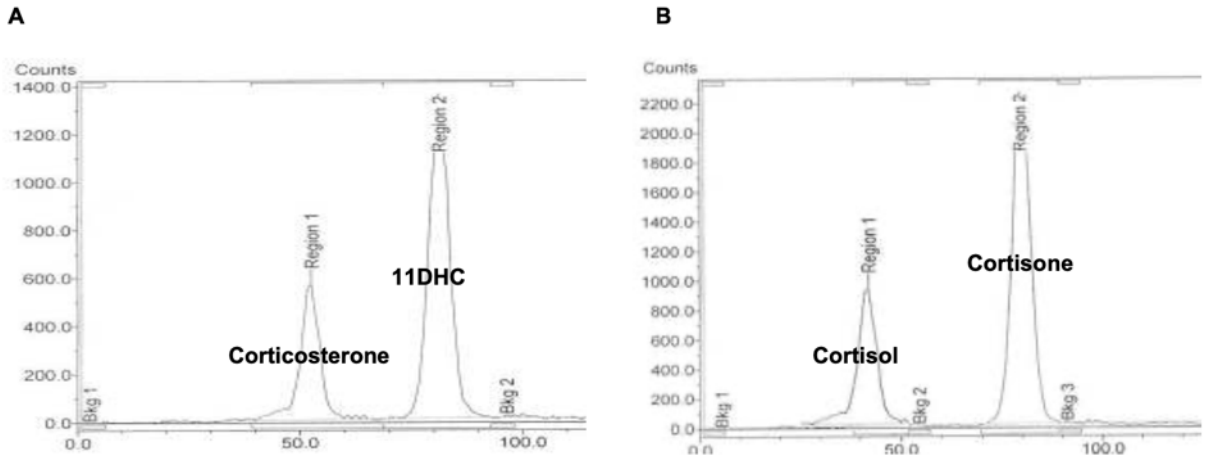


Figure 2.10. Illustrative Bioscan traces of 11β-HSD1 oxo-reductase activity in (A) mouse cell line (C2C12) and (B) human cell lines (HepG2, Dermal fibroblasts, and HEK293).

2.13.1. Production of ^{3}H-11DHC.

Tritiated 11-dehydrocorticosterone (^{3}H-11DHC) is not commercially available unlike tritiated corticosterone (^{3}H-corticosterone), therefore, tritiated corticosterone [^{3}H-corticosterone (GE Healthcare, UK) was utilized to generate ^{3}H-11DHC in a conversion reaction of 11β-HSD2 dehydrogenase activity using mouse placenta. In a glass tube, 20µl of ^{3}H-corticosterone (1mCi/mL) was incubated with 250 µg of homogenized mouse placenta in 500µl of 0.1M phosphate buffer (pH7.4), with 500 µM NAD^{+}. The conversion was measured after overnight incubation in a water bath at 37°C. To extract steroids 5mL of dichloromethane was added and vortexed in the tubes for 10 seconds. Organic and aqueous phases were separated by centrifugation for 10 minutes at 1000 g. The aqueous phase was aspirated off with a Pasteur pipette and the organic phase containing the steroids was evaporated at 55°C using an air-blowing sample concentrator (Techne, New Jersey, US). Steroids were resuspended by adding 10 µl of dichloromethane and spotted

onto a single point of a silica-coated thin layer chromatography plate (Thermo Fisher, UK) using a Pasteur pipette. To avoid contamination, 11-dehydrocorticosterone and unlabeled standards of corticosterone were spotted on the silica plate 5cm from the spotted labelled steroids. Steroids were then separated by thin layer chromatography using 200mL of chloroform: ethanol (ratio of 92:8) as the mobile phase for 1.5 hours.

To establish the position of ^{3}H-11DHC, the silica plates were read using a Bioscan 200 Imaging Scanner (Lab Logic, UK). The silica at the corresponding position to ^{3}H-11DHC was pencil marked and then scraped into a glass test tube and eluted in 1000mL of ethanol overnight at 4°C. The eluted ^{3}H-11DHC and silica were separated by centrifugation at 1000 g for 5 minutes. Radioactivity of 3H-11DHC was determined by spotting 2µl of stock by thin layer chromatography and the number of counts was determined using the Bioscan 200 Imaging Scanner. The stock was then diluted in ethanol to give ~1000 counts/µl.

2.14. Transfection of HepG2 and C2C12

Cells were seeded in 6 well plates at the optimum density (between 1.1 to 2.2 *10^{5} cells per well as specified in chapter 4) and incubated at 37°C under 5% CO2. After 24 hours, cells were transfected using lipofectamine (Lipofectamine ® 3000, Invitrogen, UK) as follows **Table 2.6**:

Table 2.6. Lipofectamine protocol for cell transfection in 6 well plates.

Reagent	Volume
Opti-MEM™ I medium	250 µL
Lipofectamine	3.25 µL
P3000™ reagent	0.5 µL
DNA amount concentration should be (0.5–5 µg/µL)	250 ng

After 48 hours, transfection was confirmed by visualization of GFP expression by fluorescence microscopy. Cells were then harvested for western blotting, gene expression, and protein determination. For 11β-HSD1 activity, the media was changed 36 hours after transfection with media containing (H^3-11DHC in C2C12), or (H^3-cortisone in HepG2), and the enzyme activity was measured 48 hours after transfection as described in **section 2.12.**

The plasmids used for transfection were kindly given by Dr Oyvind Stromland. Cells were transfected with constructs targeting ER (ER-PARP1cd and ER-EGFP) **Figures** (**2.11 and 2.12)** or mitochondria (Mito-PARP1cd and Mito-EGFP) **Figures (2.13 and 2.14)**. The EGFP plasmids were used as controls in our experiments, as they contain everything in the PARP plasmid except the PARP1 catalytic domain.

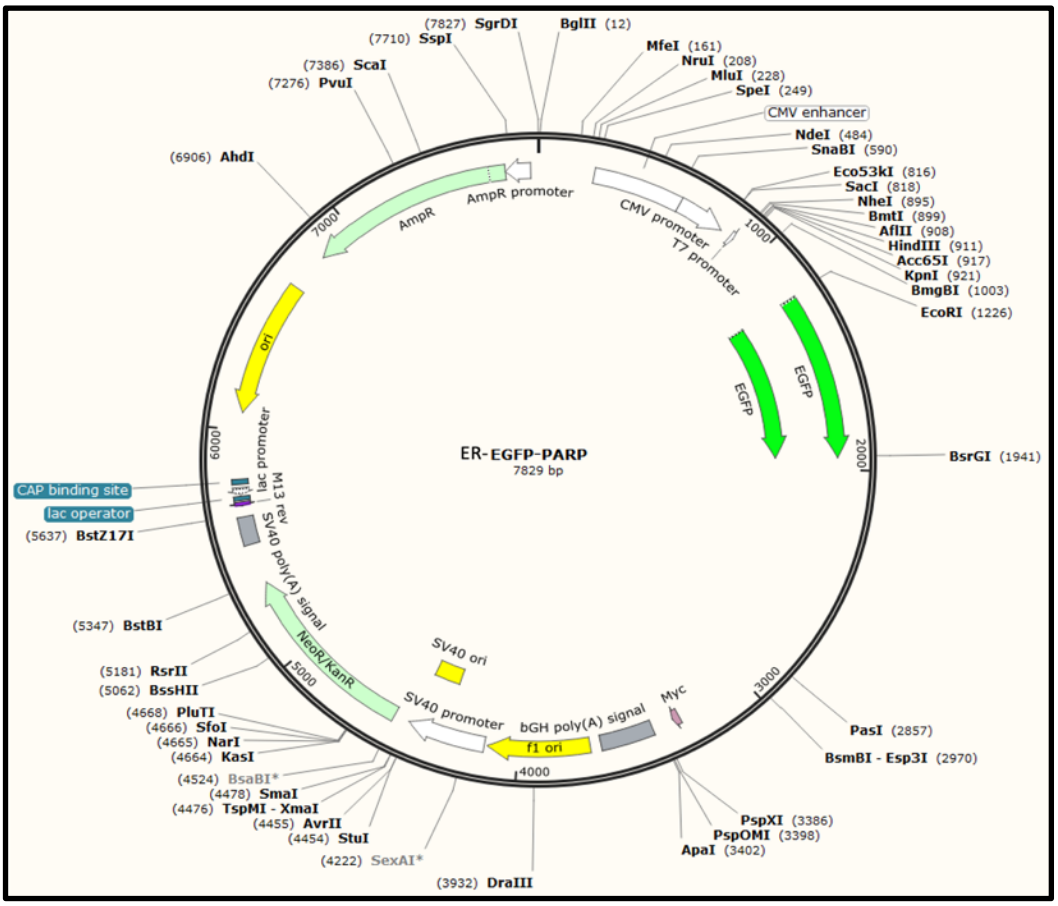


Figure 2.11. Graphic illustration of ER-PARP plasmid map displaying the restriction enzyme sites and the main components of the sequence.

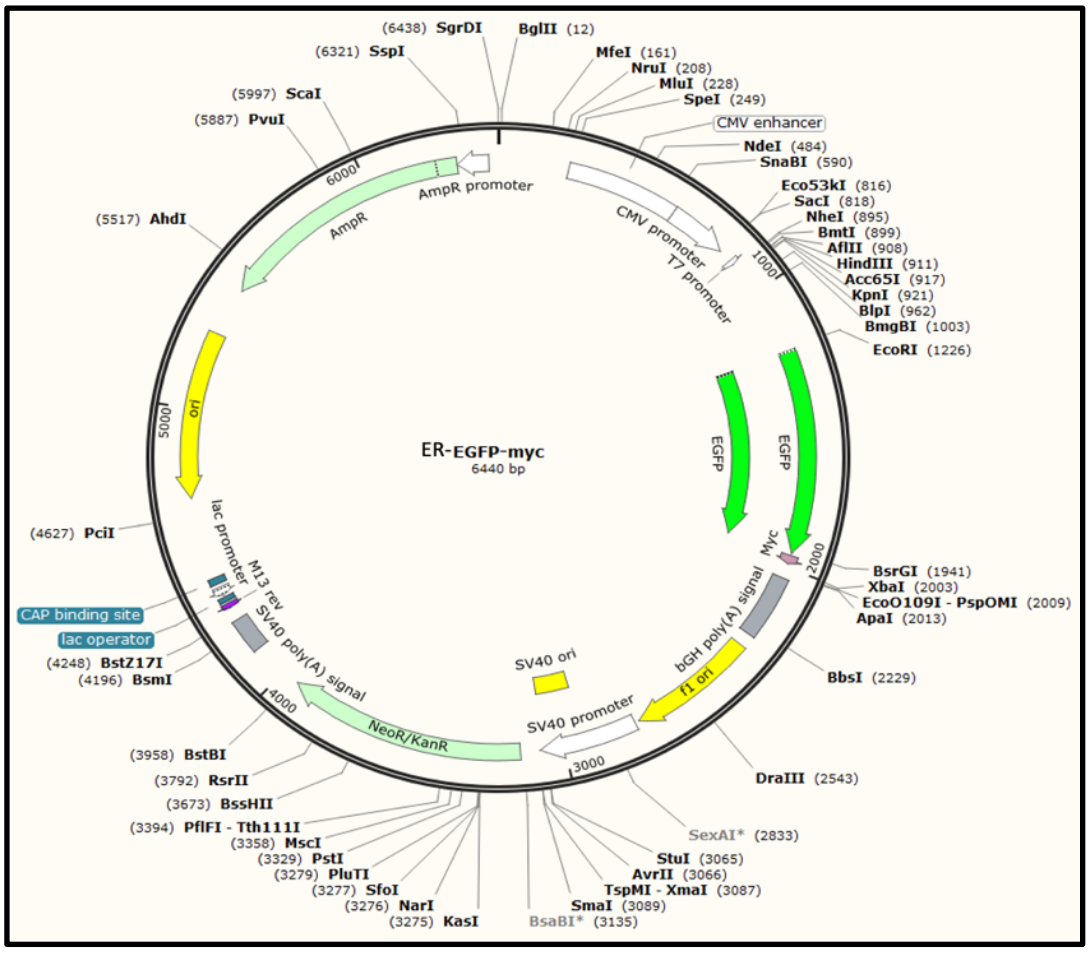


Figure 2.12 Graphic illustration of ER-EGFP plasmid map displaying the restriction enzyme sites and the main components of the sequence.

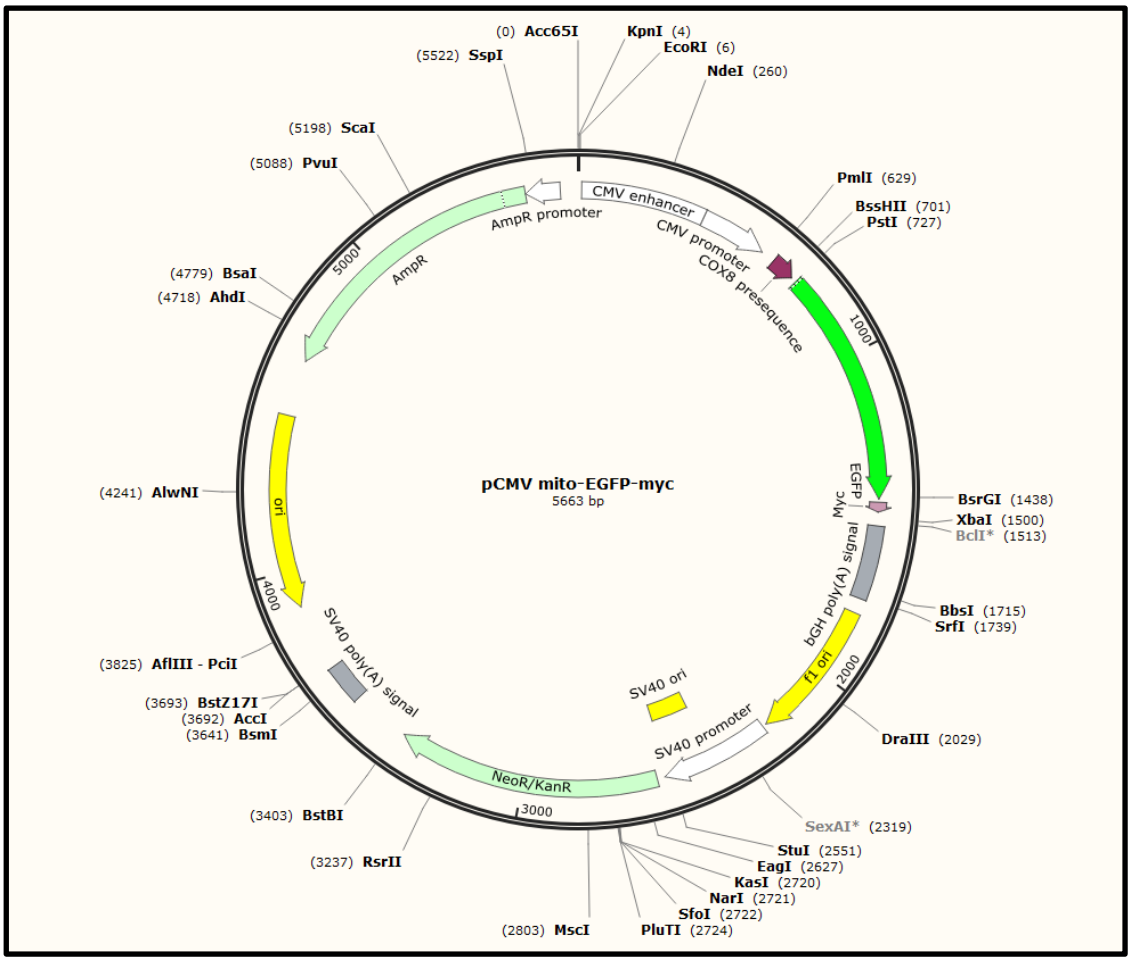


Figure 2.13. Graphic illustration of Mito-EGFP plasmid map displaying the restriction enzyme sites and the main components of the sequence.

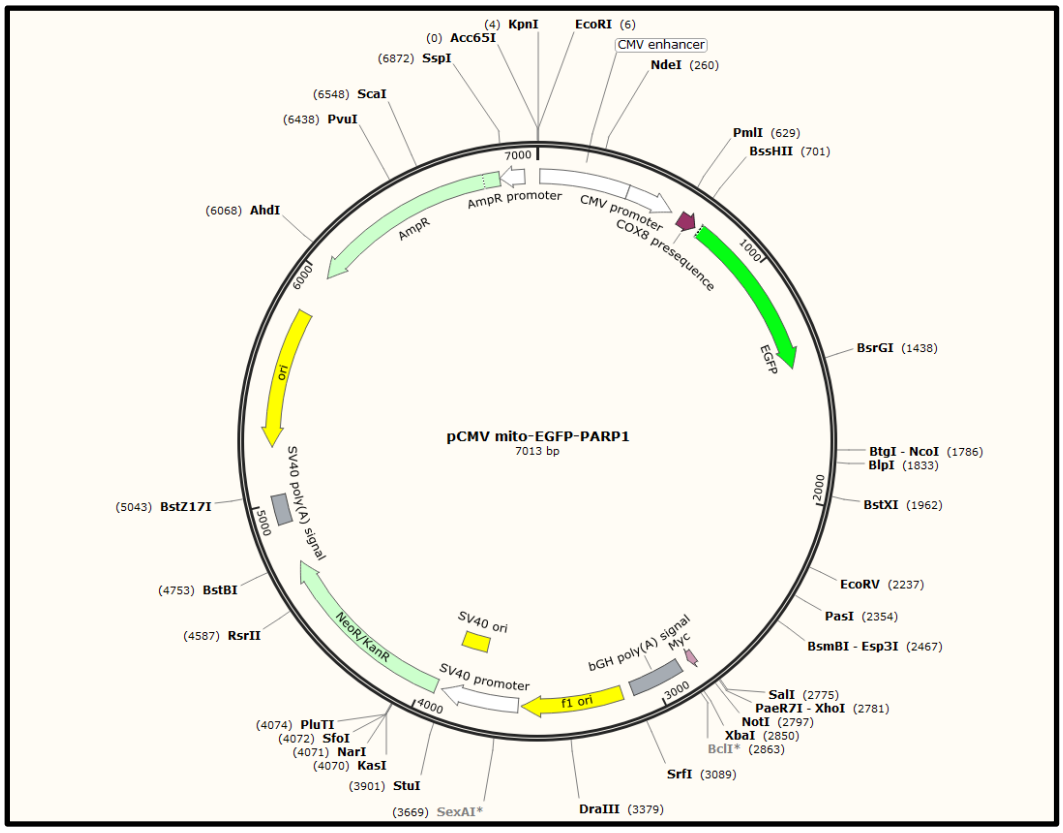


Figure 2.14. Graphic illustration of Mito-PARP plasmid map displaying the restriction enzyme sites and the main components of the sequence.

2.15. Statistical analysis.

All statistical analyses have been carried out using the GraphPad™ Prism version 9 software. Ordinary one-way ANOVA analysis has been conducted with the assumption of equal stadnard deviations and Dunnett's multiple comparison test was used. Differences were considered statistically significant, when $p<0.05$. Statistical significance was shown by * $p<0.05$, ** $p<0.01$, *** $p<0.001$, **** $p<0.0001$, when comparing to the control group and by $^{\#}$ $p<0.05$, $^{\#\#}$ $p<0.01$, $^{\#\#\#}$ $p<0.001$, $^{\#\#\#\#}$ $p<0.0001$, when comparing to an FK866-treated experimental group. Experiments were repeated at least 3 times, number of independent experiments is stated in the respective figure legend.

Chapter 3

Targeting NAD^+ metabolism to modulate 11β-Hydroxysteroid dehydrogenase type1 activity in the ER of mouse and human cells

3.1 Introduction

Skeletal muscle is the largest organ in the human body; it accounts for approximately 50% of the total body mass. Its main functions in the body are mechanical movement and shaping of the body. In metabolism, the skeletal muscle is the primary site of carbohydrate and fatty acid metabolism and serves as a reservoir of amino acids (Wolfe, 2006). Skeletal muscle has a high plasticity, which can adapt to changes in structural and metabolic stress conditions (i.e., exercise, hypoxia, and nutrition) (Smith and Muscat, 2005).

Sarcopenia is the most common pathological condition associated with skeletal muscle NAD^+ homeostasis, energy metabolism, and aging. It is characterized by a progressive loss of skeletal muscle mass and mechanical functions that can impair daily life activity. In addition, sarcopenia increases the risk of metabolic conditions such as osteoporosis, type 2 diabetes mellitus, and the metabolic syndrome (Kim and Choi, 2013). The phenotype of sarcopenia is associated with excess GC levels in patients with Cushing syndrome (Morgan et al., 2014). Furthermore, the rate of protein synthesis in a C2C12 skeletal muscle model is reduced due to dexamethasone treatment (Wang et al., 2016). These findings suggest the importance of GCs regulation in skeletal muscle and the risk of protein degradation and muscle wasting.

The liver is a vital organ that is central to many physiological body functions. Therefore, it represents an ideal model for investigating the biochemical and physiological NAD(H) and NADP(H) metabolism (Kendrick et al., 2011). The liver undergoes enormous metabolic modifications during feeding and fasting. It is the main organ responsible for detoxifying chemicals and regulating the body's metabolic activity, such as gluconeogenesis,

synthesis of amino acids, and lipoprotein synthesis. Most metabolic actions are linked to NAD(H) or NADP(H). For example, β-hydroxybutyrate dehydrogenase uses NAD(H) to convert ketone bodies during fasting, while postprandial NADPH is used as a cofactor for lipid and cholesterol synthesis (Kersten, 1999). The metabolism of alcohol occurs mainly within the liver and produces NADH within the mitochondria and cytosol (Isselbacher and Greenberger, 1964).

Glucocorticoids have many actions that increase lipid accumulation in the liver and interfere with tissue repair contributing to the pathogenesis of fibrosis (Fede et al., 2012). In addition, a previous study in mice on a high-fat diet showed that 11 β-HSD1 deficiency protects from liver steatosis and increases the risk of dyslipidemia in transgenic 11 β-HSD1 overexpressing mice (Morton et al., 2001, Paterson et al., 2004). Therefore, it is important to understand the mechanism that controls ER redox homeostasis and 11 β-HSD1 enzyme activity in metabolically active tissues such as muscle and liver.

The aim of my first results chapter is to study ER-cytosol NAD/NAD precursor cross talk. Firstly, I will investigate the capacity of FK866 and NR to modulate the level of NAD and NADH in the cytosol. Secondly, I will examine the impact of NAD(H) manipulation on the oxo-reductase activity of 11β-HSD1 enzyme as a biosensor of ER NAD(P)(H) availability. Thirdly, I will examine the effect of NAD^+ manipulation on the 11β-HSD1 dehydrogenase activity in a H6PDH knock out cell model. Finally, we aim to examine the generalizability of 11β-HSD1 modulation by FK866 and NR in multiple cell types (mouse myotubes cell line **C2C12**, primary mouse myotubes, human hepatocellular carcinoma cell line **HepG2**, human dermal fibroblasts **HDFn**, and human kidney cell line **HEK293**).

3.2. Results

3.2.1. NAD^+ /NADH manipulation by FK866 and NR in C2C12 mouse myotubes.

To examine ER-cytosol NAD^+ cross-talk in C2C12 myotubes, we examined NAD^+ manipulation by NAMPT inhibitor (FK866) and NAD^+ precursor (NR). As we expected, the availability of NAD^+ increased after administration of NR (0.5mM; 48h), while FK866 (100nM; 48h) markedly depleted NAD^+. Administration of FK866 co-treated with NR rescued NAD^+, as shown in (**Figure 3.1 (A)**)**.** Similar results were also shown for NADH, suggesting that NR can bypass the effects of NAMPT inhibition by FK866 (**Figure 3.1 (B)**).

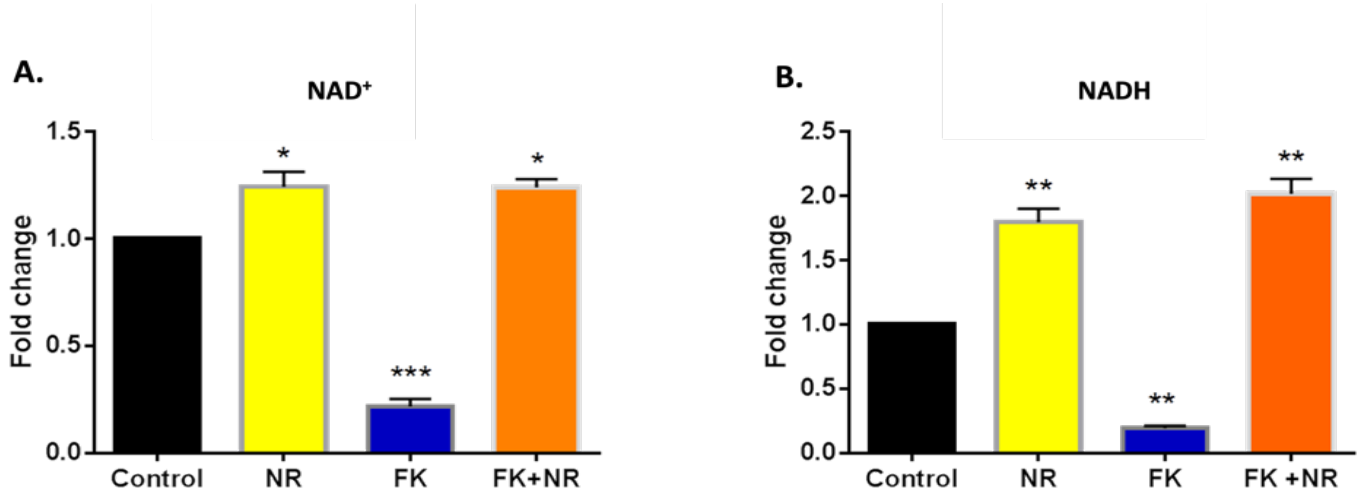


Figure 3.1. NAD⁺ manipulation with FK866 and NR in differentiated C2C12 myotubes.

The availability of **A.** NAD⁺ and **B.** NADH expressed as fold change. Control (no treatment), FK866 (100nM; 48h), NR (0.5mM; 48h), FK866+NR (48h). Results of N=3 independent experiments are shown as fold change**,** for which values were referred to controls (set =1). Statistically significant differences were designated by * ($p<0.05$), *** ($p<0.001$), when compared to control and $^{\#}$ ($p<0.05$), $^{\#\#}$ ($p<0.01$), when compared to FK866-treated cells.

3.2.2. The effect of NAD^+/NADH manipulation on 11β-HSD1 enzyme activity in C2C12 myotubes.

We then examined our hypothesis that manipulating NAD^+ availability in the cytosol could affect ER NAD^+ and, therefore, the NADPH-dependent enzyme 11β-HSD1. After 24 hours of FK866 and NR treatment, no change was seen in 11β-HSD1 enzyme activity; however, more prolonged exposure of C2C12 myotubes to FK866 depleted the enzyme activity, which was rescued when co-administrated with NR for 48 hours. Interestingly, 24 hours of NR treatment did not affect 11β-HSD1 activity compared to the control (**Figure 3.2**).

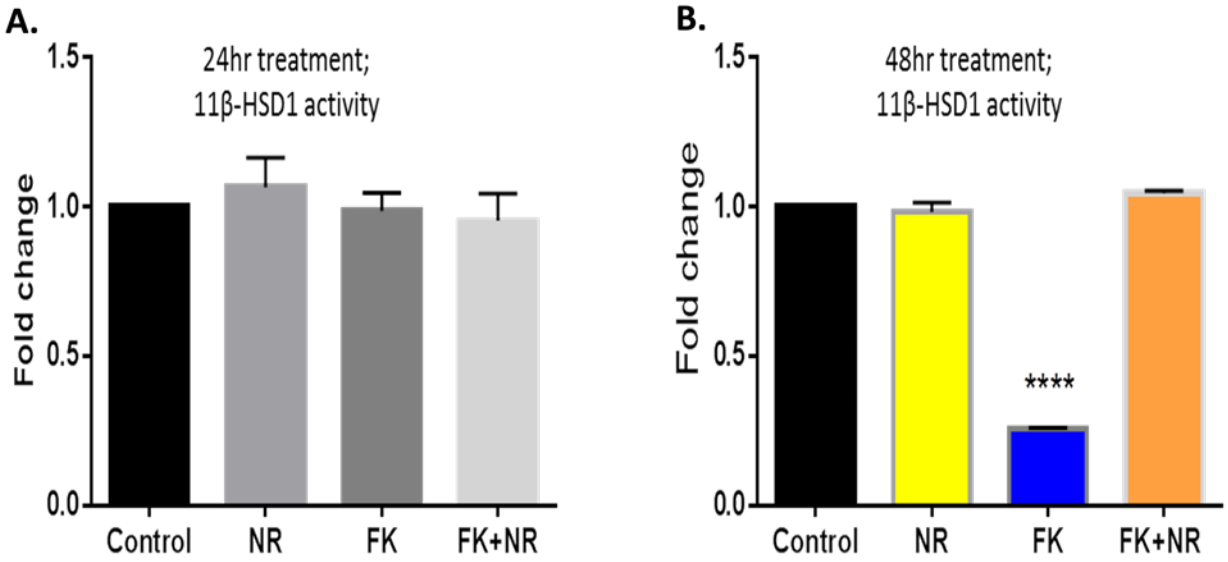


Figure 3.2. 11β-HSD1 activity in C2C12 myotubes in response to nucleotides manipulation by FK866 and NR. A. 11β-HSD1 activity after 24 hours of treatment with NR (0.5mM) and FK866 (100nM) **B.** 11β-HSD1 activity after 48 hours of treatment with NR (0.5mM) and FK866 (100nM). Results of N=3 independent experiments are shown as fold change, for which values were referred to controls (set =1). Statistically significant differences compared to control were designated by **** ($p<0.0001$).

3.2.3. Time course of 11β-HSD1 oxo-reductase activity in response to NAD^+ manipulation by FK866 and NR in C2C12 myotubes.

Our previous results showed that NR treatment requires more than 24 hours to replete NAD^+ and restore 11β-HSD1 activity. Therefore, we examined the time point effect of NR treatment on 11β-HSD1 activity to identify the required time to impact enzyme activity. Results indicate that NR can rescue 11β-HSD1 even at a short time of treatment (30 min). Additionally, enzyme activity correlated with NAD^+ rescue time by NR treatment and restored the total enzyme activity after 24 hours (**Figure 3.3**).

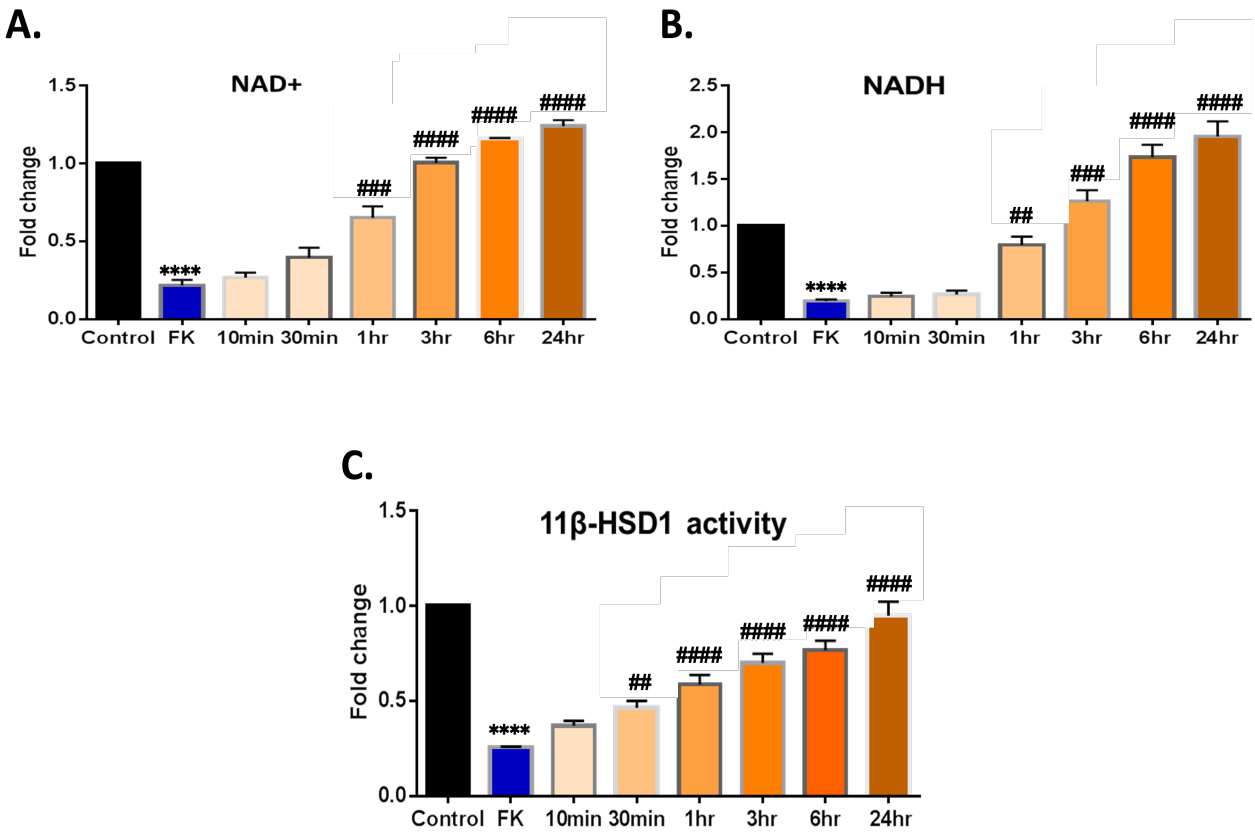


Figure 3.3. Time course of 11β-HSD1 oxo-reductase activity in response to NAD^+ manipulation by FK866 and NR in C2C12 myotubes.

A. NAD^+ level and **B.** NADH level expressed as fold change. **C.** The activity of 11β-HSD1 expressed as the percentage of H^3 11Dihydro-corticosterone to H^3 corticosterone conversion. Control (no treatment), FK866 at (100nM; 48 hours), NR (0.5 mM; 10min, 30min, 1h, 3h, 6h, 24 h). Results of N=3 independent experiments are shown as fold change, for which values were referred to controls (set =1). Statistically significant differences compared to control were designated by **** ($p<0.0001$). Statistically significant differences compared to FK866-treated cells were designated by $^{\#\#}$ ($p<0.01$), $^{\#\#\#}$ ($p<0.001$), $^{\#\#\#\#}$ ($p<0.0001$).

3.2.4. 11β-HSD1 oxo-reductase activity in WT mouse myotubes in response to FK866 and NR.

We then examined the same hypothesis in primary wild-type mouse myotubes. 11β-HSD1 activity was significantly decreased after 48 hours of FK866 treatment and rescued by NR co-administrated for 48 hours, as seen in C2C12. The enzyme activity corresponded with NR rescue at 30 min, 6 hours, and 24 hours (**Figure 3.4**).

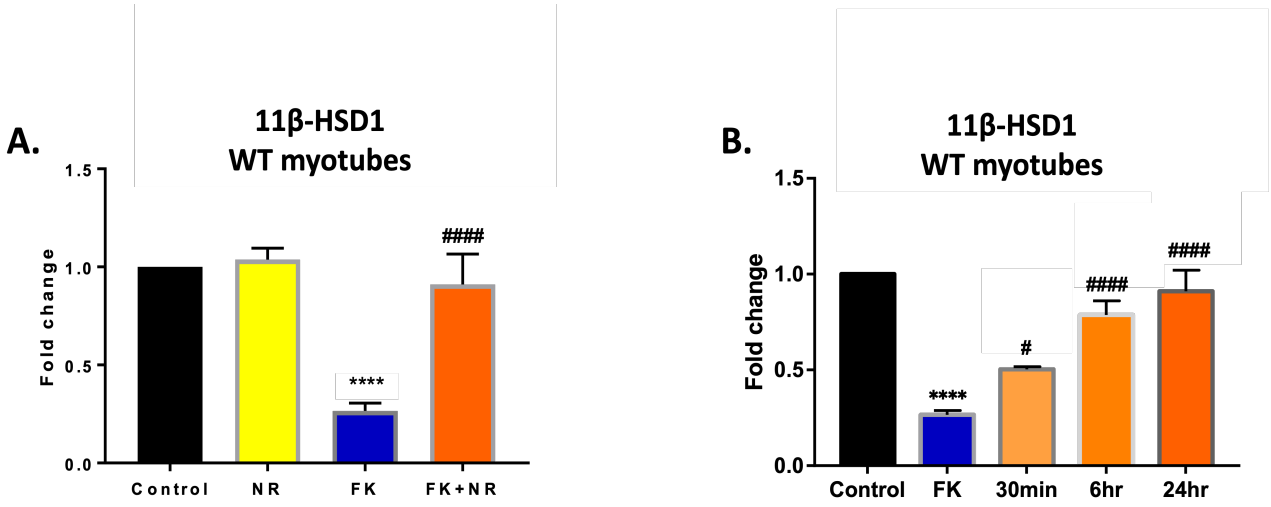


Figure 3.4. The effect of NAD^+ manipulation by FK866 and NR on 11β-HSD oxo-reductase activity in WT mouse myotubes.

A. The activity of 11β-HSD1 expressed as fold change of H^3 11-DHC to H^3 corticosterone conversion. Control (no treatment), NR (0.5mM; 24h) FK866 (100nM; 48h), FK866+NR (48h). **B.** The activity of 11 β-HSD1 expressed as fold change of H^3 11-DHC to H^3 corticosterone conversion. Control (no treatment), FK866 (100nM; 48 hours) NR (0.5mM; 30min, 6h, 24h). Results of N=3 independent experiments are shown as fold change, for which values were referred to controls (set =1). Statistically significant differences were designated by **** ($p<0.0001$), when compared to control and by $^{\#}$ ($p<0.05$), $^{\#\#\#\#}$ ($p<0.0001$), when compared to FK866-treated cells.

3.2.5. 11β-HSD1 dehydrogenase activity in H6PDH mouse myotubes.

To examine how the pentose phosphate pathway regulates 11β-HSD1 enzyme activity, we assessed 11β-HSD1 activity in H6PDH KO mouse myotubes. In the absence of H6PDH, it seemed that 11β-HSD1 favoured a dehydrogenase activity converting active steroid (corticosterone) to inactive steroid (11-DHC) utilizing NADP as a cofactor. This reaction occurs independent of NADPH or G6P. After modulating NAD^+ level with FK866 and NR, 11β-HSD1 dehydrogenase activity was also depleted, as seen in the oxo-reductase reaction. The effect on the dehydrogenase activity in H6PDH KO suggests that FK866 and NR treatment can affect ER NADP availability (**Figure 3.5**)**.**

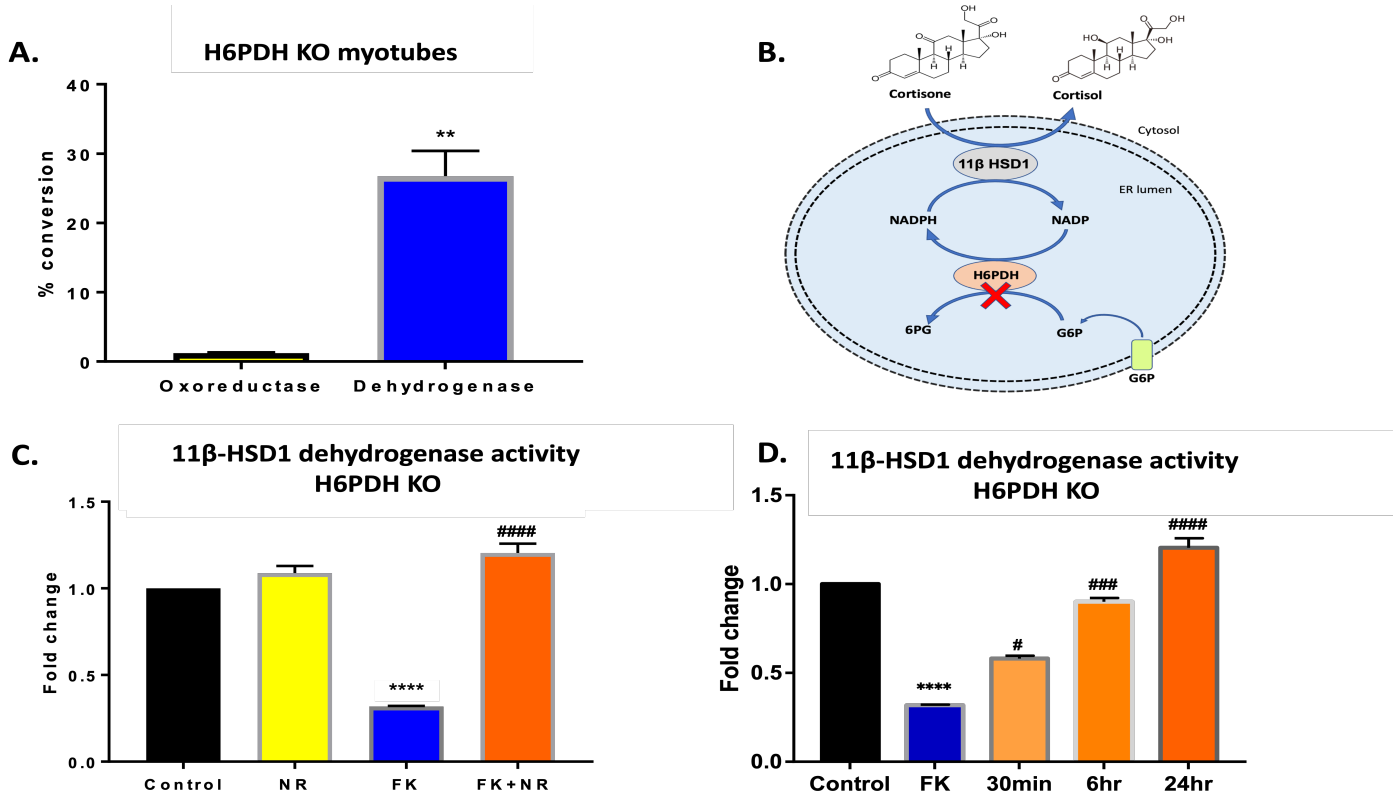


Figure 3.5. 11β-HSD1 dehydrogenase activity in H6PDH mouse myotubes.

11β-HSD1 shift to dehydrogenase activity in H6PDH KO mouse myotubes (Lavery et al., 2006). **B**. Diagram showing H6PDH KO transform 11β-HSD1 to dehydrogenase activity. **C.** Dehydrogenase activity expressed as fold change. Control (no treatment), NR (0.5mM; 24h) FK866 (100nM; 48 h), FK866+NR (48hours). **D.** Dehydrogenase activity of 11 β - HSD1 expressed as fold change. Control (no treatment), FK866 (100nM; 48 hours) NR (0.5mM; 30min, 6h, 24h). Results of N=3 independent experiments are shown as fold change, for which values were referred to controls (set =1). Statistically significant differences were shown by **** ($p<0.0001$), when compared to control. When compared to FK866- treated cells, statistically significant differences were designated by $^{\#}$ ($p<0.05$), $^{\#\#\#}$ ($p<0.001$), $^{\#\#\#\#}$ ($p<0.0001$), when compared to FK866-treated cells.

All of the previous work was done in cooperation with Dr. Yasir ElHassan. Due to variability in the enzyme activity between different replicants, we expressed 11β-HSD1 activity in fold change instead of pmol/mg of protein/h. Our observation indicated the same pattern of enzyme activity within each replicant.

3.2.6. The effect of NAD^+ manipulation by FK866 and NR on the liver's 11β-HSD oxo-reductase and dehydrogenase activity.

In order to examine the validity of our previous results in C2C12 and primary myotubes, we repeated the same experiment in different cell types. It was shown that the HepG2 cell line appears to be a close model of in vivo gluconeogenesis and hepatic metabolism (Sefried et al., 2018) and 11β-HSD1 activity (Ignatova et al., 2009). A similar result was also seen in the HepG2 cell line in our study. NAMPT depletion with FK866 (100nM; 48h) depleted NAD^+ and NADH, which were restored with co-administration of NR (0.5 mM; 24 hours) (**Figure 3.6**). The effect of NAD^+ manipulation corresponded with the oxo-reductase activity of 11β-HSD1. The decrease in the 11β-HSD1 activity was significant by more than 60% after treatment with FK866 (100nM; 48h, $p=0.0016$). After treatment with NR (0.5mM; 4h and 24h), the enzyme activity doubled after 4 hours ($p=0.0057$), and the activity was fully restored after 24h ($p=0.0006$).

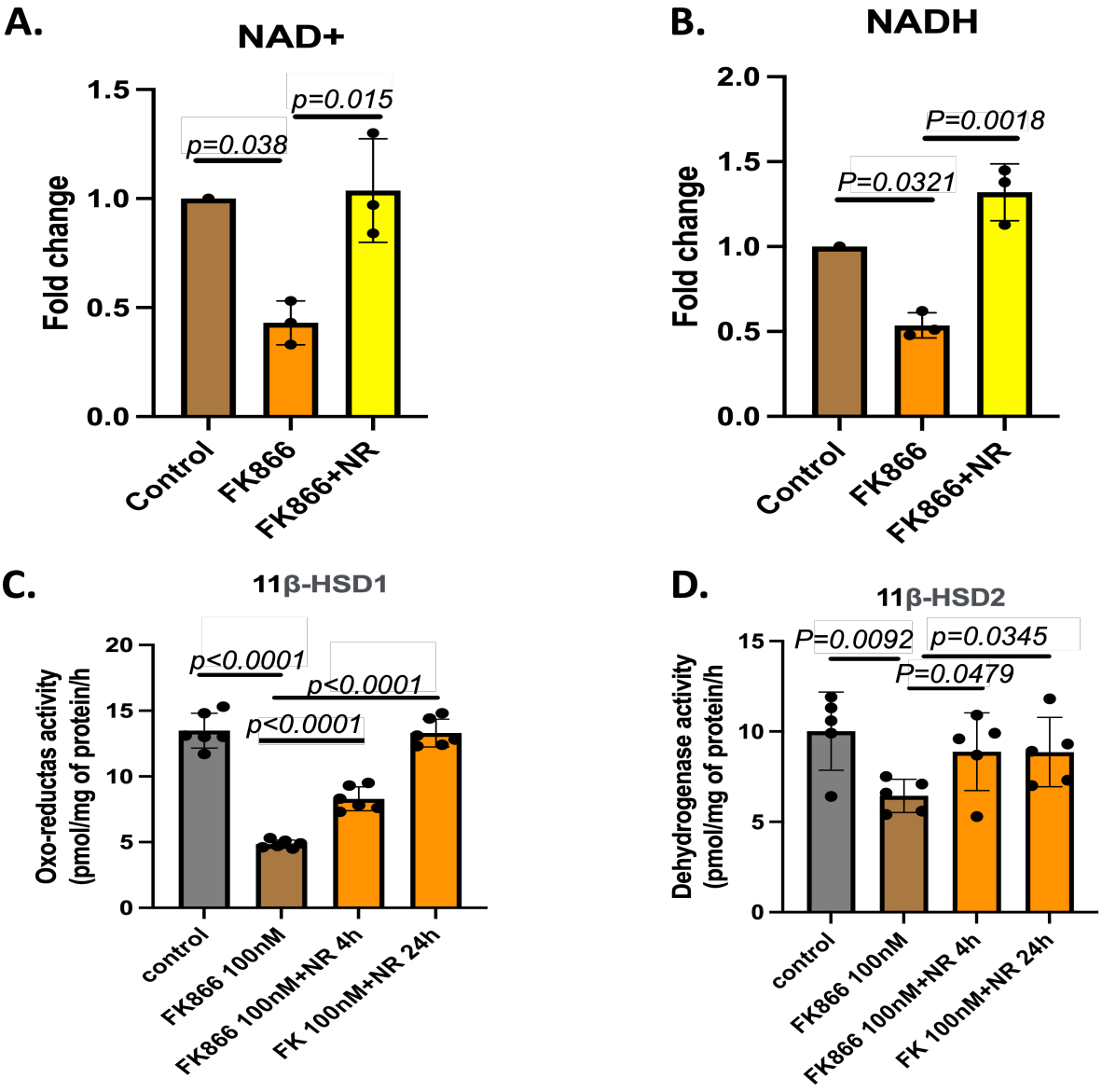

A.
NAD+
Fold change
1.5
1.0
0.5
0.0
p=0.038
p=0.015
Control
FK866
FK866+NR
B.
NADH
Fold change
2.0
1.5
1.0
0.5
0.0
P=0.0321
P=0.0018
Control
FK866
FK866+NR
C.
11β-HSD1
Oxo-reductas activity
(pmol/mg of protein/h
20
15
10
5
0
p<0.0001
p<0.0001
p<0.0001
control
FK866 100nM
FK866 100nM+NR 4h
FK 100nM+NR 24h
D.
11β-HSD2
Dehydrogenase activity
(pmol/mg of protein/h
15
10
5
0
P=0.0092
p=0.0345
P=0.0479
control
FK866 100nM
FK866 100nM+NR 4h
FK 100nM+NR 24h

Figure 3.6. The effect of NAD^+ manipulation by FK866 and NR on 11β-HSD oxo-reductase and dehydrogenase activity in HepG2 cells.

A. After FK866 treatment, NAD^+ levels decreased 0.5 fold (p=0.038 compared to control) and were fully repleted with NR treatment (p=0.015 compared to FK866-treated cells). **B.** NADH level decreased 0.5 fold (p=0.032 compared to control) and was repleted with NR treatment (p=0.0018 compared to FK866 treated cells). Results of N=3 independent experiments are shown as fold change, for which values were referred to controls (set =1). **C.** 11β-HSD oxo-reductase activity was depleted by FK866 for 48h (p<0.0001 compared to control) and repleted by NR treatment (4h, p<0.0001, and 24h, p<0.0001, compared to FK866-treated cells). Results of N=6 independent experiments are shown. **D.** 11β-HSD dehydrogenase activity decreased by approx. 40% (p=0.0092 compared to control) after FK866-treatment and was restored with NR treatment (4h, p=0.047, and 24h p=0.034, compared to FK866-treated cells). Control (no treatment), FK866 at (100nM; 48h), NR (0,5 mM; 4h, 24h). Results of N=5 independent experiments are shown.

3.2.7. The effect of NAD^+ manipulation by FK866 and NR on 11β-HSD oxo-reductase in dermal fibroblasts (HDFn).

In HDFn, the activity of 11β-HSD1 was not sufficient to convert H^3 cortisone to active H^3 cortisol. Higher 11β-HSD1 activity was previously seen in fibroblasts induced by an inflammatory factor, e.g. tumor necrosis factor (TNFα) compared to control (Hardy et al., 2006a). Therefore, we used TNFα to boost 11 β-HSD1 activity. The enzyme activity increased by 5fold after treatment with TNF-α (10 ng/ml; 48h) (**Figure 3.7 (A)**). However, after treatment with FK866 for 48 hours, the enzyme activity was depleted by more than 70% compared with TNFα-treated cells (p=0.0029). Treatment with NR for 24h was able to reverse the effect of FK866 and restore the total enzyme activity (p=0.0006 compared to FK866-treated cells) (**Figure 3.7 (B)**).

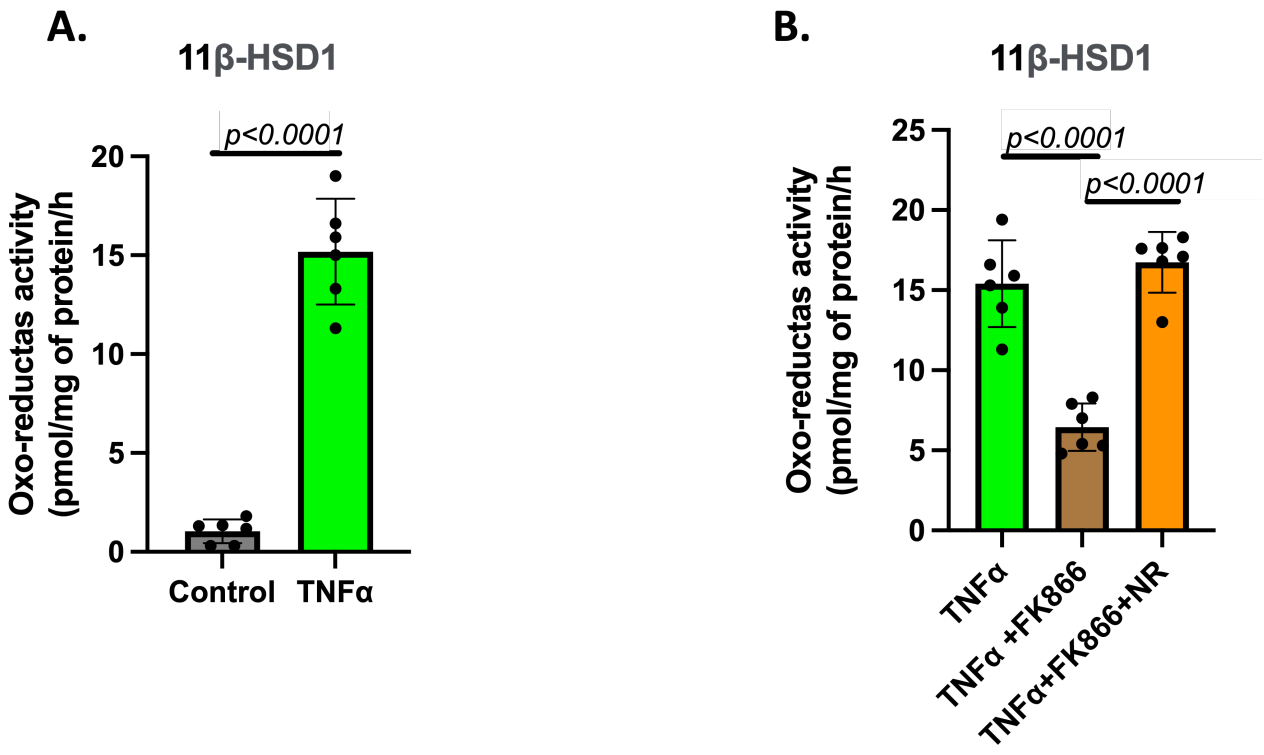


Figure 3.7. The effect of NAD⁺ manipulation by FK866 and NR on 11β-HSD oxo-reductase after enzyme boosting by TNFα in dermal fibroblast.

A. Boosting of 11β-HSD oxo-reductase activity by tumor necrosis factor (TNFα,10ng/ml;24h) expressed as the percentage of H^3 cortisone to H^3 cortisol conversion. The enzyme activity increased approx. 15fold compared to control ($p<0.0001$). **B.** The activity of 11 β-HSD1 expressed as the percentage of H^3 cortisone to H^3 cortisol conversion showed more than 70% depletion of enzyme activity ($p<0.0001$ compared to control). Enzyme activity was restored with NR treatment ($p<0.0001$ compared to FK866-treated cells). TNFα (10ng/ml;48hours), FK866 (100nM; 48 hours), NR (0,5 mM; 24hours hours). Results of N=6 independent experiments are shown.

3.2.8. The effect of NAD^+ manipulation by FK866 and NR on 11β-HSD2 dehydrogenase activity in the kidney.

To examine the effect of NAD^+/NADP manipulation on 11 β-HSD2 dehydrogenase activity, we used HEK293, because they showed a high 11 β-HSD2 expression (Brown et al., 1996). Our results indicate a similar effect of FK866 on dehydrogenase activity and restoring enzyme activity with NR treatment. Furthermore, this effect was consistent with NAD^+ depletion and rescue by FK866 (100nM; 48h) and NR (0.5mM; 24h), respectively, as shown in (**Figure 3.8**).

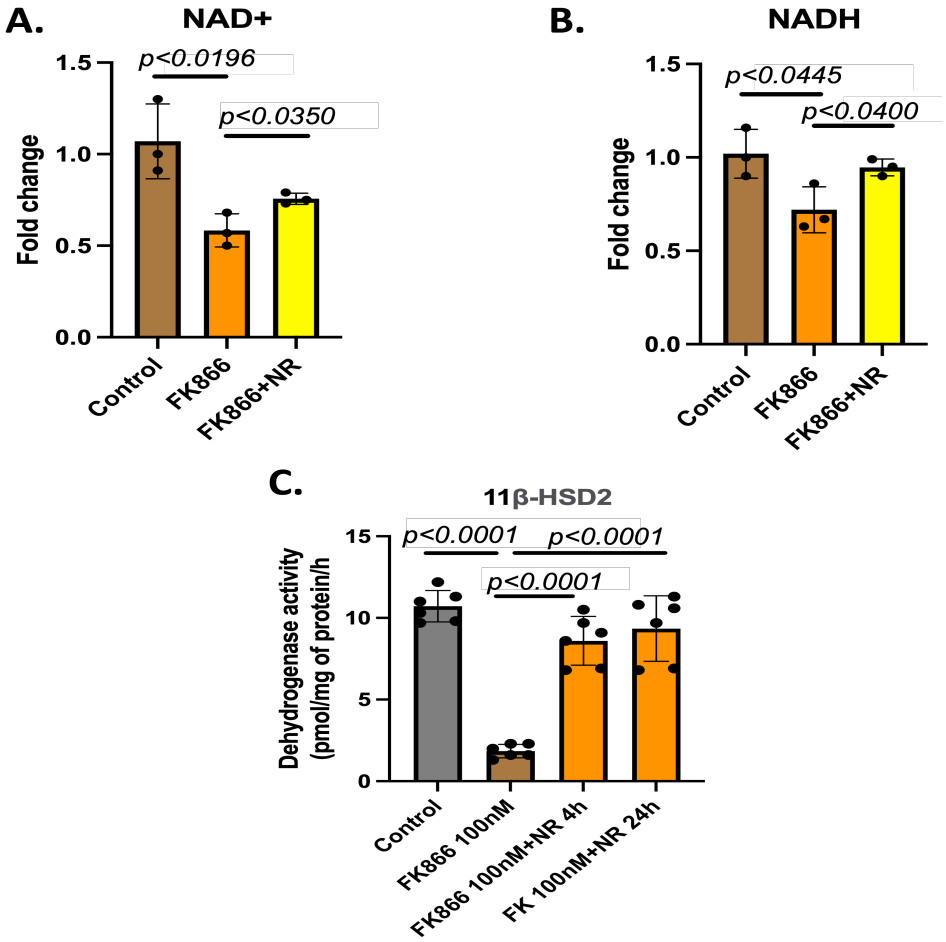


Figure 3.8. The effect of NAD⁺ manipulation by FK866 and NR on 11β-HSD2 dehydrogenase activity in the human kidney cell line (HEK293).

A. NAD⁺ level was decreased by 45% after FK866 treatment (p=0.019 compared to control) and repleted with NR treatment (p=0.035 compared to FK866-treated cells) **B.** NADH level was similarly manipulated with FK866 (100nM; 48h, p=0.044 compared to control) and NR (0.5mM; 24h, p=0.040 compared to FK866-treated cells). Results of N=3 independent experiments are shown as fold change, for which values were referred to controls (set =1). **C.** The activity of 11 β-HSD2 expressed as the percentage of H^3 cortisol to H^3 cortisone conversion was markedly depleted with FK866 (p<0.0001 compared to control), and the activity was restored after treatment with NR (4h, 24h, p<0.0001 compared to FK866 treatment). Control (no treatment), FK866 at (100nM; 48 hours), NR (0,5 mM; 4,24hours). Results of N=6 independent experiments are shown.

3.3. Discussion

NAD is an essential compound required as a cofactor for many cellular processes, and its availability is crucial to maintain NAD-dependent enzyme activity. NAD is present in two forms, oxidized NAD^+ (electron acceptor) and reduced NADH (electron donor). The cellular NAD^+ and NADH pools are regulated by maintaining the balance between biosynthesis (via *de novo*, Preiss-Handler, or salvage pathways) and consumption by NAD-dependent reactions. Therefore, the availability of NAD^+ and NADH is determined by the rate of biosynthesis and consumption, while the ratio of NAD to NADH is critical for maintaining redox homeostasis.

ER is a subcellular organelle with a prominent role in cell functions via synthesis, transfer, and modification of proteins and maintenance of calcium storage. The ER lumen is an active site for cortisol metabolism via NADPH-dependent enzyme 11β-HSD1. *In vivo*, this enzyme predominantly acts as oxo-reductase, catalyzing the conversion of cortisone to cortisol, supported by a high luminal NADPH/NADP ratio. However, it is unknown whether this ratio is maintained only by the activity of the H6PDH enzyme in the pentose phosphate pathway or if a mechanism allows NAD^+/NADH transport from the cytosol into the ER.

The current knowledge explaining the different NAD^+ pools between the cytosol and ER/SR needs to be enhanced. In contrast, unique mechanisms controling NAD(H) exchange is known for other cellular organelles. For example, the supply of cytosolic NAD(P)(H) to the mitochondria is under the control of biochemical shuttling systems, e.g. the malate-aspartate shuttle. In the nucleus, the nucleotide level does not differ from the cytosol due to nuclear permeability to cytosolic NAD^+.

There is evidence suggesting that NADH has access to the liver microsomal membrane after incubation for 60 min and significantly increased 11 β-HSD1 enzyme activity (McCormick et al., 2006). This observation indicates that the microsomal membrane might be permeable, allowing NAD(H) transport. In addition, the same study showed that pentose phosphate pathway inhibition by norepinephrine (NE) and dehydroepiandrosterone (DHEA) reduced 11 β-HSD1 oxo-reductase activity in intact rodent adipocytes (McCormick et al., 2006). These findings imply that 11 β-HSD1 oxo-reductase activity relies on the pentose phosphate pathway as a source of NADPH. This was supported by the observation that SR NADPH is controlled by the activity of G6PDH and the pentose phosphate pathway and that 11 β-HSD1 acts as dehydrogenase enzyme in G6PDH knock-out mice. Our results on H6PDH knock-out mice showed that in addition to depletion of oxo-reductase activity induced by lack of NADH generated from H6PDH, FK866 incubation depleted 11 β-HSD1 dehydrogenase activity, suggesting that the cytosolic availability of NAD^+ determines the enzyme direction. These findings indicate that H6PDH does not exclusively control 11 β-HSD1 oxo-reductase activity and the cytosolic NAD^+ level.

To study the cytosolic and ER/SR NAD^+ cross-talk, we used FK866 for 48h to inhibit NAMPT (a rate-limiting enzyme in the NAD^+ biosynthesis pathway) and depleted NAD^+ levels in the cytosol. The viability of C2C12 myotubes in response to FK866 treatment was investigated using caspase activity (Fletcher et al., 2017). It was suggested in this study that the cells were still viable after 48 of FK866 treatment, while beyond that, the viability decreased, and the apoptotic marker (caspase-3/7 activity) started to increase. Results in C2C12 mouse myotubes showed that FK866 depleted NAD/NADH, which was

rescued with NR treatment at 48 hours. This NAD/NADH level alteration reflected a similar effect on the intraluminal 11 β-HSD1 oxo-reductase activity. To examine the time required to rescue NAD/NADH and, consequently, enzyme activity, NR treatment was administered at a different time after NAD/NADH depletion with FK866 for 48 hours. The oxo-reductase activity corresponded with NAD/NADH rescue suggesting that 11 β-HSD1 was able to sense the fluctuation in NAD/NADH availability rescue induced by NR treatment as short as 30 min and restored the total enzyme activity after 24 hours. Similar results were also shown in primary muscle myotubes.

In order to validate our observation on skeletal muscle myotubes, we examined the effect of NAD^+ manipulation on multiple cell types. Similar results were shown in the hepatic cell line HepG2 after 48 hours of FK866 treatment at 100 nM. After NAD^+ repletion with NR (0.5 mM, 4h), the enzyme activity was rescued by more than 90%, and restored the total activity after 24 hours. In human dermal fibroblasts (HDFn), the enzyme activity is induced after 48 hours of TNF treatment, as shown in the previous study (Hardy et al., 2006b). Following the previous findings, treatment with FK866 (100nM, 48h) was enough to lower the oxo-reductase activity by more than 70% significantly. Furthermore, after NAD repletion by NR (0.5 mM, 24h), the active cortisol conversion was fully restored. In contrast, osteosarcoma cell lines and human primary osteoblasts express both enzymes 11 β-HSD1 and 11 β-HSD2, while the predominant enzyme activity was shown to be the dehydrogenase activity, i.e. inactivation of cortisol (Bland et al., 1999). Similarly, the human kidney cell line Hek293 is known to have low expression of 11 β-HSD1 and high expression of 11 β-HSD2 (Krozowski et al., 1995). These data explain the absence of 11 β-HSD1 oxo-reductase activity in these cell lines.

In conclusion, our data on C2C12, HepG2, and HDFn suggest a possible mechanism for NAD^+ entry into the ER/SR. This is possibly due to a shuttling system similar to the mitochondria or a luminal NAD^+ kinase that controls for cytosol and ER/SR NAD(H) communication.

Chapter 4

Optimization of HepG2 and C2C12 transfection to examine Poly-ADP-Ribose Formation as a Biosensor for NAD^+ pools in the Endoplasmic Reticulum

4.1. Introduction

Transfection is the process of inserting a foreign material (DNA/RNA) in order to create a genetically modified cell. Optimizing suitable cultural conditions is a critical step in any effective transfection procedure. Each cell type has unique features that require a distinctive approach to produce successful transfection. Cells can be stably or transiently transfected based on the nature of the nucleic acid introduced (Recillas-Targa, 2006). In stable transfection, the foreign gene integrates with the cellular genome and allows for the passing of the DNA to the next generations. In transient transfection, the nucleic acid temporarily exists in the cell but does not integrate with the cellular genome. With the cellular division, the expression of the foreign gene will gradually decrease until gone. The advantage of transient transfection is that it allows short-term and rapid investigation of transformed genes or overexpressed proteins.

PARPs are a group of enzymes located in different subcellular compartments consuming NAD^+ and producing polymers of PAR. These polymers can be detected via attachment to a specific antibody. It was shown that stable transfection of Hek293 with cytosolic catalytically active PARP (PARPcd) significantly depleted total cellular NAD^+ level by 20% compared to control expressing EGFP only (Dölle et al., 2010). In addition, this study indicated that the viability of the transfected cells did not diminish, excluding the possible cytotoxic effect of cytosolic PARP overexpression (Dölle et al., 2010). Therefore, subcellular localization of NAD^+-dependent enzyme (PARP) activity is reported by the formation of PAR, which is inversely proportional to the organelle NAD^+ content.

This chapter aims to establish a model of ER-PARP overexpression in the liver (HepG2) and mouse muscle cells (C2C12) by optimizing suitable culture conditions for efficient transfection**.** We adjusted the cell number, transfection time, DNA concentration, and PAR detection by Western blot. In the next chapter, we will use this model to investigate whether ER can maintain NAD^+ availability through cytosolic NAD^+ repletion.

4.2. Results

4.2.1. Plasmid DNA quality after restriction digest with XbaI and EcoRI

We started by examining the plasmids used for our experiment to confirm the correct structure based on the cleaved sizes after restriction digestion with XbaI and EcoRI. (**Figure 4.1**).

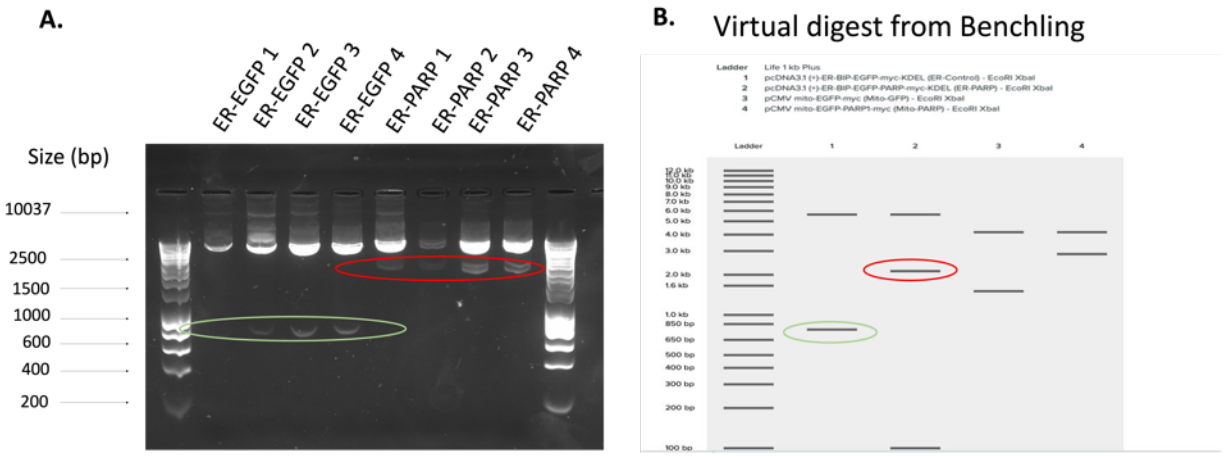


Figure 4.1. Gel electrophoresis of the plasmid DNA after restriction digestion with XbaI and EcoRI.

A. ER-EGFP and ER-PARP plasmid DNA fragments separated based on their sizes compared with **B.** Simulated gel predicted the fragment sizes by virtual digestion. The sizes of ER-EGFP (1-4) fragments ~ 3000 & 600 and ER-PARP (1-4) ~ 3000 & 1900, corresponded with the fragment sizes of virtual digest.

4.2.2. Transfection of HepG2 cells with vectors encoding ER-PARP1cd, ER-EGFP, mitochondrial PARP1cd and mitochondrial-EGFP

4.2.2.1. Optimization of lipofectamine for HepG2 transfection

We started a pilot experiment in our first transfection to transfect the HepG2 cell line with vectors encoding ER-PARP1cd and ER-EGFP. To optimize transfection efficiency in ER PARP1cd, two concentrations of lipofectamine were used (0.75 µl and 1.5 µl) as recommended by manufacturer‘s protocol (Invitrogen). Protein expression was observed by the intrinsic fluorescence of the EGFP fraction of the constructs. The transfection efficiency was good for all transfected cells, while the green fluorescence from the ER-PARP1cd plasmid was weaker than the control and the mito-PARP1cd plasmids. A higher concentration of lipofectamine did not improve transfection efficiency (**Figure 4.2**).

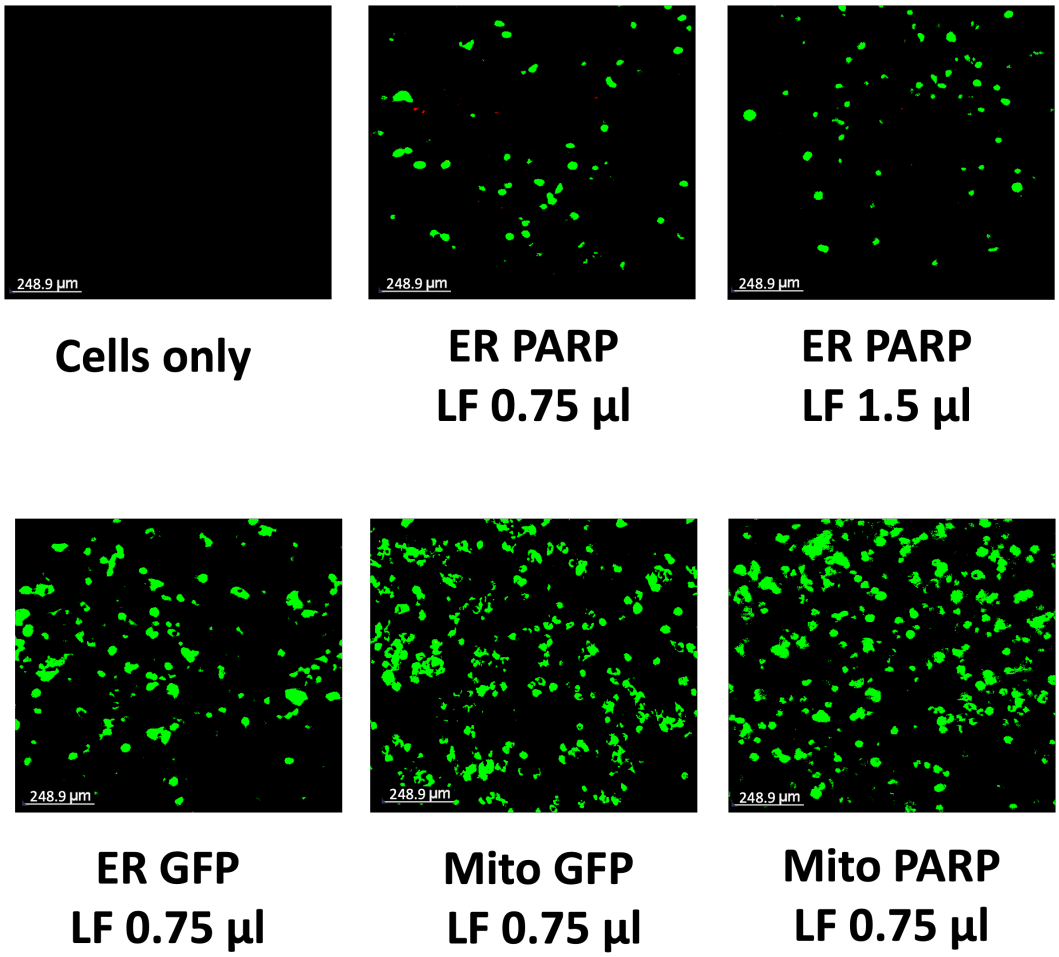


Figure 4.2. Transfection of HepG2 cells with vectors encoding ER-PARP1cd, ER-EGFP, mitochondrial PARP1cd and mitochondrial EGFP.

Cells were transfected with lipofectamine (LF 0.75 µl) in ER-EGFP, Mito-EGFP and Mito-PARP1cd, and (LF 0.75 µl and 1.5 µl) in ER-PARP1cd. Fluorescence was detected in all transfected cells, with a lower fluorescence in cells expressing ER-PARP1cd. No difference was seen with increased lipofectamine concentration in cells transfected with ER PARP1cd.

4.2.2.2. Transfection efficiency of different ER-PARP plasmids

We aimed to examine four different preparations of ER-PARP1cd plasmids to use the optimal plasmid that has the highest transfection efficiency for our next transfection. No difference in the signal intensity was noticeable between the four ER-PARP1cd plasmids (**Figure 4.3**).

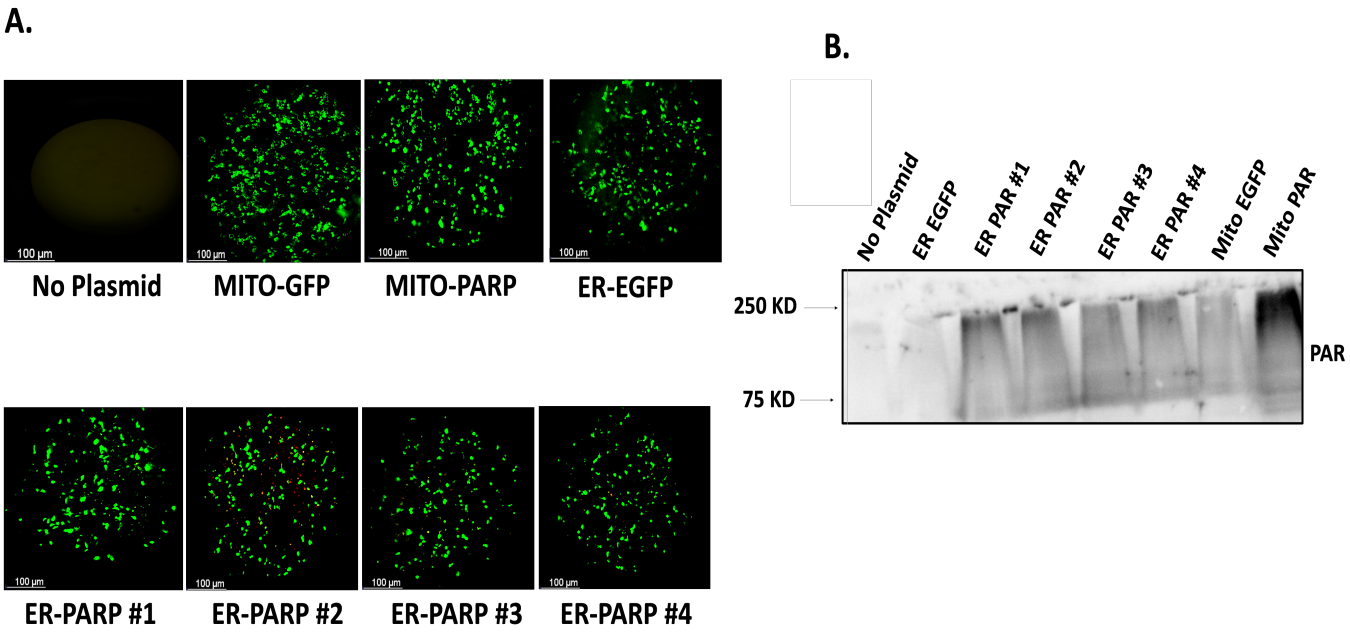


Figure 4.3. Transfection of HepG2 with vectors encoding ER-PARP1cd (four plasmid preparations), ER-GFP, mitochondrial PARP1cd and mitochondrial EGFP.

A. Fluorescence was seen in all cells expressing the EGFP portion of all different constructs. No fluorescence was detected in cells without plasmid (lipofectamine only). Fluorescence was detected in cells transfected with ER PARPs, with a slightly better transfection seen in ER PARP#1. **B.** Immunoblot analysis of lysate from transfected HepG2 transiently expressing PARP1cd or EGFP-PARP1cd targeted to ER or mitochondria. PAR formation revealed an equal signal in all different PARP plasmids with more detectable PAR formation in Mito-PARP1cd. No PAR formation was detected in ER-EGFP and cells with no plasmid (lipofectamine only).

4.2.2.3. Transfection of HepG2 at a density of 2.2*10^5 cells/well

HepG2 cell lines have a high proliferation rate (average doubling time is 48h) and tend to grow in clusters. These characteristics make it difficult to adjust the right confluence during transfection. We started with transfecting HepG2 at a density of 2.2 *10^5 cells/well. Then, we transfected the cells with constructs targeted to the ER (ER-PARP1cd and ER-EGFP) and constructs targeting mitochondria (mito-PARP1cd and mito-EGFP) as a control of transfection. The green fluorescence protein (GFP) expression indicates transfection efficiency, which showed a better expression in cells transfected with mitochondrial constructs than in cells transfected with ER constructs (**Figure 4.4 (A)**). These findings are in line with the strong PAR signal in Mito-PARP1cd, as seen in the Western blot image (**Figure 4.4 (B)**).

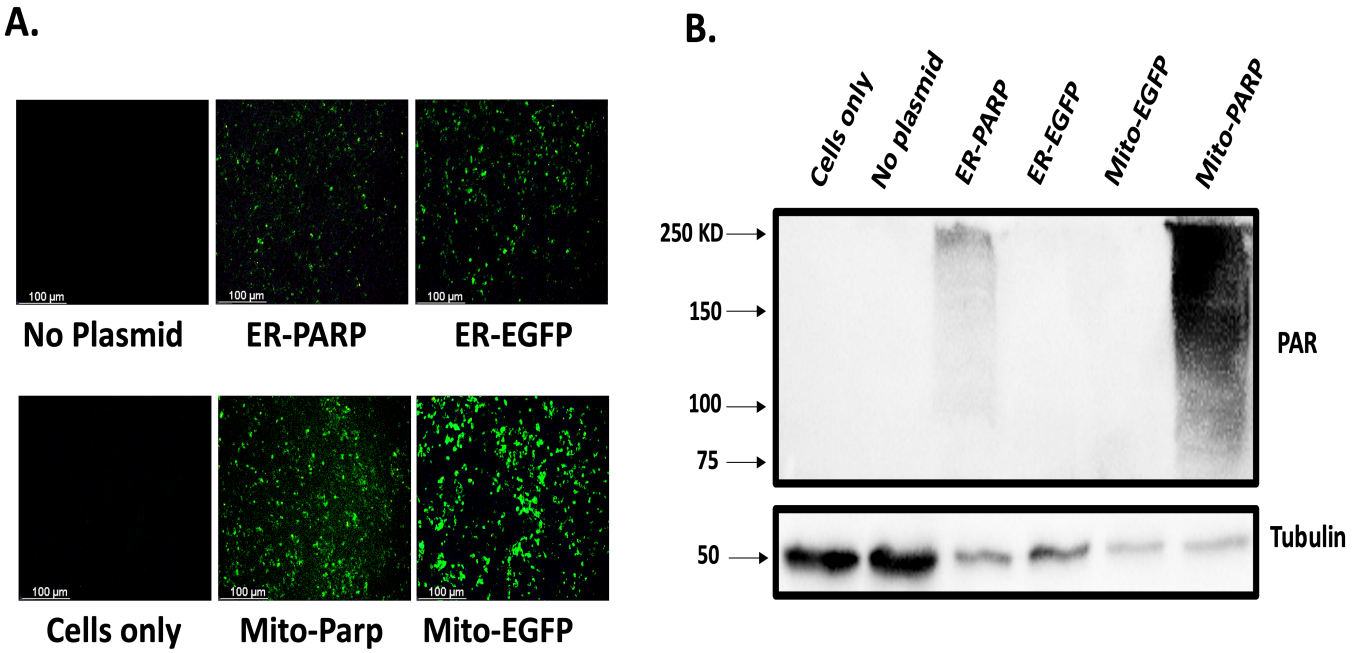


Figure 4.4. Transfection of HepG2 at a density of 2.2 *10^5 cells/well with vectors encoding ER-PARPcd, ER-EGFP, mitochondrial PARPcd and mitochondrial EGFP.

A. Fluorescence was seen in all transfected cells, with a higher fluorescence in mito-PARP and Mito-EGFP. No fluorescence was seen in cells only and without plasmid. **B.** Immunoblot analysis of cell lysate expressing PARPcd or EGFP-PARPcd targeted to ER and mitochondria. PAR immunoblotting analysis using PAR antibody revealed detectable PAR formation in cells expressing mito-PARP and low signal in ER-PARP. No signal was detected in cell lysate expressing ER-EGFP, Mito EGFP, no plasmid, and cells only. Protein was transferred to blotting membrane using the wet transfer method. β tubulin was used as loading control.

4.2.2.4. Transfection of HepG2 at a density of 1.1 *10^5 cells/well

To establish an ER PARP1cd overexpression model, we focused on optimizing the transfection technique of HepG2 with ER constructs only. To avoid contact inhibition that decreases DNA uptake, we started with a cell density of 1.1 *10^5 cells/well. We showed a low transfection efficiency indicated by the expression of GFP (**Figure 4.5 (A)**). A Western blotting image revealed low PAR formation corresponding with the low protein concentration (**Figure 4.5 (B)**).

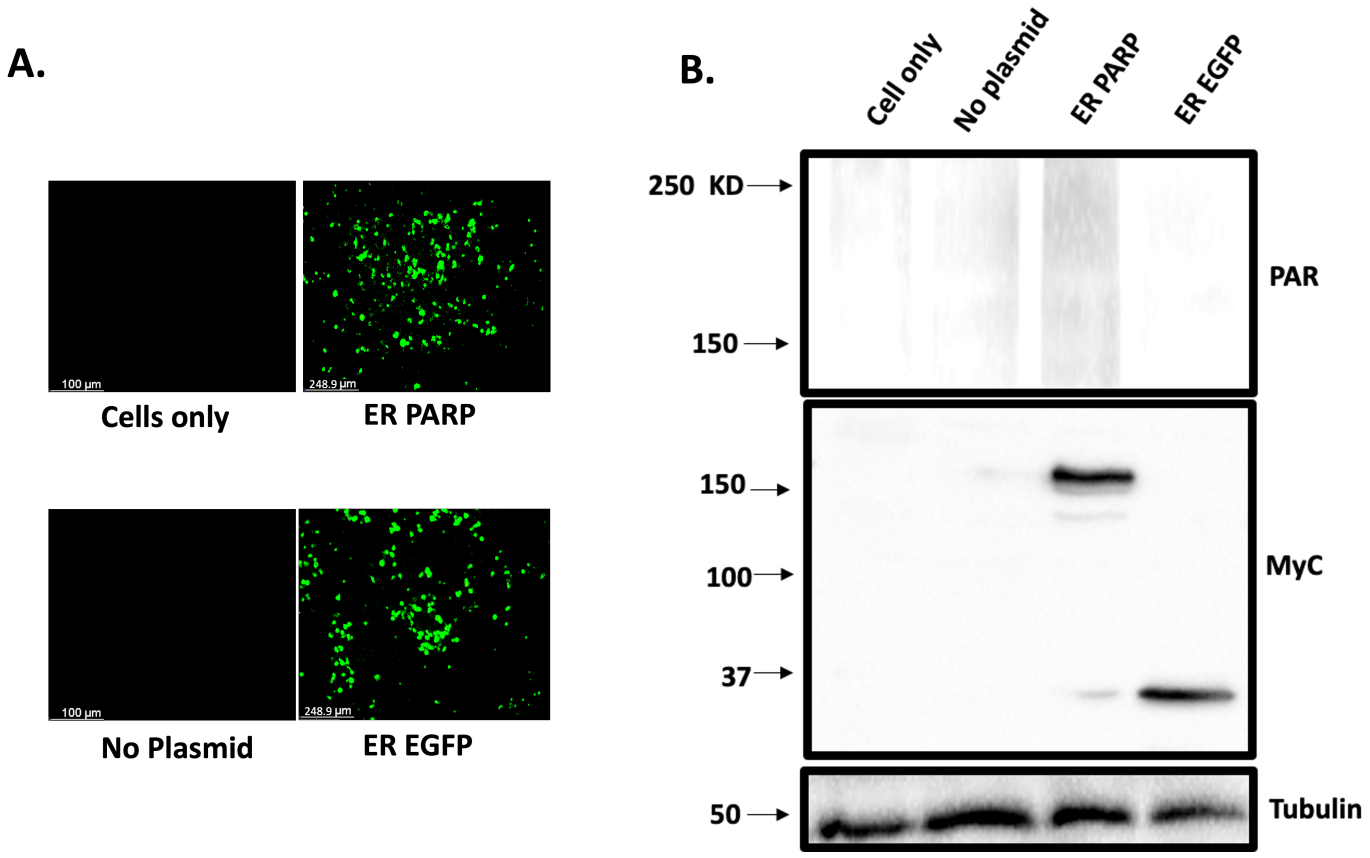


Figure 4.5 Immunofluorescence and Western blotting images of transfected HepG2 48h after transfection (at a confluence of 1.1* 10^5 cells/well).

A. Fluorescence was seen in cells transfected with ER-PARP and ER EGFP. No fluorescence was seen in cells only and cells without plasmid (lipofectamine only). **B.** Immunoblot analysis of cell lysate expressing PARPcd or EGFP-PARPcd targeted to ER. PAR immunoblotting analysis revealed detectable PAR formation in cells expressing ER-PARPcd with a low signal intensity. Proteins were transferred to the blotting membrane using the semi-dry transfer method. No increase in PAR formation was seen in cells only, no plasmid, and ER-EGFP. Protein overexpression was detected by C-terminal Myc-tag. β tubulin was used as loading control.

4.2.2.5. Transfection of HepG2 at a density of 1.5 *10^5 cells/well

Then we increased cell number to improve transfection efficiency. No significant change in green fluorescence compared to the previous cell number was detected (**Figure 4.6 (A)**). Western blotting images did not show a strong PAR signal in cell lysate of ER-PARP1cd compared to other cell lysates (**Figure 4.6 (B)**).

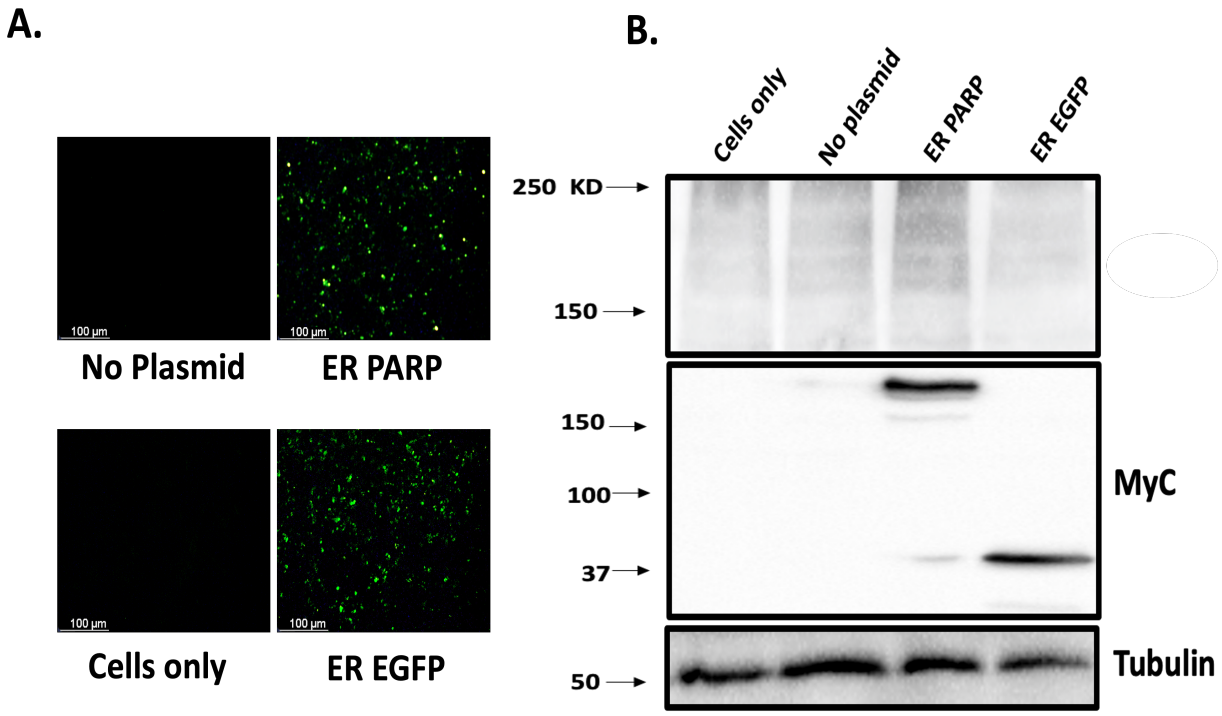


Figure 4.6. Transfection of HepG2 at a density of 1.5 *10^5 cells/well with vectors encoding ER-PARP1cd, ER-EGFP.

A. Fluorescence was seen in cells transfected with ER-PARP1cd and ER EGFP. No fluorescence was seen in cells only and cells without plasmid (lipofectamine only). **B.** Immunoblot analysis of cell lysate expressing PARP1cd or EGFP-PARPcd targeted to ER. PAR immunoblotting analysis using PAR antibody revealed slightly higher PAR formation in cells expressing ER-PARP1cd. Protein was transferred to blotting membrane using the wet transfer method. Protein overexpression was detected by C-terminal Myc-tag. β tubulin was used as loading control.

4.2.2.6. Transfection of HepG2 at a density of 2.5 *10^5 cells/well

At a cell density of 2.2*10^5 cells/well, GFP expression indicates a better transfection efficiency in ER-PARPcd and ER-EGFP (**Figure 4.7 (A)**). In addition, PAR formation was shown in the Western blotting image as a smeared band (**Figure 4.7 (B)**). In the previous transfection, we transferred western blotting gel using the semi-dry transfer technique. Due to the high molecular weight of PAR, this technique needed to be improved for transferring the PAR. It was suggested that transferring high molecular weight proteins requires a longer transferring time accomplished by the wet transfer technique (Blancher and Jones, 2001). We showed that the PAR signal improved using the wet transfer technique.

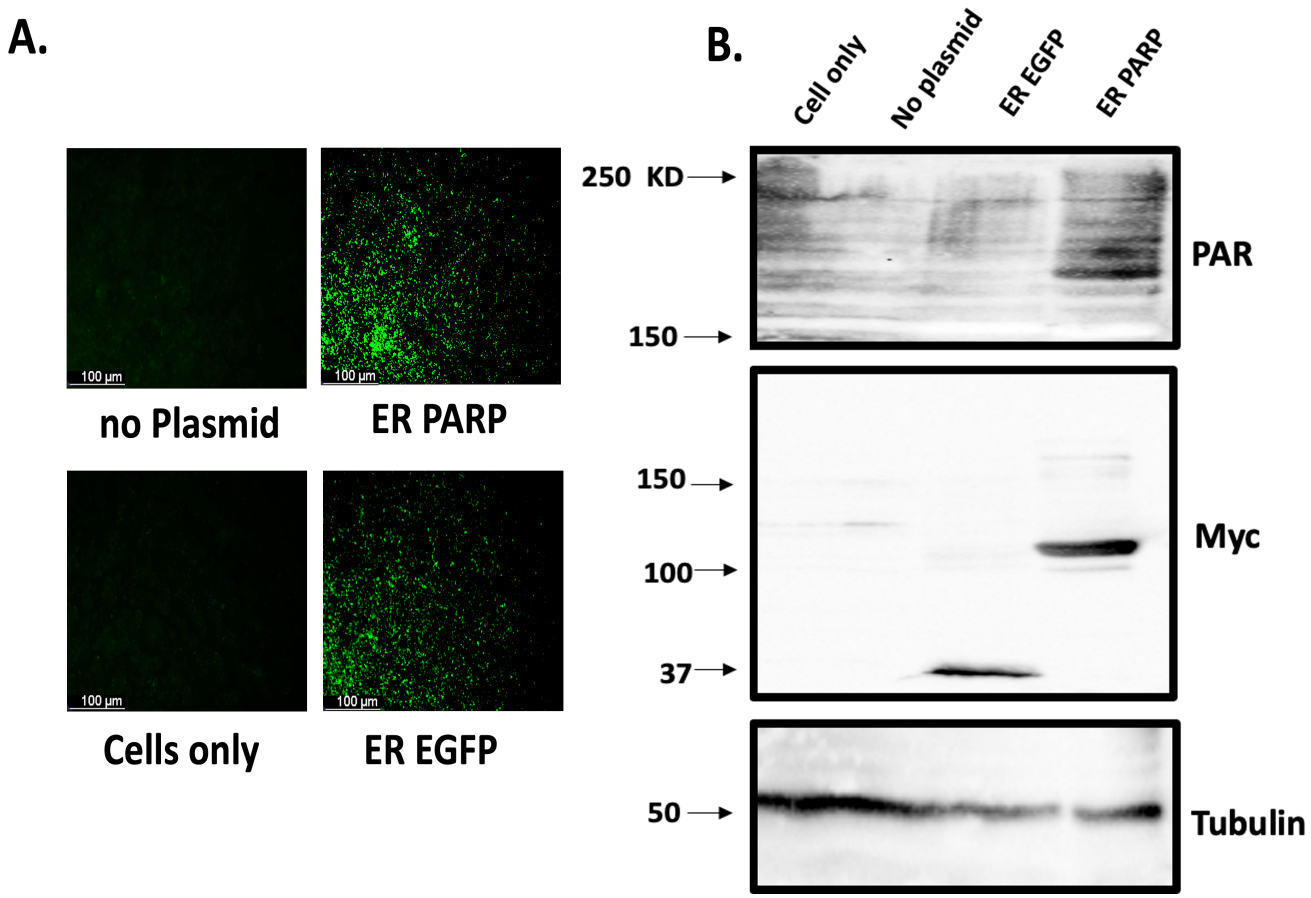


Figure 4.7. Transfection of HepG2 at a density of 2.5 *10^5 cells/well with vectors encoding ER-PARPcd, ER-EGFP.

A. Fluorescence was seen in cells transfected with ER-PARPcd and ER EGFP. No fluorescence was seen in cells only and cells without plasmid (lipofectamine only). **B.** Immunoblot analysis of cell lysate expressing PARPcd or EGFP-PARPcd targeted to ER. PAR immunoblotting analysis using PAR antibody revealed detectable PAR formation in cells expressing ER-PARPcd compared to ER-EGFP, no plasmid, and cells only. Protein was transferred to the blotting membrane using the wet transfer method. No increase in PAR formation was seen in cells only, no plasmid, and ER-EGFP. Protein overexpression was detected by C-terminal Myc-tag. β tubulin was used as loading control.

4.2.2.7. Increasing DNA concentration to improve transfection efficiency

Since the amount of DNA required for optimal transfection widely varies between different plasmids and cell types, we tested how increasing DNA amount improves transfection efficiency. By doubling the DNA amount (1000 ng), the PAR signal significantly improved compared to the previous transfection with lower DNA concentration (**Figure 4.8 (B)**). In addition, a fluorescence microscope image revealed a slightly better green fluorescence signal than in the previous transfection (**Figure 4.8 (A)**).

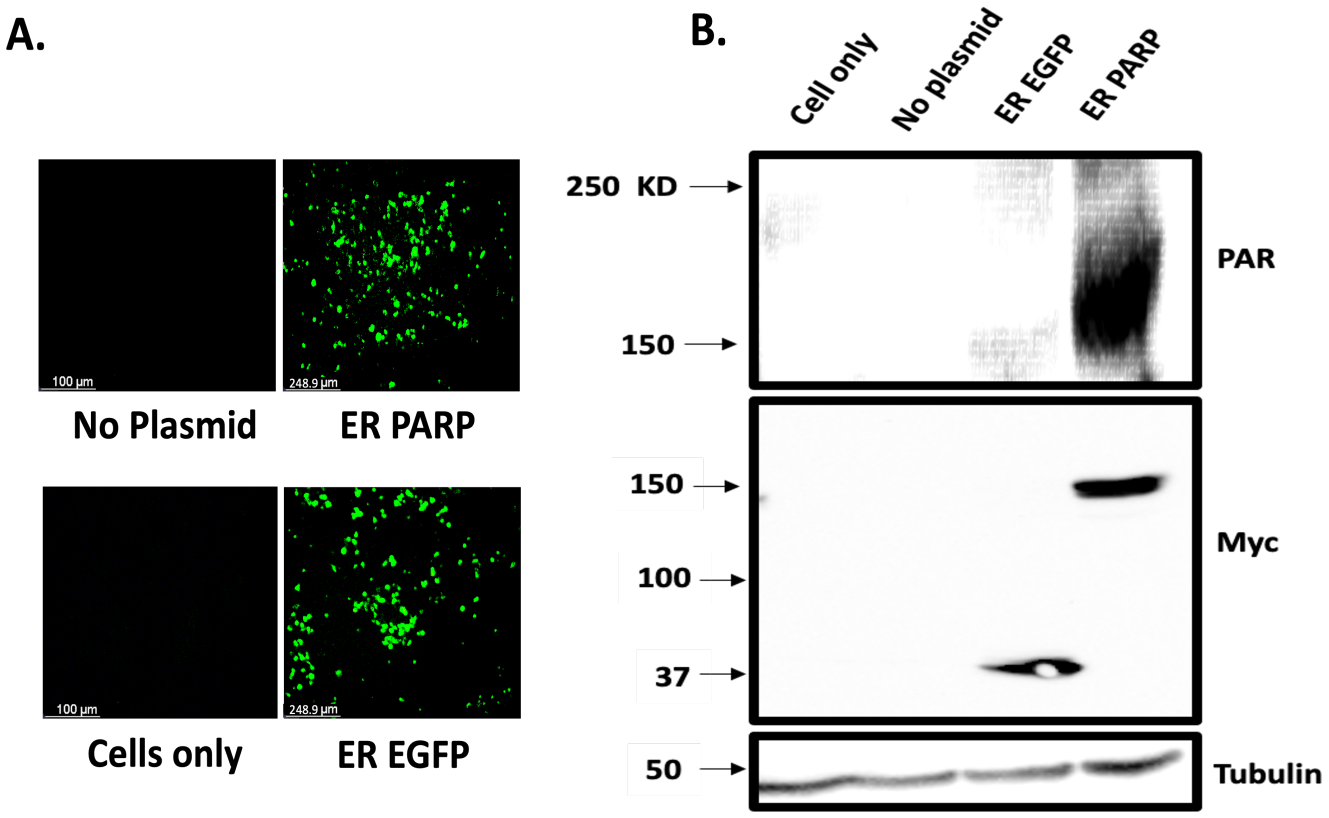


Figure 4.8. Transfection of HepG2 at a density of 2.2 *10^5 cells/well with vectors encoding ER-PARPcd, ER-EGFP with double DNA amount (1000 ng).

A. Fluorescence was seen in cells transfected with ER-PARP and ER EGFP. No fluorescence was seen in cells only and cells without plasmid. **B.** Immunoblot analysis of cell lysate expressing PARPcd or EGFP-PARPcd targeted to ER. PAR immunoblotting analysis using PAR antibody revealed detectable PAR formation in cells expressing ER-PARPcd. No PAR formation was detected in cell lysate of ER-EGFP, no plasmid, and cells only. Protein was transferred to blotting membrane using wet transfer method. Protein overexpression was detected by C-terminal Myc-tag. β tubulin was used as loading control.

4.2.3. Transfection of C2C12 cells with vectors encoding ER-PARPcd and ER-EGFP.

4.2.3.1. Transfection of C2C12 at a density of $1.1*10^5$ cells/well

To validate the expression of the PARP enzyme in a different cell type, we investigated transfection efficiency in C2C12 mouse myotubes. Cells were transfected at a confluence of $1.1*10^5$ cells/well, and the green fluorescence was imaged after 24 and 48 hours. Transfection efficiency was low even after 48 hours (**Figure 4.9 (A)**). Western blot images showed a minor PAR formation in the cell lysate of ER-PARP compared to other cells (**Figure 4.9 (B)**). This low signal might be related to insufficient protein concentration.

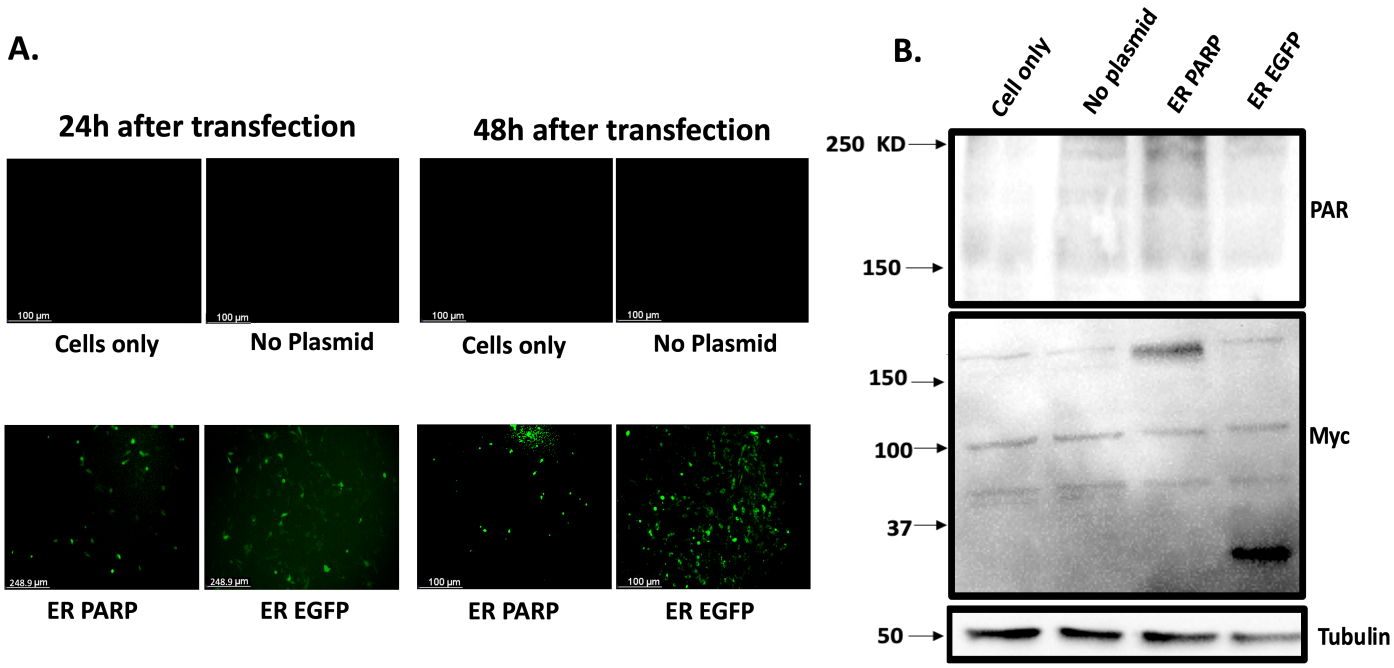


Figure 4.9. Transfection of C2C12 at a density of 1.1 *10^5 cells/well with vectors encoding ER-PARPcd, ER-EGFP.

A. Fluorescence was seen in cells transfected with ER-PARP and ER EGFP 24h and 48h post transfection. No fluorescence was seen in cells only and cells without plasmid. **B.** Immunoblot analysis of cell lysate expressing PARPcd or EGFP-PARPcd targeted to ER. PAR immunoblotting analysis using PAR antibody showed low signal of PAR formation in cells expressing ER-PARPcd. PAR formation was absent in cell lysate of ER-EGFP, no plasmid, and cells only. Protein was transferred to the blotting membrane using the wet transfer method. Protein overexpression was detected by C-terminal Myc-tag. β tubulin was used as loading control.

4.2.3.2. Transfection of C2C12 at a density of $2.2*10^5$ cells/well.

Then, we doubled the cell number to improve transfection and protein concentration. The expression of green fluorescence protein was significantly enhanced, especially after 48 hours of transfection (**Figure 4.10 (A)**). This also improved PAR formation in ER-PARP cell lysate in the Western blotting image (**Figure 4.10 (B)**). Although higher cell density improved the transfection efficiency, C2C12 started to fuse and form differentiated myotubes after 48 hours of transfection.

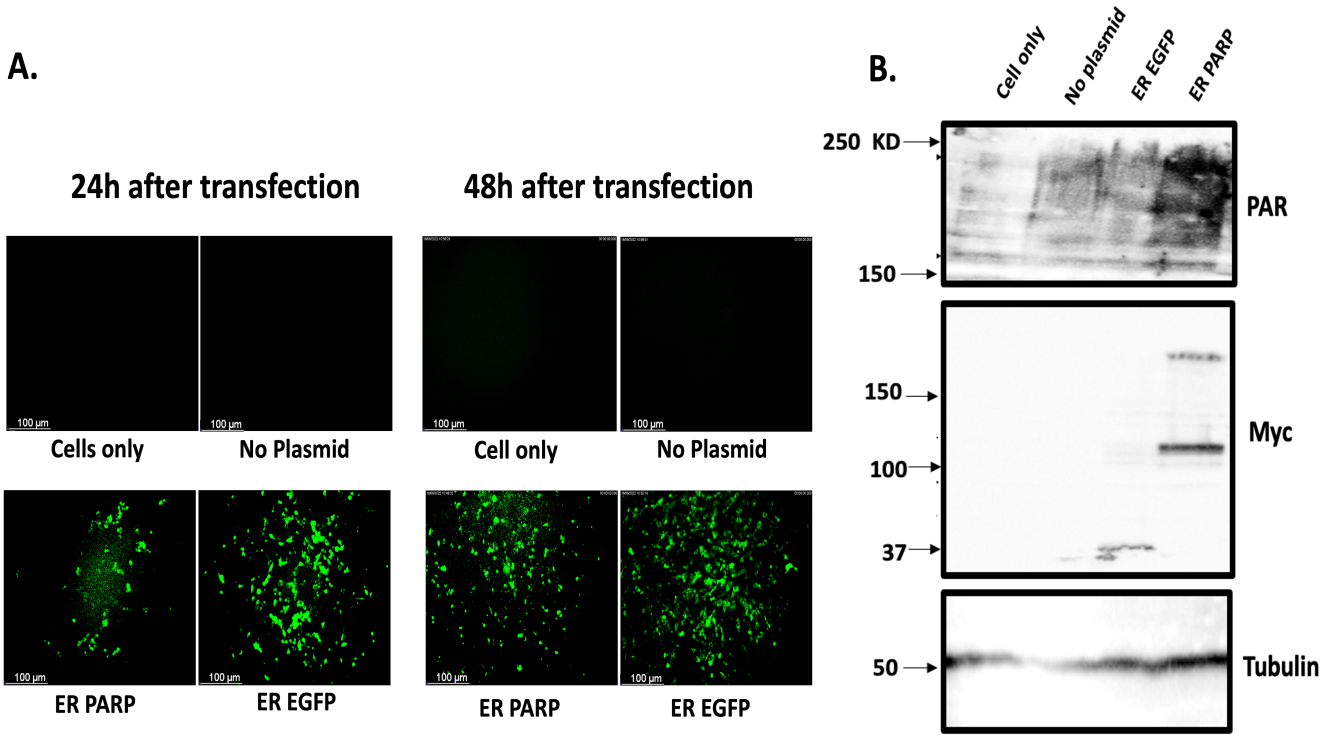


Figure 4.9. Transfection of C2C12 at a density of 2.2 *10^5 cells/well with vectors encoding ER-PARPcd, ER-EGFP.

A. Fluorescence was seen in cells transfected with ER-PARP and ER EGFP 24h and 48h post transfection. No fluorescence was seen in cells only and cells without plasmid. **B.** Immunoblot analysis of cell lysate expressing PARPcd or EGFP-PARPcd targeted to ER. PAR immunoblotting analysis using PAR antibody revealed detectable PAR formation in cells expressing ER-PARPcd. PAR formation was absent in cell lysate of ER-EGFP, no plasmid, and cells only. Protein was transferred to the blotting membrane using the wet transfer method. Protein overexpression was detected by C-terminal Myc-tag. β tubulin was used as loading control.

4.2.3.3. Transfection of C2C12 at a density of $1.5*10^5$ cells/well

To avoid the cells from reaching 100% confluence after 48 hours of transfection, cells were seeded at a density of $1.5*10^5$ cells/well. The detection of green fluorescence revealed successful transfection after 48 hours of transfection (**Figure 4.11 (A)**). Western blots displayed a high PAR signal in the cell lysate of ER-PARP compared to cells lacking PARP constructs (**Figure 4.11 (B)**).

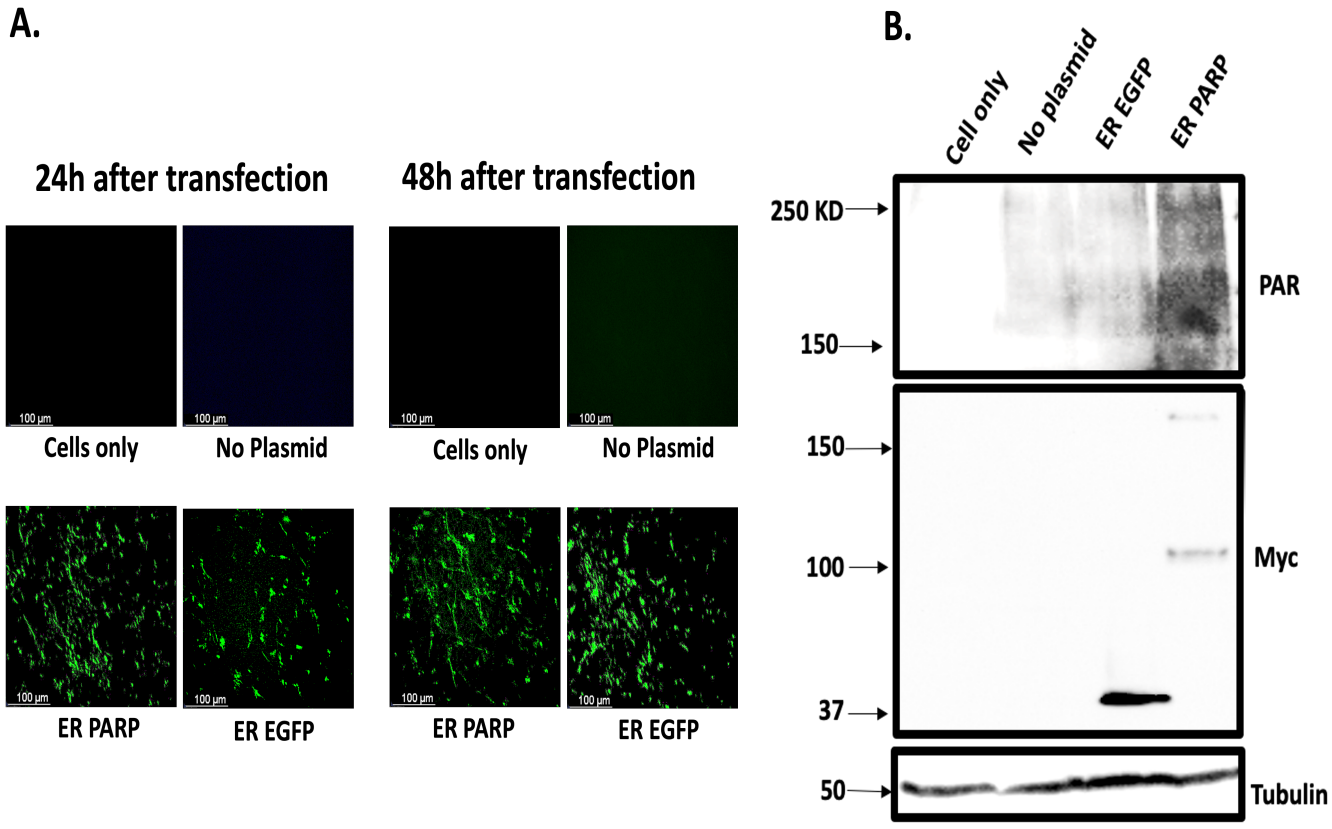


Figure 4.10. Transfection of C2C12 at density of 1.5 *10^5 cells/well with vectors encoding ER-PARPcd, ER-EGFP.

A. Fluorescence was detected in cell lysate of ER-PARP and ER EGFP after 24 hours of transfection with a better fluorescence after 48 hours. No green fluorescence was seen in cells only and cells without plasmid. **B.** Immunoblot analysis of cell lysate expressing PARPcd or EGFP-PARPcd targeted to ER. PAR immunoblotting analysis using PAR antibody revealed detectable PAR formation in cells expressing ER-PARPcd. PAR formation was absent in cell lysate of ER-EGFP, no plasmid, and cell only. Protein was transferred to the blotting membrane using the wet transfer method. Protein

overexpression was detected by C-terminal Myc-tag. β tubulin was used as loading control.

4.3. Discussion

PARPs are a group of enzymes present almost in all cell types generating polymers of PAR by utilizing NAD^+ as a cofactor. The formation of these polymers can be detected via a specific antibody (Kawamitsu et al., 1984). In a previous study, the formation of PAR was seen in cell organelles targeted with the PARP catalytic domain (Dölle et al., 2010). This observation was seen in the ER, mitochondria, peroxisomes, and Golgi apparatus. However, there was no observed diminishing in cell viability, excluding the possible cytotoxic effect of PARP overexpression targeted to these sites. In addition, total NAD^+ measurement showed a significant reduction of approximately 20% in cells transfected with PARPcd compared to control cells transfected with a construct expressing EGFP only as a result of NAD^+ uptake by PARP enzyme activity.

Transfection is the technique used to introduce a specific nucleic acid into the cell to study overexpressed genes. Several factors influence transfection efficacy, including the method of transfection, cell type/density, DNA quality/quantity, transfection reagent, and duration of transfection. It was suggested that transient transfection of different cell types (HEK293, endothelial cells, and mouse cortical neurons cells) using Lipofectamine3000 provided higher transfection efficiency and GFP expression compared with other transfection techniques (Shi et al., 2018). We used this method to transfect HepG2 and C2C12 myotubes with a vector encoding PARPcd or a control construct expressing EGFP only targeting the ER and mitochondria. The success of transfection was confirmed by the

intensity of GFP signal, Myc tag expression and formation of PAR shown in the Western blot image.

The plating density varies between multiple cell types based on how fast they grow. In HepG2, the cell number doubling time is 48.5 hours (Louisa et al., 2016) while in C2C12 myotubes, the doubling time is only 15 hours (Forterre et al., 2014). It was suggested that successful transfection is best acquired when the cells are transfected at a density of 50-80% confluence (Tanner et al., 1997, Li et al., 2010, Zhong et al., 2013). We plated 6 well plates at different cell densities to achieve the optimum confluence for transfection. Results indicate that HepG2 transfection efficiency was best seen at the plating density of 2.2 $*10^5$ cells/well, indicated by GFP expression. Transfection also improved when we increased DNA amount to 1000 ng. In C2C12 myotubes, cells were seeded at a low density as the population doubling time was too short, and the cells started to differentiate when they reached 100% confluence. We seeded the cells at three different concentrations: $1.1*10^5$, $1.5*10^5$, and $2.2*10^5$ cells/well. The optimum transfection efficiency was shown at a cell density of $1.5*10^5$ cells/well after 48 hours of transfection, which was assessed by the expression of GFP.

Unlike fluorescence microscopy, visualization of PAR formation in Western blot provides higher accuracy and sensitivity, as it represents a cumulative signal of multiple cells rather than just a single cell (Dölle et al., 2010). Although a low PAR signal was detected at low cell density ($1.1*10^5$) in both cell types, seeding the cells at a higher density improved transfection and PAR signal. In addition, by increasing the DNA amount to 1000 ng per well in HepG2, the expression of PAR significantly increased. Detection of PAR in cell

lysate expressing PARPcd in HepG2 and C2C12 verified NAD^+ consumption and depletion induced by PARP hyperactivity.

In conclusion, we established a model of ER-PARP overexpression in human liver cells (HepG2) and mouse myotubes (C2C12). Based on nucleotide consumption and formation of PAR polymers, we indicate that targeted PARP enzyme expression allows for modulation of subcellular NAD availability. In order to achieve efficient gene transfer, we compared various cell densities, amount of lipofectamine reagent, DNA concentrations, and transfection times. We were able to confirm successful transfection by visualization of GFP expression under a fluorescence microscope in both cell types. The detection of PAR signal in Western blotting images supported this observation.

CHAPTER 5

11β- Hydroxysteroid dehydrogenase1 activity as a read-out of NAD^+ depletion in a cell model of Poly-ADP Ribose polymerase overexpression

5.1. Introduction

NAD^+ distribution in the subcellular compartments, such as the mitochondria and the ER/SR, is the primary determinant of metabolic activity and redox homeostasis (Zhu et al., 2019).Therefore, balancing NAD^+ consumption and biosynthesis is essential to maintain cell functions (Strømland et al., 2021). Many NAD^+ consumers, e.g., PARPs, sirtuins, and CDs, are located in cellular compartments, including ER. It was suggested that increased PARP1 protein expression in the ER results in a higher NAD^+ consumption and increased PAR formation (Dölle et al., 2010). Therefore, to maintain NAD^+ availability, ER requires a continuous NAD^+ synthesis by NAD^+ biosynthetic enzymes or supplementation through communicating with the cytosol as a source of NAD^+.

In the previous chapter, we optimized the transfection of human liver cells (HepG2) and mouse skeletal muscle cells (C2C12) to generate a genetic model of ER NAD^+ depletion by upregulating PARP expression in the ER. We indicated that NAD^+ was depleted in cells expressing ER-PARP catalytic domain confirmed by PAR formation in Western blot images suggesting PARP hyperactivity.

In this chapter, we examine ER-cytosolic NAD(H) cross-talk in a genetic model of NAD^+ depletion using 11β-HSD1 activity as a read-out. Firstly, we examined the effect of NAD^+ precursor (NR) on restoring ER NAD availability in cells overexpressing PARP protein. Therefore, restoring ER-NAD^+ levels can be detected by increased PAR formation generated by PARP activity. Secondly, we tested whether depleted ER NAD^+ by PARP hyperactivity influenced a depletion in the activity oft he ER luminal

enzyme 11β-HSD1. Thirdly, we examined the effect of NAD^+ repletion by NR treatment in restoring the activity of 11β-HSD1. Finally, we assessed the link between PARP overexpression and the expression of genes involved in ER stress response. These experiments were done in human liver cells (HepG2) and mouse skeletal muscle cells (C2C12).

5.2. Results

5.2.1. ER-cytosol crosstalk in HepG2 overexpressing ER-PARP

5.2.1.1. NAD^+ precursor (NR) increased PAR formation

We started by investigating the role of NAD^+ repletion by NR on the formation of PAR. As expected, the Western blot image revealed a more intense PAR signal in cell lysate expressing ER-PARP1cd treated with NR (0.5 mM, 24 hours) than untreated cells expressing ER-PARP1cd (**Figure 5.1 (B)**)**.** No PAR signal was detected in cell lysate lacking ER-PARP1cd construct. GFP fluorescence indicated successful transfection by vectors encoding ER-EGFP and ER-PARP1cd (**Figure 5.1 (A)**).

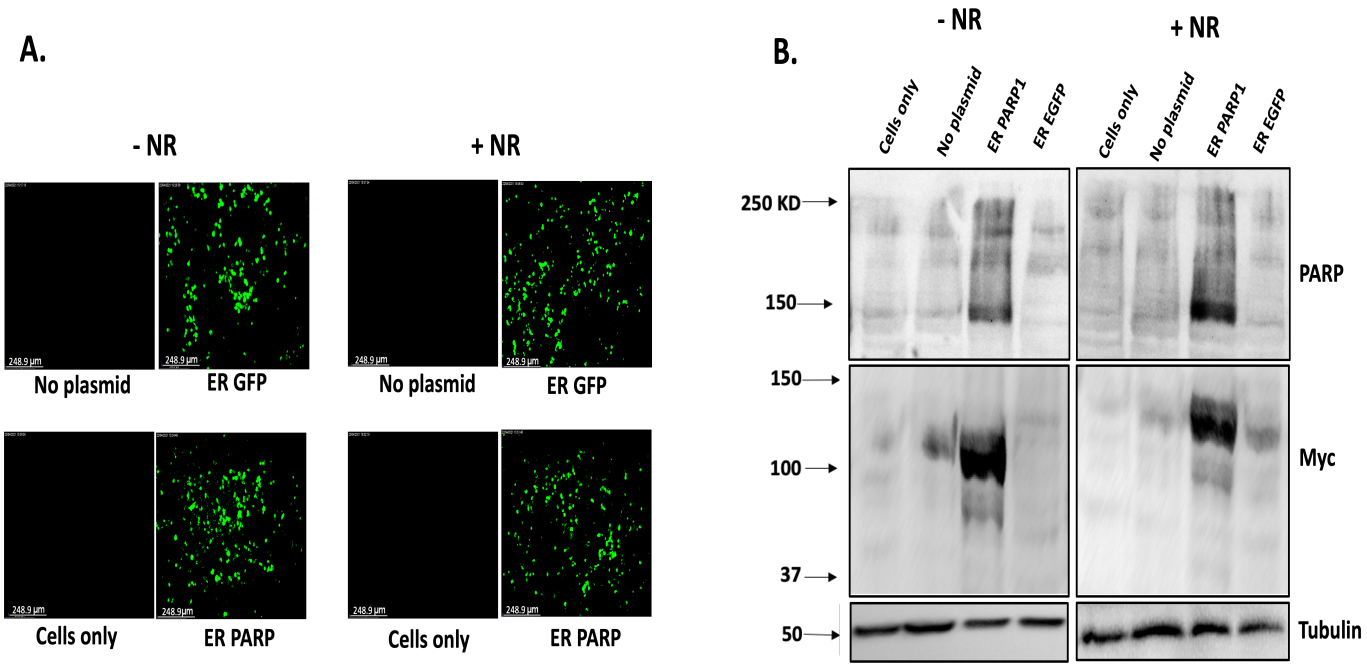


Figure 5.1. The effect of NR on PAR formation in HepG2.

A. Fluorescence was detected in cell lysate of ER-PARP1cd and ER EGFP treated and untreated with NR 48 hours after transfection. No green fluorescence was seen in cells only and cells without plasmid. **B.** Immunoblot analysis of cell lysate expressing PARPcd or EGFP-PARP1cd targeted to ER. PAR immunoblotting analysis using PAR antibody revealed detectable PAR formation in cells expressing ER-PARP1cd. PAR signal slightly improved with NR treatment. No PAR formation was seen in cell lysate of ER-EGFP, no plasmid, and cell only. Protein overexpression was detected by C-terminal Myc-tag. β tubulin was used as loading control.

5.2.1.2. 11β-HSD1 activity as a read-out of ER NAD^+ bioavailability in ER-PARP1cd overexpression cell model.

Then we examined the impact of ER NAD^+ depletion induced by PARP hyperactivity on 11β-HSD1 enzyme activity. Although the activity was decreased in all transfected cells (cells expressing ER-EGFP and ER-PARP1cd) compared to non-transfected cells (cells only and cells with lipofectamine only) (**Figure 5.2 (A)**), the depletion of the enzyme activity was more prominent in cells expressing ER-PARP1cd compared to cells expressing ER-EGFP only. However, following NR treatment, the enzyme activity was significantly restored in cells expressing ER-PARP1cd compared to untreated cells expressing the same construct (**Figure 5.2 (B)**). To confirm that 11β-HSD1 activity was not depleted due to low protein concentrations, we compared the total protein concentration among the transfected and non-transfected cells, which showed no significant difference **in (Figure 5.2 (C)**). Additionally, transfection with ER-EGFP and ER-PARP1cd constructs revealed a non-significant effect on cell viability assessed by the percentage reduction of Alamar blue (**Figure 5.2 (D)**).

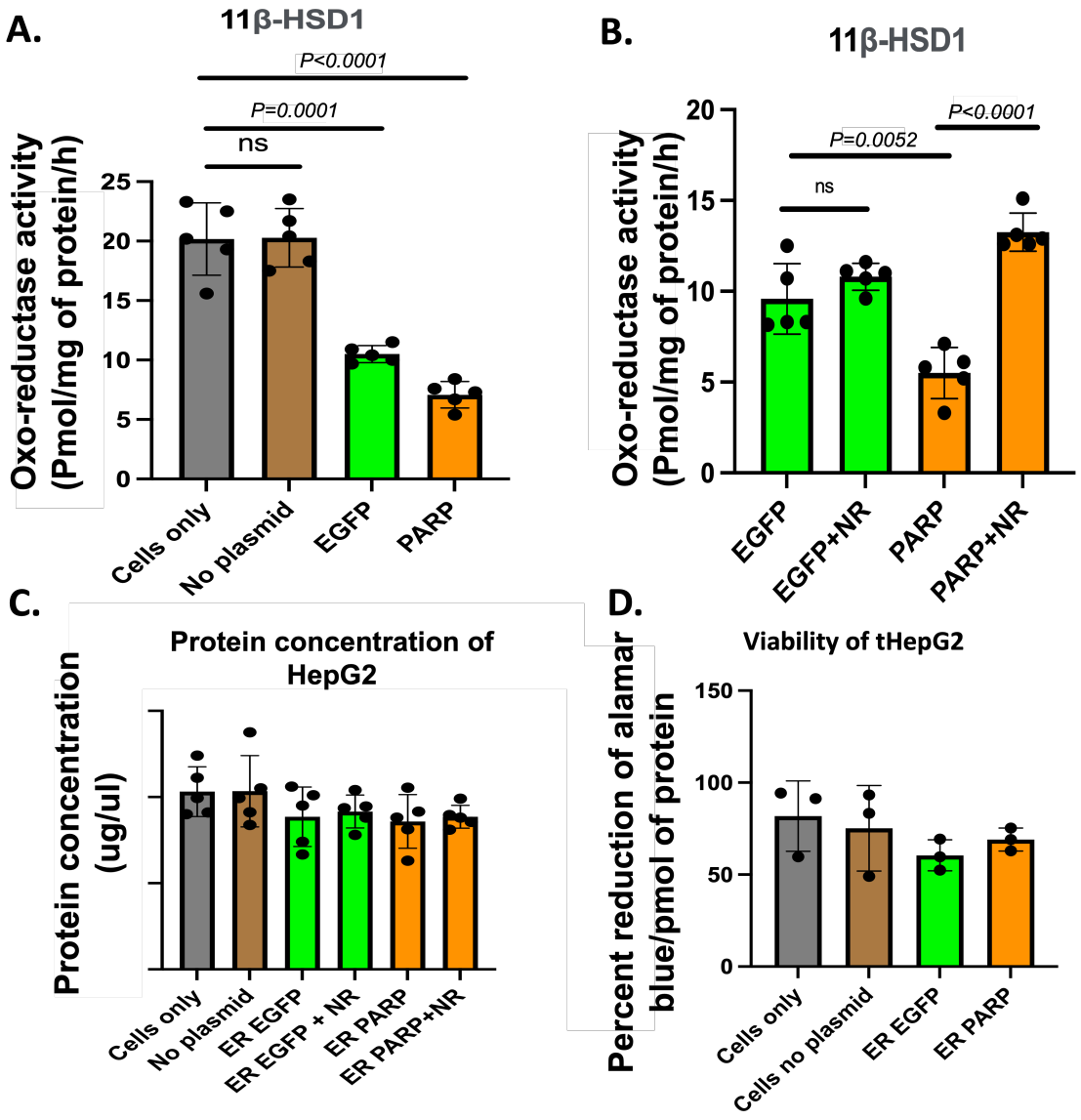


Figure 5.2. 11β-HSD1 oxo-reductase activity in transfected HepG2 (tHepG2).

A. 11β-HSD1 activity was reduced by 50% in cells expressing ER-EGFP (p=0.0004) and 65% in cells expressing ER-PARP1cd compared to cells only. **B.** Treatment with NR (0.5 mM, 24h) did not significantly improve enzyme activity in cells expressing ER-EGFP (p=0.098 compared to EGFP transfected cells), while it restored full 11β-HSD1 activity in cells expressing ER-PARP1cd (p<0.0001 copmared to PARPcd expressing cells) **C.** Protein concentration of transfected cells and controls was not altered. **D.** The viability of transfected cell was not affected as indicated by the percentage reduction of alamar blue**.** For A, B and C 5 and for D 3 independent experiments were performed.

5.2.1.3. ER stress gene expression in response to transfection with ER-PARP1cd and ER-EGFP constructs.

Although the viability of transfected HepG2 was intact, we examined whether transfection induced expression of ER stress genes. No significant changes in the expression of genes involved in ER stress response was seen in transfected and non-transfected cells (**Figure 5.3**).

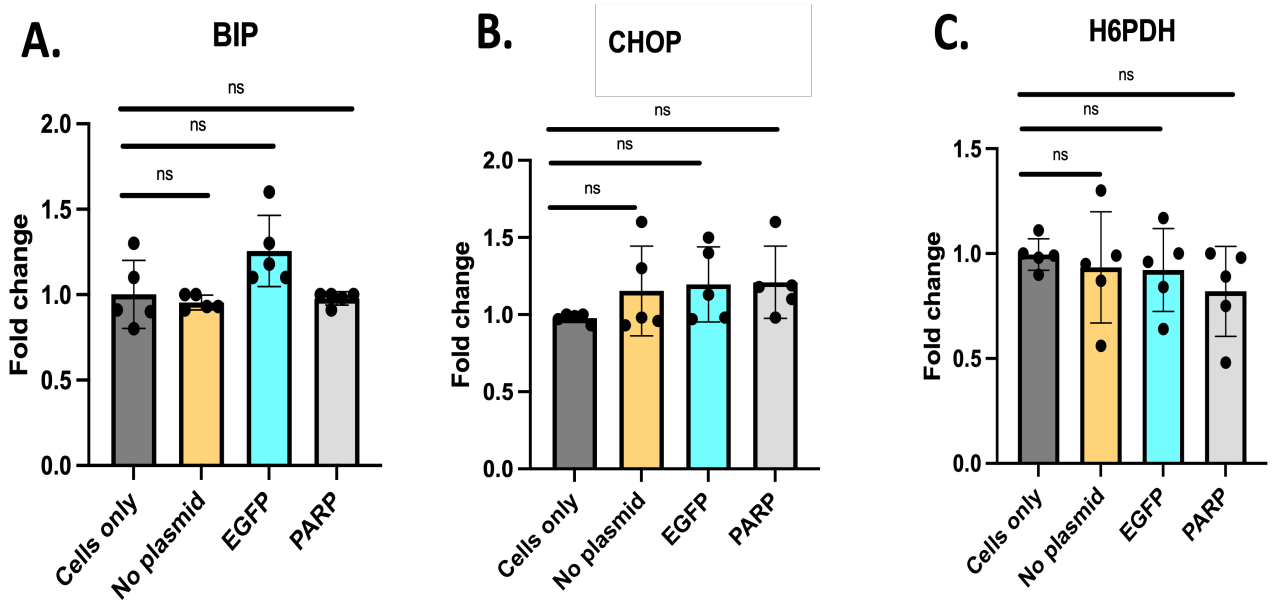


Figure 5.3. The effect of HepG2 transfection on genes involved in ER stress.

A. Binding immunoglobulin protein **(BIP**). **B.** CCAAT/enhancer binding protein homologous protein (CHOP). **C**. Hexose 6 phosphate dehydrogenase (H6PDH). A slight increase in BIP expression was seen in cells expressing ER-EGFP construct, with no increase in cells transfected with ER PARP1cd construct. No effect of transfection was seen on CHOP and H6PDH gene expressing between transfected and un-transfected cells. Gene expression was expressed as fold changes. Cells only (no treatment), no plasmid (lipofectamine only). Data from 5 independent experiments are shown.

Table 5.1. ∆Ct of genes involved in ER stress response in transfected HepG2.

Sample	BIP ∆Ct	Chop ∆Ct	H6PDH ∆Ct
Cells only	7.61	2.31	6.35
No plasmid	7.91	2.81	5.81
ER-EGFP	8.31	3.15	6.09
ER-PARP	8.77	3.41	5.98

5.2.2. Examining ER-cytosol crosstalk in C2C12 overexpressing ER-PARP1cd.

5.2.2.1. The effect of NR treatment on the formation of PAR protein.

Unlike in HepG2, the expression of PAR signal in transfected C2C12 is generally weak. This observation was seen after treatment with NR (0.5 mM, 24h). The signal was insufficient to reflect upon the signal intensity of PAR formation (**Figure 5.4 (B)**). No PAR formation was seen in cell lysate expressing ER-EGFP with and without NR treatment. Transfection was confirmed by the expression of GFP in cells transfected with ER-PARP1cd and ER-EGFP (**Figure 5.4 (A)**).

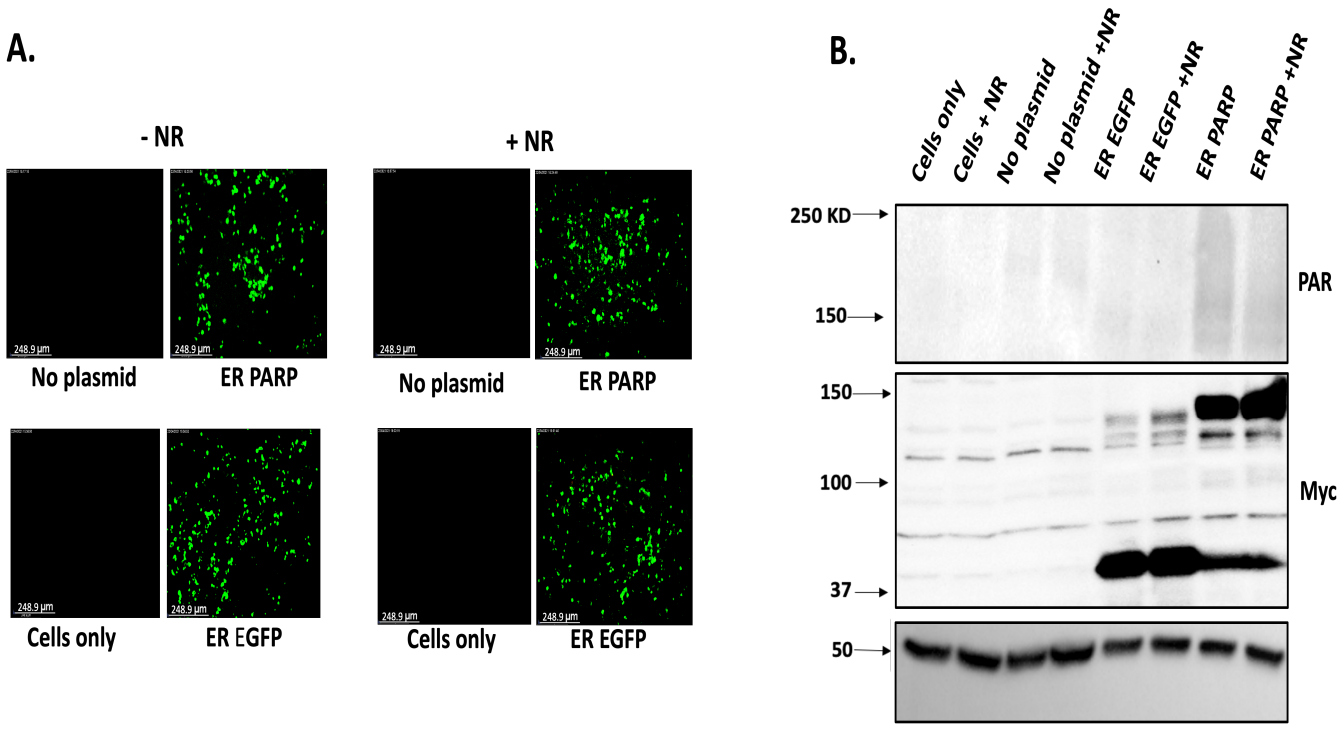


Figure 5.4. The effect of NR on PAR formation in C2C12.

A. Fluorescence was detected in cell lysate of ER-PARP1cd and ER EGFP transfected cells treated and untreated with NR 48 hours after transfection. No green fluorescence was seen in cells only and cells without plasmid. *Bar 248.9 μm.* **B.** Immunoblot analysis of cell lysate expressing PARP1cd or EGFP-PARPcd targeted to ER. PAR immunoblotting analysis using PAR antibody revealed detectable PAR formation in cells expressing ER-PARP1cd. PAR signal was also detected in cell lysate of ER-PARP treated with NR. No PAR formation was seen in cell lysate of ER-EGFP, no plasmid, and cell only. Protein overexpression was detected by C-terminal Myc-tag. β tubulin was used as loading control.

5.2.2.2. Time-point of assessing 11 β-HSD1 oxo-reductase activity in C2C12 myoblast.

To examine the activity of 11β-HSD1 as a read-out of NAD^+ modulation induced by ER-PARP1cd transfection in C2C12 myoblasts, we had to optimize the time required for the myoblasts to convert inactive 11-DHC to active corticosterone. Due to the limited transfection time (48 hours), C2C12 cannot be cultured to differentiate and form myotubes. Previously, we showed that 20 minutes is enough for C2C12 myotubes to convert ~20% of inactive 11-DHC to corticosterone. Cells were set at two different growth times (48-72 hours), and the conversion was measured after 6, 10, and 24 hours of incubation with inactive compound (H^3 11-DHC). Results showed that cells cultured for 48 hours could convert ~20 % of inactive 11-DHC after 10 hours of incubation (**Figure 5.5**). This was the time required for assessing 11β-HSD1 in transfected C2C12 myoblasts in the future.

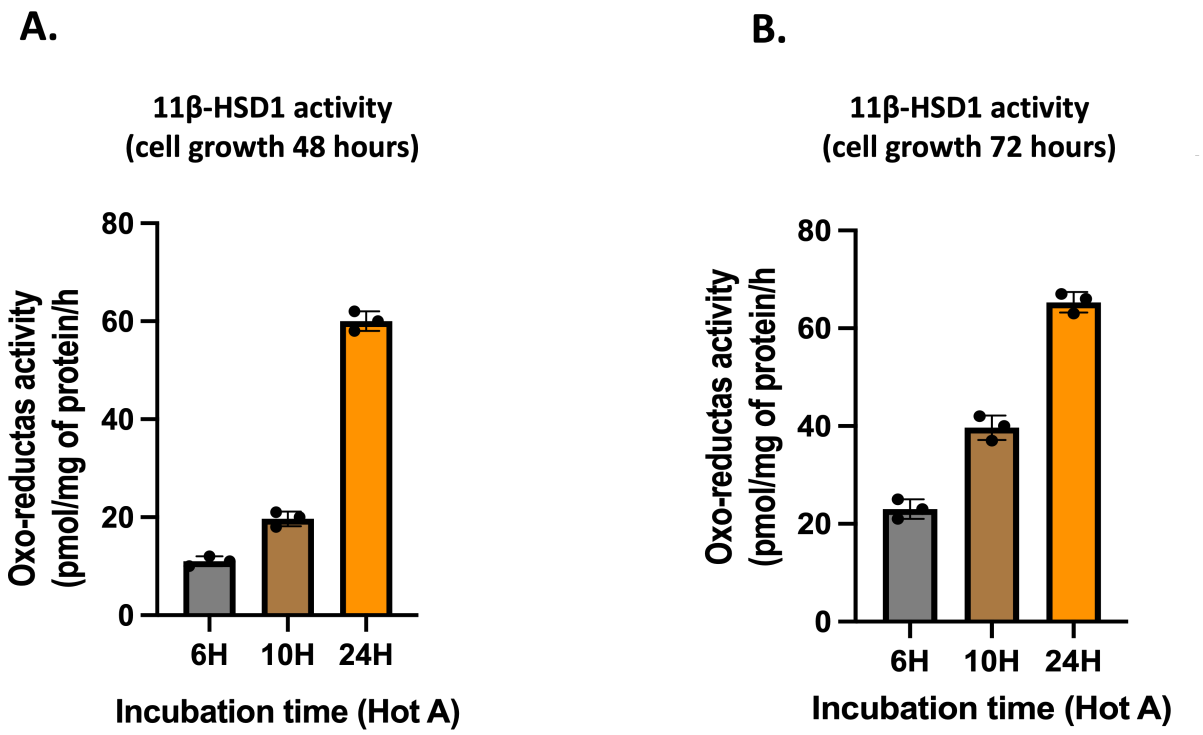


Figure 5.5. Optimization of 11 β-HSD1 oxo-reductase activity in non-transfected C2C12 myoblast.

The percent of conversion was measured after cells were grown for **A.** 48 hours and **B.** 72 hours. C2C12 myoblasts incubated with H^3 11-DHC (hot A) at different time points (6,10, 24 h) to examine the time required for conversion to H^3 corticosterone (hot B). We indicated that conversion was best seen 10 hours after incubation with H^3 11-DHC, when cells were cultured for 48 hours (approximately 20 % conversion). Data from 3 independent experiments are shown.

5.2.2.3. 11β-HSD1 activity as a read-out of ER NAD^+ bioavailability in ER-PARP1cd overexpression.

Then we examined the impact of ER NAD^+ depletion induced by PARP hyperactivity on 11β-HSD1 enzyme activity. Although lipofectamine affected the activity, as seen in cells with no plasmid (**Figure 5.6 (A)**), cells expressing ER-PARP1cd revealed more reduction in 11β-HSD1 enzyme activity compared to cells expressing ER-EGFP. The enzyme activity was restored in cells expressing ER-PARP1cd treated with NR (0.5 mM, 24h) compared to untreated cells expressing the same construct (**Figure 5.6 (B)**). Protein concentration was slightly lower in all transfected cells with no significant difference between the transfected groups (**Figure 5.6 (C)**). Cell viability was not different between transfected and non-transfected cells **(Figure 5.6 (D)**).

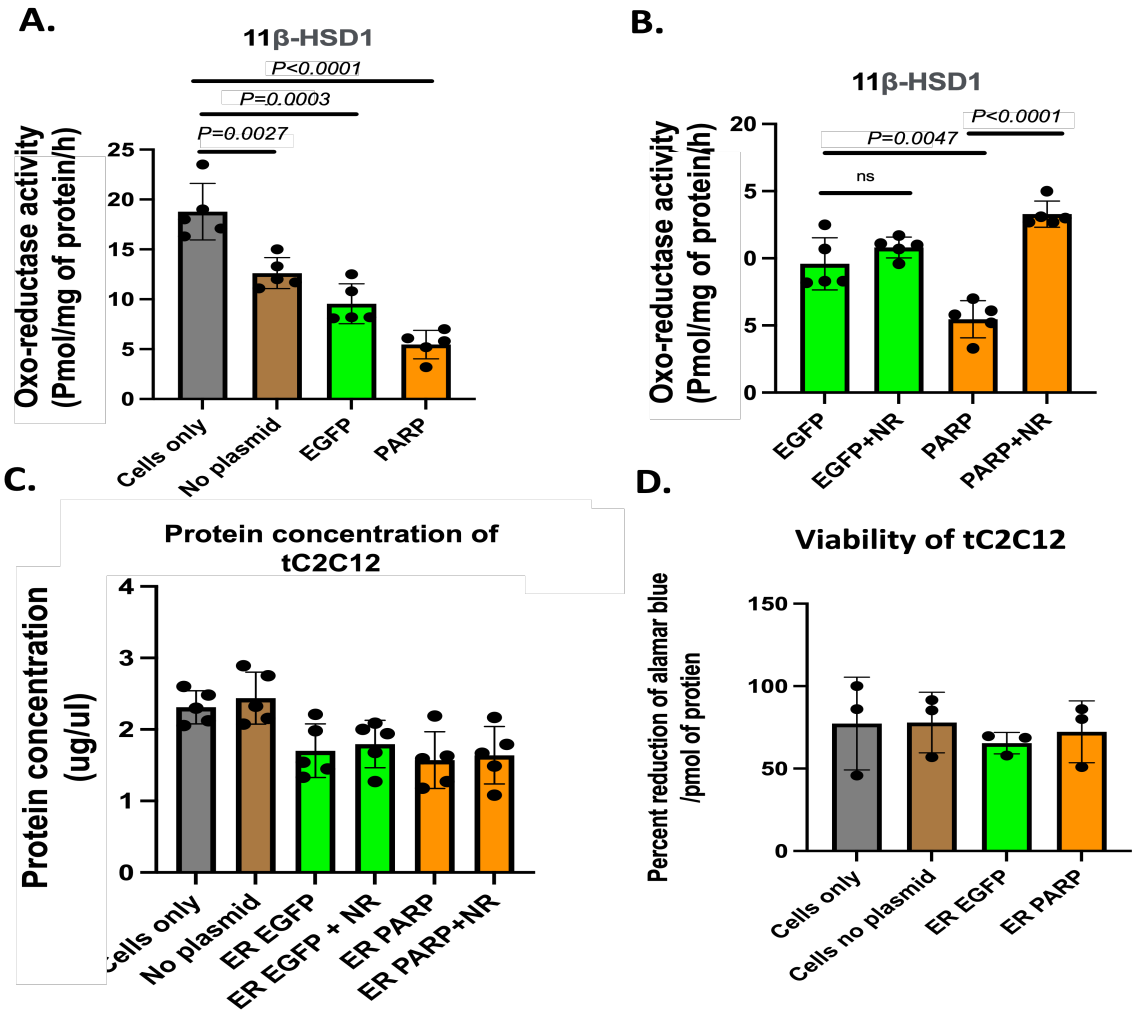


Figure 5.6. 11β-HSD1 oxo-reductase activity in transfected C2C12 (tC2C12) myotubes.

A. 11β-HSD1 activity was reduced in cells with no plasmid, cells expressing ER-EGFP and ER-PARP1cd compared to cells only (p=0.0027, p=0.0003, and p<0.0001 respectively) **B.** Treatment with NR (0.5 mM, 24h) restored 11β-HSD1 activity in 100% in cells expressing ER-PARP1cd (p<0.0001 comapred to PARPcd transfected cells). **C.** Protein concentration of transfected cells and controls was not different. **D.** The viability of transfected cell was not affected as indicated by the percentage reduction of alamar blue. For A, B and C 5 and for D 3 independent experiments were performed.

5.2.2.4. ER stress genes expression in response to transfection with ER-PARP1cd and ER-EGFP constructs.

We examined whether transfection induced the expression of ER stress genes. No significant changes in the expression of genes involved in ER stress response were seen in transfected and non-transfected cells (**Figure 5.7**).

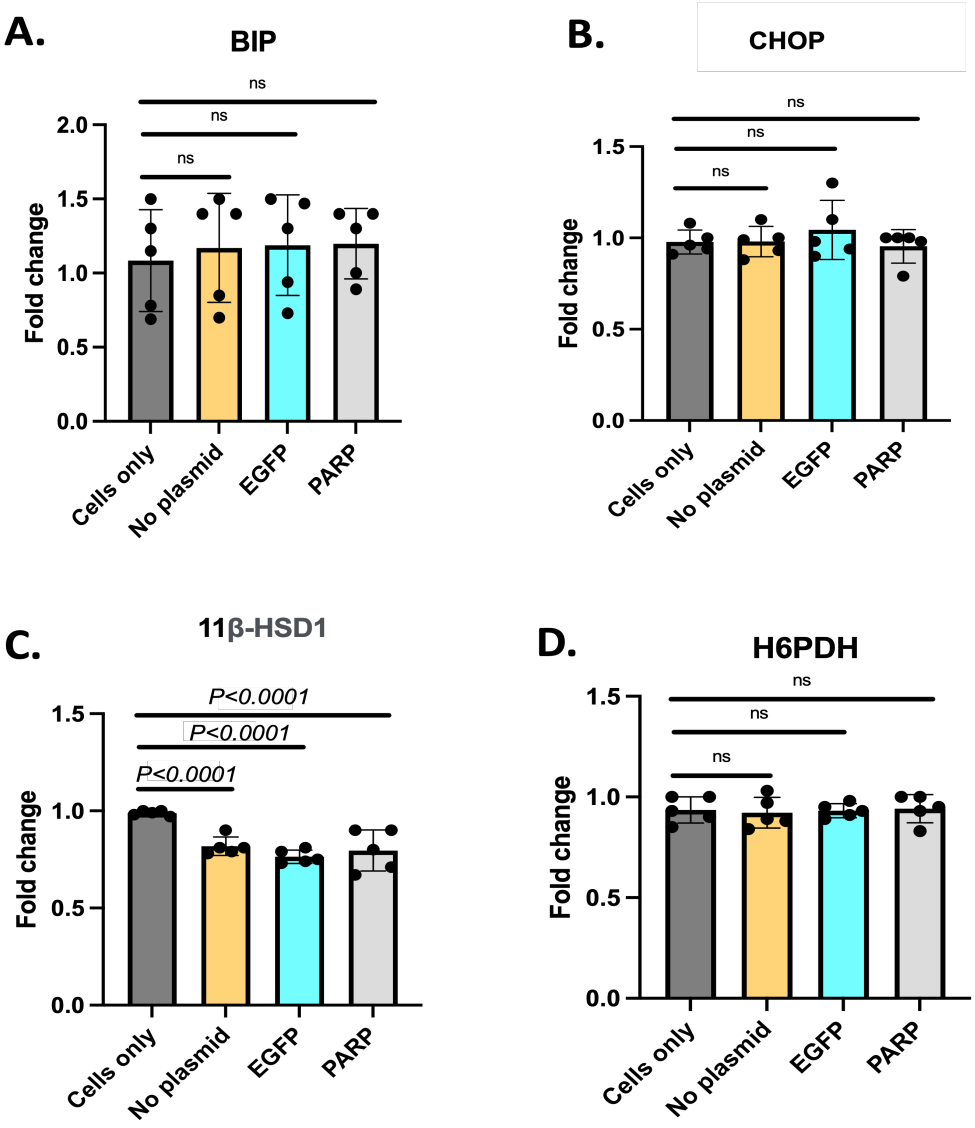


Figure 5.7. The effect of C2C12 transfection on genes involved in ER stress.

Gene expression expressed as fold changes. Cells only (no treatment), no plasmid (lipofectamine only). No significant effect of transfection was seen in the expression of **A.** Bip. **B.** CHOP **C.** The expression of 11β-HSD1 significantly decreased in all transfected cells ($p<0.0001$ compared to cells only)**. D.** H6PDH. Data from 5 independent experiments are shown.

Table 5.2. ∆Ct values of genes involved in ER stress response in transfected C2C12.

Sample	BIP ∆Ct	Chop ∆Ct	H6PDH ∆Ct	11β-HSD1 ∆Ct
Cells only	4.98	4.13	8.31	8.31
No plasmid	5.31	4.33	8.19	7.81
ER-EGFP	5.46	4.61	8.67	7.46
ER-PARP	5.13	4.11	8.97	7.53

5.3. Discussion

The ER-cytosol NAD(H) cross-talk has been examined previously in Chapter 3 by inhibiting cytosolic NAD^+ availability through FK866 that inhibits the NAMPT biosynthesis pathway to induce NAD^+ depletion. However, this chapter used a different mechanism to deplete NAD^+ by genetically targeting ER-PARP1cd to the ER, which led to increased activity of the NAD^+ dependent enzyme PARP1, and depleting ER NAD^+ availability. This model provides a different approach to investigating the cross-talk by depleting NAD^+ in the ER rather than the cytosol.

When HepG2 and C2C12 cells were targeted with ER PARP1cd fused with EGFP, the formation of PAR was seen from the cell lysate overexpressing PARP1cd. In contrast, detection of PAR formation was not seen from cell lysate expressing EGFP only. After treating transfected cells with NR (0.5 mM; 24h), detection of PAR formation slightly increased in cell lysate expressing ER-PARP1cd compared to cell lysate expressing the same construct without NR treatment, suggesting that restored cytosolic NAD^+ might have access to ER to support PAR formation. This observation was best seen in HepG2, while in C2C12, the expression of PAR was generally weaker than in HepG2, and NR treatment did not significantly enhance the expression of PAR. On the other hand, cell lysate lacking PARP1cd did not show detectable PAR formation, demonstrating the incapability of NR to increase PAR formation in the absence of catalytically active PARP.

To examine how ER-PARP overexpression impacts upon ER NAD^+ availability, we investigated the activity of ER luminal enzyme 11β-HSD1 as a read-out. As expected, NAD^+-dependent PARP1 hyperactivity reduced the oxo-reductase activity of the enzyme.

Although enzyme activity was reduced in all transfected cells (ER-PARP, ER-EGFP), cells expressing ER-PARPcd showed depleted activity by ~40% in HepG2 and ~ 50% in C2C12 compared to cells expressing ER-EGFP only. To confirm that reduced 11β-HSD1 activity is related to low NAD^+ level rather than reduced protein concentration, we checked protein concentration among transfected and non-transfected cells and saw no significant differences. In addition, cell viability was not diminished as a result of transfecting HepG2 and C2C12 with vectors encoding ER-PARP1cd and ER-EGFP.

Furthermore, we investigated the possible effect of transfection on the expression of genes involved in the ER stress response. We assessed the expression of CHOP, H6PDH, Bip, and 11β-HSD1 by qPCR, and the expression was normalized to the expression of GAPDH as a housekeeper gene. Results indicate no significant increase in the expression of ER stress genes in HepG2 and C2C12 in transfected cells compared to non-transfected cells. In addition, we indicate that NAD^+ depletion induced by ER-PARP overexpression was not sufficiently low to diminish cell viability and stimulate the ER stress response.

In conclusion, this chapter provides a different method to examine ER-cytosol NAD(H) cross-talk in a cell model where NAD^+ availability is depleted in the ER. The capacity of restoring 11β-HSD1 oxo-reductase activity by NR-induced NAD^+ repletion in cells overexpressing PARPcd suggests that ER might have access to cytosolic NAD^+ to enhance the enzyme activity.

CHAPTER 6

Final discussion and future direction

NAD^+ has been known for its central role in cellular energy production as an electron donor to generate ATP in the oxidation-reduction reactions in the TCA cycle (Houtkooper et al., 2010, Belenky et al., 2007). Its reduced and phosphorylated forms (NADH, NADP+, and NADPH) act as coenzymes for a set of cellular enzymatic reactions involved in energy metabolism, DNA repair, gene expression, and the regulation of cellular stress response

(Okabe et al., 2019, Fang et al., 2017). Evidence revealed a significant relationship between NAD^+ decline and the development of metabolic disorders such as fatty liver, skeletal muscle degeneration, and type 2 diabetes (Yoshino et al., 2011, Trammell et al., 2016b, Frederick et al., 2016, Zhou et al., 2016). Therefore, it is essential to understand the mechanisms that maintain cellular NAD^+ homeostasis.

The intracellular NAD^+ pool is separated by cellular compartments and is not equally distributed within subcellular organelles (Cambronne and Kraus, 2020). Therefore, biosynthesis of NAD^+ or supplementation by adjacent organelles is necessary to meet the subcellular organelle demand. It has been suggested that NAD^+ can transfer freely between the cytosol and the nucleus (Nikiforov et al., 2015), while in the mitochondria, the malate-aspartate shuttle system and other shuttles are known as a source of NADH (Satrústegui et al., 2007). However, the mechanism underlying the maintenance of the ER NAD^+ pool is not clearly understood.

The ER is the largest cellular organelle with a central role in maintaining Ca^{2+} homeostasis (Schwarz and Blower, 2016). In cellular metabolism, ER is the primary site for protein production, lipid biosynthesis, and glucose metabolism (Westrate et al., 2015). A balance between NAD^+ and NADH in the ER determines the optimum oxidizing and reducing

reactions to support protein folding and modification. Therefore, any disturbance in the ER redox homeostasis can stimulate ER stress responses (Gansemer et al., 2020).Many observations link a prolonged ER stress response to the progression of several diseases, such as type2 diabetes (Laybutt et al., 2007), atherosclerosis (Tsukano et al., 2010), and cancer (Fernandez et al., 2000).

In this project, we investigated the mechanism that maintains the ER NAD^+ availability, particularly the ER-cytosolic NAD^+ pool. The activity of 11 β-HSD1 enzyme was used as read-out as NADPH-dependent enzyme in the lumen of the ER. As a result of cytosolic NAD^+ depletion by the NAMPT inhibitor FK866, the oxo-reductase activity of 11 β-HSD1 significantly decreased. To examine if NAD^+ repletion with the NAD^+ precursor NR can rescue the enzyme activity, we showed that length ot treatment corresponded with the increased 11 β-HSD1 activity. In addition, our group has previously shown that the viability of C2C12 myotubes was intact in response to treatment with FK866 (100 nM, 24 hours) and NR (0.5 mM, 24 hours) (Fletcher, 2017). This observation suggests a possible communication of the ER-cytosol NAD^+ pool that allowed the ER to sense the modulation of cytosolic NAD^+ availability. Then we investigated the generalizability of these results in multiple metabolically active cell types, including mouse skeletal muscle myotubes (C2C12), a human hepatocellular carcinoma cell line (HepG2), human dermal fibroblasts (HDFn), and human kidney cell line (HEK293). Similar findings were observed in all cell types, suggesting that it is not a tissue-specific response but a common cellular mechanism that allowed NAD^+ entry into the ER to maintain redox homeostasis.

Due to the difficulty of measuring the subcellular NAD^+ pool, indirect visualization of compartment-specific NAD^+ availability was assessed in mitochondria, Golgi apparatus, cytosol, and ER (Dölle et al., 2010). This study indicated the availability of subcellular NAD^+ by detecting PAR polymers generated by the activity of the NAD^+-dependent enzyme PARP1. In addition, we established a genetically modified model of ER-PARP overexpression by targeting the catalytic domain of PARP1 into the ER to induce NAD^+ depletion. This model allowed assessment of the cross-talk by depleting ER NAD^+ level rather than cytosolic NAD^+ depletion by FK866.

We transfected two cell lines (C2C12 and HepG2) with vector encoding ER-PARPcd to induce PARP overexpression in the ER and vector encoding ER-EGFP only as a control. Due to the variability in cellular characteristics, we had to optimize the proper transfection conditions for each cell line. These conditions included cell density at the time of transfection, plasmid DNA concentration, transfection time, and the technique used for protein transfer. Successful transfection was indicated by the expression of GFP visualize by fluorescence microscopy. At the same time, PARP overexpression increased PAR signal formation, as seen in Western blot images of cell lysate expressing ER-PARPcd.

Then we assessed if ER NAD^+ depletion, induced by PARP hyperactivity, impacted 11 β-HSD1 oxo-reductase activity. Results showed that cells expressing ER-PARPcd has depleted 11 β-HSD1 compared to cells expressing ER-EGFP only. This observation was seen in both cell types, with no diminished cell viability in transfected cells. Repletion of NAD^+ with NR supplementation rescued ER NAD^+ availability as indicated by restored 11 β-HSD1 activity. Our observation suggests that ER could access cytosolic NAD^+ that

recompensates the consumption of ER NAD^+ by PARP activity. Then we assessed the impact of transfection with PARPcd on the expression of genes involved in ER stress response. No apparent effect was seen on the ER stress genes suggesting that NAD^+ was not low enough to induce ER stress.

There are several limitations in this project, which took time to complete due to the impact of the Covid-19 pandemic. First, the majority of our experiments were conducted *in vitro* cell models. The main disadvantage of these in vitro models is lacking the capability to represent the complexity of organs and interactions between different cell types (Ghallab, 2013). Second, despite the previous observation showing intact cell viability in C2C12 after treatment with FK866 and NR (Fletcher et al., 2017), this was not examined in other cell lines using caspase activity. However, we assessed the viability of the cells by the reduction of Alamar blue and the expression of genes linked to the ER stress response. Thirdly, although a previous study confirmed the expression of 11 β-HSD1 genes in HepG2 (Ignatova et al., 2009), this was not shown in this thesis. This could be related to the low sensitivity of TaqMan probes we used to detect 11 β-HSD1 gene expression. Fourthly, after we examined the cross talk in a model of NAD manipulation by FK866 and NR in C2C12, HepG2, HDFn, and HEK293, only two cell lines have been studied using the PAPR-induced NAD^+ depletion model. Due to the limited time and optimizing transfection procedures, studying PARP overexpression in HDFn and HEK293 was beyond the scope of this thesis.

Future research would include *in vivo* studies to fully understand mechanisms and factors that determine ER-cytosol NAD^+ cross talk. In this project, we considered NAD^+ depletion

based on PARP and PAR formation activity. This approach might be improved by measuring the actual NAD^+ level in cellular compartments by cell fractionation technique (Simpson and Pepperkok, 2006). To confirm the localization of PARP in the ER, it would be required to fuse PARPcd with ER marker binding immunoglobulin protein (BiP) (Haas, 1994). This would differentiate between protein accumulation in the ER and the cellular intermembrane space.

In conclusion, this thesis examined the association between cellular glucocorticoids and NAD^+ metabolism to investigate how the NAD^+ pool is regulated and maintained in the ER. Results suggests a possible ER-cytosol communication that allows NAD^+ entry into the ER. Two different methods were used to deplete the cellular NAD^+ pool. First, we used a NAMPT inhibitor (FK866) to deplete cytosolic NAD^+. Second, we induced ER NAD^+ depletion by genetically overexpressing ER-PARPcd as NAD^+ consuming enzyme. The ability of NAD^+ repletion with NR to rescue the ER NAD^+ pool and restore the activity of 11 β-HSD1 was validated in multiple cell types. This data would advance our understanding of the critical cellular biology and physiology that maintain ER NAD^+/NADH redox homeostasis. Further research is required to assess the cross-talk *in vivo* models, considering the complexity of the subcellular interactions in a living organism. **Figure 6.1** is showing an overview of results generated in this thesis.

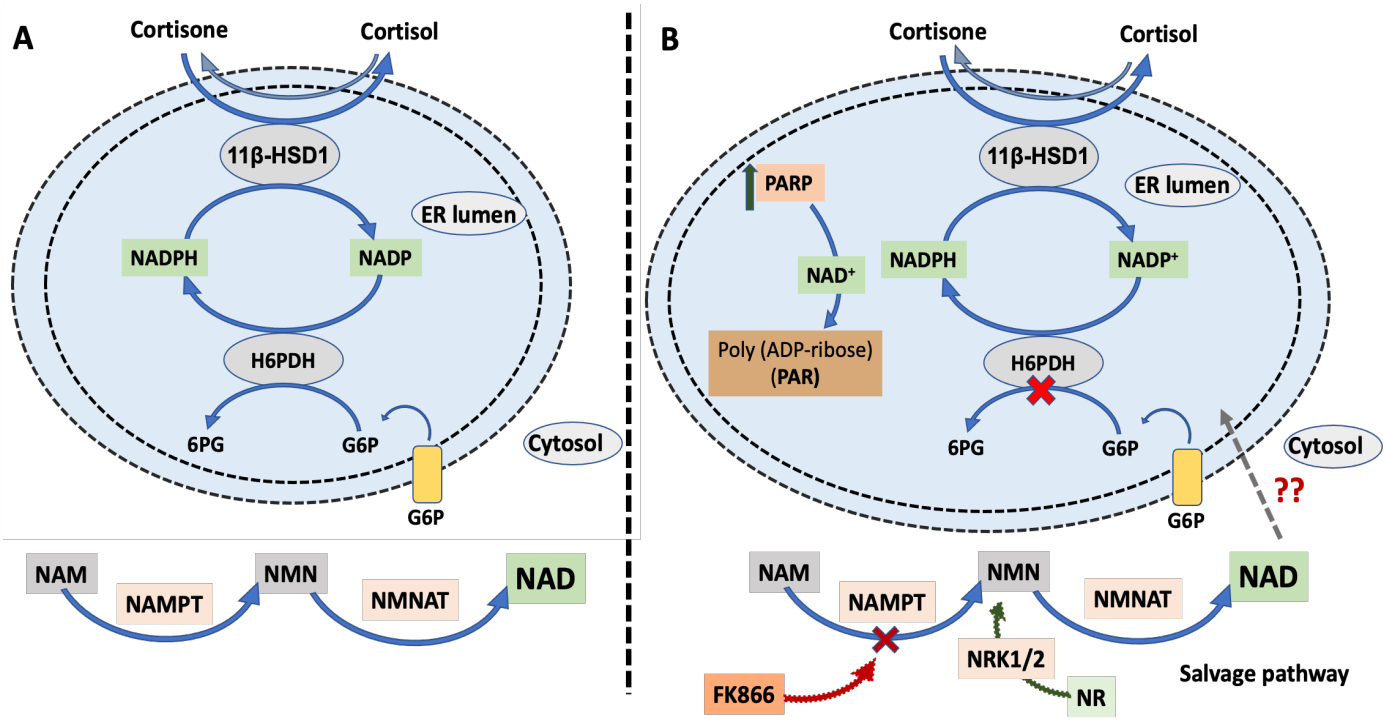


Figure 6.1. Schematic figure illustrating the results generated in this thesis.

A. 11 β-Hydroxysteroid dehydrogenase type 1 (11 β-HSD1) orientation in the endoplasmic reticulum and its connection with hexose-6-phosphate dehydrogenase (H6PDH). The glucose-6-phosphate (G6P) transporter and H6PDH system are required for G6P transfer to the H6PDH enzyme. G6P binds to H6PDH to generate 6-phospho-gluconolactone (6PG), which results in the production of NADPH within the ER lumen. The NADPH generated is used by 11 β-HSD1 to convert cortisone to cortisol. **B.** We examined the ER-cytosolic NAD^+ cross talk by modulating cytosolic NAD^+ with FK866 and NR using 11 β-HSD1 activity as a readout. This was examined in multiple cell types including H6PDH knock out mouse myoblasts. Additionally, we introduced a catalytically active ER-PARP plasmid to induce ER-PARP overexpression and deplete ER NAD^+. Results suggest that a ER-cytosolic NAD^+ communication might exist as indicated by the correspondence of 11 β-HSD1 activity with NAD^+ availability and repletion with NR.

References

AKSOY, P., ESCANDE, C., WHITE, T. A., THOMPSON, M., SOARES, S., BENECH, J. C. & CHINI, E. N. 2006a. Regulation of SIRT 1 mediated NAD dependent deacetylation: a novel role for the multifunctional enzyme CD38. *Biochem and biophys res commun.,* 349**:** 353-359.

AKSOY, P., WHITE, T. A., THOMPSON, M. & CHINI, E. N. 2006b. Regulation of intracellular levels of NAD: a novel role for CD38. *Biocheml and biophys res commun,* 345**:** 1386-1392.

ALVAREZ-GONZALEZ, R. & JACOBSON, M. K. 1987. Characterization of polymers of adenosine diphosphate ribose generated in vitro and in vivo. *Biochemistry,* 26**:** 3218-3224.

AUBRY, E. M. & ODERMATT, A. 2009. Retinoic acid reduces glucocorticoid sensitivity in C2C12 myotubes by decreasing 11β-Hydroxysteroid Dehydrogenase Type 1 and glucocorticoid receptor activities. *Endocrinol,* 150**:** 2700-2708.

BAI, P., CANTÓ, C., OUDART, H., BRUNYÁNSZKI, A., CEN, Y., THOMAS, C., YAMAMOTO, H., HUBER, A., KISS, B. & HOUTKOOPER, R. H. 2011. PARP-1 inhibition increases mitochondrial metabolism through SIRT1 activation. *Cell metabolism,* 13**,** 461-468.

BAMBERGER, C. M., SCHULTE, H. M. & CHROUSOS, G. P. 1996. Molecular determinants of glucocorticoid receptor function and tissue sensitivity to glucocorticoids. *Endocrine Reviews,* 17**,** 245-261.

BANHEGYI, G., BENEDETTI, A., FULCERI, R. & SENESI, S. 2004. Cooperativity between 11beta-hydroxysteroid dehydrogenase type 1 and hexose-6-phosphate dehydrogenase in the lumen of the endoplasmic reticulum. *J Biol Chem,* 279**,** 27017-21.

BÁNHEGYI, G. B., LUSINI, L., PUSKÁS, F., ROSSI, R., FULCERI, R., BRAUN, L., MILE, V. R., DI SIMPLICIO, P., MANDL, J. & BENEDETTI, A. 1999. Preferential Transport of Glutathione versusGlutathione disulfide in Rat Liver Microsomal Vesicles. *Journal of Biological Chemistry,* 274**,** 12213-12216.

BANKS, A. S., KON, N., KNIGHT, C., MATSUMOTO, M., GUTIÉRREZ-JUÁREZ, R., ROSSETTI, L., GU, W. & ACCILI, D. 2008. SirT1 gain of function increases energy efficiency and prevents diabetes in mice. *Cell metabolism,* 8**,** 333-341.

BELENKY, P., BOGAN, K. L. & BRENNER, C. 2007. NAD+ metabolism in health and disease. *Trends Biochem Sci,* 32**,** 12-9.

BERGER, F., RAMÍREZ-HERNÁNDEZ, M. A. H. & ZIEGLER, M. 2004. The new life of a centenarian: signalling functions of NAD (P). *Trends in biochemical sciences,* 29**,** 111-118.

BIEGANOWSKI, P. & BRENNER, C. 2004. Discoveries of nicotinamide riboside as a nutrient and conserved NRK genes establish a Preiss-Handler independent route to NAD+ in fungi and humans. *Cell,* 117**,** 495-502.

BLANCHER, C. & JONES, A. 2001. SDS-PAGE and western blotting techniques. *Metastasis research protocols: volume I: analysis of cells and tissues***,** 145-162.

BLAND, R., WORKER, C. A., NOBLE, B. S., EYRE, L. J., BUJALSKA, I. J., SHEPPARD, M. C., STEWART, P. M. & HEWISON, M. 1999. Characterization of 11beta-hydroxysteroid

dehydrogenase activity and corticosteroid receptor expression in human osteosarcoma cell lines. *J Endocrinol,* 161**,** 455-64.
BLAU, H. M., PAVLATH, G. K., HARDEMAN, E. C., CHIU, C.-P., SILBERSTEIN, L., WEBSTER, S. G., MILLER, S. C. & WEBSTER, C. 1985. Plasticity of the differentiated state. *Science,* 230**,** 758-766.
BOGAN, K. L. & BRENNER, C. 2008. Nicotinic acid, nicotinamide, and nicotinamide riboside: a molecular evaluation of NAD+ precursor vitamins in human nutrition. *Annual review of nutrition,* 28**,** 115-130.
BOLLET, A. J. 1992. Politics and pellagra: the epidemic of pellagra in the US in the early twentieth century. *The Yale journal of biology and medicine,* 65**,** 211.
BRAIDY, N., BERG, J., CLEMENT, J., KHORSHIDI, F., POLJAK, A., JAYASENA, T., GRANT, R. & SACHDEV, P. 2019. Role of nicotinamide adenine dinucleotide and related precursors as therapeutic targets for age-related degenerative diseases: rationale, biochemistry, pharmacokinetics, and outcomes. *Antioxidants & Redox Signaling,* 30**,** 251-294.
BROWN, R., DIAZ, R., ROBSON, A., KOTELEVTSEV, Y., MULLINS, J., KAUFMAN, M. & SECKL, J. 1996. The ontogeny of 11 beta-hydroxysteroid dehydrogenase type 2 and mineralocorticoid receptor gene expression reveal intricate control of glucocorticoid action in development. *Endocrinology,* 137**,** 794-797.
CAMBRONNE, X. A. & KRAUS, W. L. 2020. Location, Location, Location: Compartmentalization of NAD(+) synthesis and functions in mammalian cells. *Trends Biochem Sci,* 45**,** 858-873.
CANTÓ, C., GERHART-HINES, Z., FEIGE, J. N., LAGOUGE, M., NORIEGA, L., MILNE, J. C., ELLIOTT, P. J., PUIGSERVER, P. & AUWERX, J. 2009. AMPK regulates energy expenditure by modulating NAD+ metabolism and SIRT1 activity. *Nature,* 458**,** 1056-1060.
CANTÓ, C., HOUTKOOPER, R. H., PIRINEN, E., YOUN, D. Y., OOSTERVEER, M. H., CEN, Y., FERNANDEZ-MARCOS, P. J., YAMAMOTO, H., ANDREUX, P. A., CETTOUR-ROSE, P., GADEMANN, K., RINSCH, C., SCHOONJANS, K., SAUVE, A. A. & AUWERX, J. 2012. The NAD(+) precursor nicotinamide riboside enhances oxidative metabolism and protects against high-fat diet-induced obesity. *Cell Metab,* 15**,** 838-47.
CANTÓ, C., MENZIES, K. J. & AUWERX, J. 2015. NAD+ metabolism and the control of energy homeostasis: a balancing act between mitochondria and the nucleus. *Cell metabolism,* 22**,** 31-53.
CATON, P. W., NAYUNI, N. K., KIESWICH, J., KHAN, N. Q., YAQOOB, M. M. & CORDER, R. 2010. Metformin suppresses hepatic gluconeogenesis through induction of SIRT1 and GCN5. *Journal of Endocrinology,* 205**,** 97.
CHAMBON, P., WEILL, J. & MANDEL, P. 1963. Nicotinamide mononucleotide activation of a new DNA-dependent polyadenylic acid synthesizing nuclear enzyme. *Biochemical and biophysical research communications,* 11**,** 39-43.
CHANG, H.-C. & GUARENTE, L. 2014. SIRT1 and other sirtuins in metabolism. *Trends in Endocrinolo & Metabolism,* 25**,** 138-145.
CHEN, S., NOVICK, P. & FERRO-NOVICK, S. 2013. ER structure and function. *Current opinion in cell biology,* 25**,** 428-433.

COLLARD, F., COLLET, J.-F., GERIN, I., VEIGA-DA-CUNHA, M. & VAN SCHAFTINGEN, E. 1999. Identification of the cDNA encoding human 6-phosphogluconolactonase, the enzyme catalyzing the second step of the pentose phosphate pathway. *FEBS Letters,* 459**,** 223-226.

COOPER, M. S., WALKER, E. A., BLAND, R., FRASER, W. D., HEWISON, M. & STEWART, P. M. 2000. Expression and functional consequences of 11beta-hydroxysteroid dehydrogenase activity in human bone. *Bone,* 27**,** 375-81.

CSALA, M., BÁNHEGYI, G. & BENEDETTI, A. 2006. Endoplasmic reticulum: A metabolic compartment. *FEBS Letters,* 580**,** 2160-2165.

CUYÀS, E., VERDURA, S., LLORACH-PARÉS, L., FERNÁNDEZ-ARROYO, S., JOVEN, J., MARTIN-CASTILLO, B., BOSCH-BARRERA, J., BRUNET, J., NONELL-CANALS, A. & SANCHEZ-MARTINEZ, M. 2018. Metformin is a direct SIRT1-activating compound: computational modeling and experimental validation. *Frontiers in endocrinology,* 9**,** 657.

DALL, M., TRAMMELL, S. A., ASPING, M., HASSING, A. S., AGERHOLM, M., VIENBERG, S. G., GILLUM, M. P., LARSEN, S. & TREEBAK, J. T. 2019. Mitochondrial function in liver cells is resistant to perturbations in NAD+ salvage capacity. *Journal of Biological Chemistry,* 294**,** 13304-13326.

DE FIGUEIREDO, L. F., GOSSMANN, T. I., ZIEGLER, M. & SCHUSTER, S. 2011. Pathway analysis of NAD+ metabolism. *Biochemical Journal,* 439**,** 341-348.

DI STEFANO, M. & CONFORTI, L. 2013. Diversification of NAD biological role: the importance of location. *The FEBS journal,* 280**,** 4711-4728.

DÖLLE, C., HVIDSTEN SKOGE, R., R VANLINDEN, M. & ZIEGLER, M. 2013. NAD biosynthesis in humans-enzymes, metabolites and therapeutic aspects. *Current topics in medicinal chemistry,* 13**,** 2907-2917.

DÖLLE, C., NIERE, M., LOHNDAL, E. & ZIEGLER, M. 2010. Visualization of subcellular NAD pools and intra-organellar protein localization by poly-ADP-ribose formation. *Cellular and molecular life sciences,* 67**,** 433-443.

DOLLE, C., SKOGE, R. H., VANLINDEN, M. R. & ZIEGLER, M. 2013. NAD biosynthesis in humans--enzymes, metabolites and therapeutic aspects. *Curr Top Med Chem,* 13**,** 2907-17.

DOLLERUP, O. L., CHRISTENSEN, B., SVART, M., SCHMIDT, M. S., SULEK, K., RINGGAARD, S., STØDKILDE-JØRGENSEN, H., MØLLER, N., BRENNER, C. & TREEBAK, J. T. 2018. A randomized placebo-controlled clinical trial of nicotinamide riboside in obese men: safety, insulin-sensitivity, and lipid-mobilizing effects. *The American journal of clinical nutrition,* 108**,** 343-353.

DOLOPIKOU, C., KOURTZIDIS, I. A., MARGARITELIS, N. V., VRABAS, I. S., KOIDOU, I., KYPAROS, A., THEODOROU, A. A., PASCHALIS, V. & NIKOLAIDIS, M. G. 2020. Acute nicotinamide riboside supplementation improves redox homeostasis and exercise performance in old individuals: a double-blind cross-over study. *European journal of nutrition,* 59**,** 505-515.

DU, L., ZHANG, X., HAN, Y. Y., BURKE, N. A., KOCHANEK, P. M., WATKINS, S. C., GRAHAM, S. H., CARCILLO, J. A., SZABÓ, C. & CLARK, R. S. B. 2003. Intra-mitochondrial Poly(ADP-ribosylation) Contributes to NAD+ Depletion and Cell Death Induced by Oxidative Stress*. *Journal of Biological Chemistry,* 278**,** 18426-18433.

ERION, D. M., YONEMITSU, S., NIE, Y., NAGAI, Y., GILLUM, M. P., HSIAO, J. J., IWASAKI, T., STARK, R., WEISMANN, D. & YU, X. X. 2009. SirT1 knockdown in liver decreases basal hepatic glucose production and increases hepatic insulin responsiveness in diabetic rats. *Proceedings of the National Academy of Sciences,* 106**,** 11288-11293.

FANG, E. F., LAUTRUP, S., HOU, Y., DEMAREST, T. G., CROTEAU, D. L., MATTSON, M. P. & BOHR, V. A. 2017. NAD+ in aging: molecular mechanisms and translational implications. *Trends in molecular medicine,* 23**,** 899-916.

FAWCETT, D. W. 1966. Atlas of fine structure.

FEDE, G., SPADARO, L., TOMASELLI, T., PRIVITERA, G., GERMANI, G., TSOCHATZIS, E., THOMAS, M., BOULOUX, P. M., BURROUGHS, A. K. & PURRELLO, F. 2012. Adrenocortical dysfunction in liver disease: a systematic review. *Hepatology,* 55**,** 1282-1291.

FERNANDEZ, P. M., TABBARA, S. O., JACOBS, L. K., MANNING, F. C., TSANGARIS, T. N., SCHWARTZ, A. M., KENNEDY, K. A. & PATIERNO, S. R. 2000. Overexpression of the glucose-regulated stress gene GRP78 in malignant but not benign human breast lesions. *Breast cancer research and treatment,* 59**,** 15-26.

FLETCHER, R. 2017. *Vitamin B3 salvage and NAD\(^+\) metabolism in skeletal muscle.* University of Birmingham.

FLETCHER, R. S., RATAJCZAK, J., DOIG, C. L., OAKEY, L. A., CALLINGHAM, R., DA SILVA XAVIER, G., GARTEN, A., ELHASSAN, Y. S., REDPATH, P., MIGAUD, M. E., PHILP, A., BRENNER, C., CANTO, C. & LAVERY, G. G. 2017. Nicotinamide riboside kinases display redundancy in mediating nicotinamide mononucleotide and nicotinamide riboside metabolism in skeletal muscle cells. *Molecular Metabolism,* 6**,** 819-832.

FORTERRE, A., JALABERT, A., BERGER, E., BAUDET, M., CHIKH, K., ERRAZURIZ, E., DE LARICHAUDY, J., CHANON, S., WEISS-GAYET, M. & HESSE, A.-M. 2014. Proteomic analysis of C2C12 myoblast and myotube exosome-like vesicles: a new paradigm for myoblast-myotube cross talk? *PloS one,* 9**,** e84153.

FREDERICK, D. W., LORO, E., LIU, L., DAVILA, A., CHELLAPPA, K., SILVERMAN, I. M., QUINN, W. J., GOSAI, S. J., TICHY, E. D. & DAVIS, J. G. 2016. Loss of NAD homeostasis leads to progressive and reversible degeneration of skeletal muscle. *Cell metabolism,* 24**,** 269-282.

FRICKER, R. A., GREEN, E. L., JENKINS, S. I. & GRIFFIN, S. M. 2018. The influence of nicotinamide on health and disease in the central nervous system. *International Journal of Tryptophan Research,* 11**,** 1178646918776658.

FRIEDMAN, J. R. & VOELTZ, G. K. 2011. The ER in 3D: a multifunctional dynamic membrane network. *Trends Cell Biol,* 21**,** 709-17.

GANSEMER, E. R., MCCOMMIS, K. S., MARTINO, M., KING-MCALPIN, A. Q., POTTHOFF, M. J., FINCK, B. N., TAYLOR, E. B. & RUTKOWSKI, D. T. 2020. NADPH and Glutathione Redox Link TCA Cycle Activity to Endoplasmic Reticulum Homeostasis. *iScience,* 23**,** 101116.

GAO, H. & XU, X. 2012. The cyanobacterial NAD kinase gene sll1415 is required for photoheterotrophic growth and cellular redox homeostasis in Synechocystis sp. strain PCC 6803. *Journal of bacteriology,* 194**,** 218-224.

GARTEN, A., PETZOLD, S., KÖRNER, A., IMAI, S.-I. & KIESS, W. 2009. Nampt: linking NAD biology, metabolism and cancer. *Trends in Endocrinology & Metabolism,* 20**,** 130-138.

GARTEN, A., SCHUSTER, S., PENKE, M., GORSKI, T., DE GIORGIS, T. & KIESS, W. 2015. Physiological and pathophysiological roles of NAMPT and NAD metabolism. *Nature Reviews Endocrinology,* 11**,** 535-546.

GATHERCOLE, L. L., LAVERY, G. G., MORGAN, S. A., COOPER, M. S., SINCLAIR, A. J., TOMLINSON, J. W. & STEWART, P. M. 2013. 11β-Hydroxysteroid dehydrogenase 1: translational and therapeutic aspects. *Endocrine reviews,* 34**,** 525-555.

GHALLAB, A. 2013. In vitro test systems and their limitations. *Excli j,* 12**,** 1024-6.

GINGRICH, W. & SCHLENK, F. 1944. Codehydrogenase I and Other Pyridinium Compounds as V-Factor for Hemophilus influenzae and H. parainfluenzae. *Journal of bacteriology,* 47**,** 535-550.

GROSSMAN, A., PERRY, L., SCHALLY, A. V., REES, L., NIEUWENHUYZEN KRUSEMAN, A. C., TOMLIN, S., COY, D. H., COMARU-SCHALLY, A.-M. & BESSER, G. M. 1982. NEW HYPOTHALAMIC HORMONE, CORTICOTROPIN-RELEASING FACTOR, SPECIFICALLY STIMULATES THE RELEASE OF ADRENOCORTICOTROPIC HORMONE AND CORTISOL IN MAN. *The Lancet,* 319**,** 921-922.

GUARENTE, L. 2014. Linking DNA damage, NAD+/SIRT1, and aging. *Cell metabolism,* 20**,** 706-707.

GUSE, A. H., DA SILVA, C. P., BERG, I., SKAPENKO, A. L., WEBER, K., HEYER, P., HOHENEGGER, M., ASHAMU, G. A., SCHULZE-KOOPS, H. & POTTER, B. V. 1999. Regulation of calcium signalling in T lymphocytes by the second messenger cyclic ADP-ribose. *Nature,* 398**,** 70-73.

HAAS, I. 1994. BiP (GRP78), an essential hsp70 resident protein in the endoplasmic reticulum. *Experientia,* 50**,** 1012-1020.

HAMMAMI, M. M. & SIITERI, P. K. 1991. Regulation of 11 beta-hydroxysteroid dehydrogenase activity in human skin fibroblasts: enzymatic modulation of glucocorticoid action. *J Clin Endocrinol Metab,* 73**,** 326-34.

HARDEN, A. & YOUNG, W. J. 1906. The alcoholic ferment of yeast-juice. *Proceedings of the Royal Society of London. Series B, Containing Papers of a Biological Character,* 77**,** 405-420.

HARDY, R., FILER, A., COOPER, M., PARSONAGE, G., RAZA, K., HARDIE, D., RABBITT, E., STEWART, P., BUCKLEY, C. & HEWISON, M. 2006a. Differential expression, function and response to inflammatory stimuli of 11??-hydroxysteroid dehydrogenase type 1 in human fibroblasts: A mechanism for tissue-specific regulation of inflammation. *Arthritis research & therapy,* 8**,** R108.

HARDY, R. S., FILER, A., COOPER, M. S., PARSONAGE, G., RAZA, K., HARDIE, D. L., RABBITT, E. H., STEWART, P. M., BUCKLEY, C. D. & HEWISON, M. 2006b. Differential expression, function and response to inflammatory stimuli of 11β-hydroxysteroid dehydrogenase type 1 in human fibroblasts: a mechanism for tissue-specific regulation of inflammation. *Arthritis research & therapy,* 8**,** R108.

HEGYI, J., SCHWARTZ, R. A. & HEGYI, V. 2004. Pellagra: dermatitis, dementia, and diarrhea. *International journal of dermatology,* 43**,** 1-5.

HERCEG, Z. & WANG, Z. Q. 2001. Functions of poly(ADP-ribose) polymerase (PARP) in DNA repair, genomic integrity and cell death. *Mutat Res,* 477**,** 97-110.
HERITAGE, D. & WONDERLIN, W. F. 2001. Translocon pores in the endoplasmic reticulum are permeable to a neutral, polar molecule. *Journal of Biological Chemistry,* 276**,** 22655-22662.
HOTAMISLIGIL, G. S. 2010. Endoplasmic Reticulum Stress and the Inflammatory Basis of Metabolic Disease. *Cell,* 140**,** 900-917.
HOUTKOOPER, R. H., CANTO, C., WANDERS, R. J. & AUWERX, J. 2010. The secret life of NAD+: an old metabolite controlling new metabolic signaling pathways. *Endocr Rev,* 31**,** 194-223.
HOUTKOOPER, R. H., PIRINEN, E. & AUWERX, J. 2012. Sirtuins as regulators of metabolism and healthspan. *Nature reviews Molecular cell biology,* 13**,** 225-238.
HOWARD, M., GRIMALDI, J. C., BAZAN, J. F., LUND, F. E., SANTOS-ARGUMEDO, L., PARKHOUSE, R., WALSETH, T. F. & LEE, H. C. 1993. Formation and hydrolysis of cyclic ADP-ribose catalyzed by lymphocyte antigen CD38. *Science,* 262**,** 1056-1059.
HUDSON, D. A., GANNON, S. A. & THORPE, C. 2015. Oxidative protein folding: From thiol–disulfide exchange reactions to the redox poise of the endoplasmic reticulum. *Free Radical Biology and Medicine,* 80**,** 171-182.
HWANG, C., SINSKEY, A. J. & LODISH, H. F. 1992. Oxidized redox state of glutathione in the endoplasmic reticulum. *Science,* 257**,** 1496-1502.
IGNATOVA, I. D., KOSTADINOVA, R. M., GOLDRING, C. E., NAWROCKI, A. R., FREY, F. J. & FREY, B. M. 2009. Tumor necrosis factor-α upregulates 11β-hydroxysteroid dehydrogenase type 1 expression by CCAAT/enhancer binding protein-β in HepG2 cells. *American journal of physiology-endocrinology and metabolism,* 296**,** E367-E377.
IMAI, S.-I., ARMSTRONG, C. M., KAEBERLEIN, M. & GUARENTE, L. 2000. Transcriptional silencing and longevity protein Sir2 is an NAD-dependent histone deacetylase. *Nature,* 403**,** 795-800.
IMAI, S.-I. & GUARENTE, L. 2014. NAD+ and sirtuins in aging and disease. *Trends in cell biology,* 24**,** 464-471.
ISSELBACHER, K. J. & GREENBERGER, N. J. 1964. Metabolic effects of alcohol on the liver. *New England Journal of Medicine,* 270**,** 351-356.
ITO, S., MURPHY, C. G., DOUBROVINA, E., JASIN, M. & MOYNAHAN, M. E. 2016. PARP inhibitors in clinical use induce genomic instability in normal human cells. *PloS one,* 11**,** e0159341.
JAVLE, M. & CURTIN, N. 2011. The role of PARP in DNA repair and its therapeutic exploitation. *British journal of cancer,* 105**,** 1114-1122.
JUAREZ-SALINAS, H., LEVI, V., JACOBSON, E. & JACOBSON, M. 1982. Poly (ADP-ribose) has a branched structure in vivo. *Journal of Biological Chemistry,* 257**,** 607-609.
JUKARAINEN, S., HEINONEN, S., RÄMÖ, J. T., RINNANKOSKI-TUIKKA, R., RAPPOU, E., TUMMERS, M., MUNIANDY, M., HAKKARAINEN, A., LUNDBOM, J. & LUNDBOM, N. 2016. Obesity is associated with low NAD+/SIRT pathway expression in adipose tissue of BMI-discordant monozygotic twins. *The Journal of Clinical Endocrinology,* 101**,** 275-283.

KAWAMITSU, H., HOSHINO, H., OKADA, H., MIWA, M., MOMOI, H. & SUGIMURA, T. 1984. Monoclonal antibodies to poly (adenosine diphosphate ribose) recognize different structures. *Biochemistry,* 23**,** 3771-3777.

KENDRICK, A. A., CHOUDHURY, M., RAHMAN, S. M., MCCURDY, C. E., FRIEDERICH, M., VAN HOVE, J. L., WATSON, P. A., BIRDSEY, N., BAO, J., GIUS, D., SACK, M. N., JING, E., KAHN, C. R., FRIEDMAN, J. E. & JONSCHER, K. R. 2011. Fatty liver is associated with reduced SIRT3 activity and mitochondrial protein hyperacetylation. *Biochem J,* 433**,** 505-14.

KERSTEN, S. 1999. Seydoux J, Peters JM, Gonzalez FJ, Desvergne B, and Wahli W. *Peroxisome proliferator-activated receptor alpha mediates the adaptive response to fasting. J Clin Invest,* 103**,** 1489-1498.

KIESWICH, J., SAYERS, S. R., SILVESTRE, M. F., HARWOOD, S. M., YAQOOB, M. M. & CATON, P. W. 2016. Monomeric eNAMPT in the development of experimental diabetes in mice: a potential target for type 2 diabetes treatment. *Diabetologia,* 59**,** 2477-2486.

KIM, J. H., JOHANNES, L., GOUD, B., ANTONY, C., LINGWOOD, C. A., DANEMAN, R. & GRINSTEIN, S. 1998. Noninvasive measurement of the pH of the endoplasmic reticulum at rest and during calcium release. *Proceedings of the National Academy of Sciences,* 95**,** 2997-3002.

KIM, J. S., YOON, C. S. & PARK, D. R. 2014. NAMPT regulates mitochondria biogenesis via NAD metabolism and calcium binding proteins during skeletal muscle contraction. *J Exerc Nutrition Biochem,* 18**,** 259-66.

KIM, T. N. & CHOI, K. M. 2013. Sarcopenia: definition, epidemiology, and pathophysiology. *Journal of bone metabolism,* 20**,** 1-10.

KNEEN, M., FARINAS, J., LI, Y. & VERKMAN, A. 1998. Green fluorescent protein as a noninvasive intracellular pH indicator. *Biophysical journal,* 74**,** 1591-1599.

KOEHN JR, C. & ELVEHJEM, C. 1937. Further Studies on the Concentration of the Anti-pellagra Factor. *Journal of Biological Chemistry,* 118**,** 693-699.

KOH, D. W., LAWLER, A. M., POITRAS, M. F., SASAKI, M., WATTLER, S., NEHLS, M. C., STÖGER, T., POIRIER, G. G., DAWSON, V. L. & DAWSON, T. M. 2004. Failure to degrade poly (ADP-ribose) causes increased sensitivity to cytotoxicity and early embryonic lethality. *Proceedings of the National Academy of Sciences,* 101**,** 17699-17704.

KRAUS-FRIEDMANN, N. 1984. Hormonal regulation of hepatic gluconeogenesis. *Physiological reviews,* 64**,** 170-259.

KRIETSCH, J., ROULEAU, M., PIC, É., ETHIER, C., DAWSON, T. M., DAWSON, V. L., MASSON, J.-Y., POIRIER, G. G. & GAGNÉ, J.-P. 2013. Reprogramming cellular events by poly (ADP-ribose)-binding proteins. *Molecular aspects of medicine,* 34**,** 1066-1087.

KROZOWSKI, Z., MAGUIRE, J. A., STEIN-OAKLEY, A. N., DOWLING, J., SMITH, R. E. & ANDREWS, R. K. 1995. Immunohistochemical localization of the 11 beta-hydroxysteroid dehydrogenase type II enzyme in human kidney and placenta. *The Journal of Clinical Endocrinology & Metabolism,* 80**,** 2203-2209.

LAVERY, G. G., WALKER, E. A., DRAPER, N., JEYASURIA, P., MARCOS, J., SHACKLETON, C. H., PARKER, K. L., WHITE, P. C. & STEWART, P. M. 2006. Hexose-6-phosphate dehydrogenase knock-out mice lack 11β-hydroxysteroid

dehydrogenase type 1-mediated glucocorticoid generation. *Journal of Biological Chemistry,* 281**,** 6546-6551.
LAYBUTT, D., PRESTON, A., ÅKERFELDT, M., KENCH, J., BUSCH, A., BIANKIN, A. & BIDEN, T. 2007. Endoplasmic reticulum stress contributes to beta cell apoptosis in type 2 diabetes. *Diabetologia,* 50**,** 752-763.
LEE, H. C. 2006. Structure and enzymatic functions of human CD38. *Molecular medicine,* 12**,** 317-323.
LEE, J., KIM, H., LEE, J. E., SHIN, S.-J., OH, S., KWON, G., KIM, H., CHOI, Y. Y., WHITE, M. A. & PAIK, S. 2018. Selective cytotoxicity of the NAMPT inhibitor FK866 toward gastric cancer cells with markers of the epithelial-mesenchymal transition, due to loss of NAPRT. *Gastroenterology,* 155**,** 799-814. e13.
LI, C., QIAN, T., HE, R., WAN, C., LIU, Y. & YU, H. 2021. Endoplasmic reticulum–plasma membrane contact sites: Regulators, mechanisms, and physiological functions. *Frontiers in Cell and Developmental Biology,* 9**,** 627700.
LI, M., HUSIC, N., LIN, Y., CHRISTENSEN, H., MALIK, I., MCIVER, S., DANIELS, C. M. L., HARRIS, D. A., KOTZBAUER, P. T. & GOLDBERG, M. P. 2010. Optimal promoter usage for lentiviral vector-mediated transduction of cultured central nervous system cells. *Journal of neuroscience methods,* 189**,** 56-64.
LI, X. 2013. SIRT1 and energy metabolism. *Acta Biochim Biophys Sin,* 45**,** 51-60.
LIGHTMAN, S. L. & CONWAY-CAMPBELL, B. L. 2010. The crucial role of pulsatile activity of the HPA axis for continuous dynamic equilibration. *Nature Reviews Neuroscience,* 11**,** 710-718.
LONG, W., WEI, L. & BARRETT, E. J. 2001. Dexamethasone inhibits the stimulation of muscle protein synthesis and PHAS-I and p70 S6-kinase phosphorylation. *American Journal of Physiology-Endocrinology And Metabolism,* 280**,** E570-E575.
LOUISA, M., SUYATNA, F. D., WANANDI, S. I., ASIH, P. B. S. & SYAFRUDDIN, D. 2016. Differential expression of several drug transporter genes in HepG2 and Huh-7 cell lines. *Advanced Biomedical Research,* 5.
MAGNI, G., AMICI, A., EMANUELLI, M., ORSOMANDO, G., RAFFAELLI, N. & RUGGIERI, S. 2004. Enzymology of NAD+ homeostasis in man. *Cell Mol Life Sci,* 61**,** 19-34.
MANDL, J., MÉSZÁROS, T., BÁNHEGYI, G., HUNYADY, L. & CSALA, M. 2009. Endoplasmic reticulum: nutrient sensor in physiology and pathology. *Trends in Endocrinology & Metabolism,* 20**,** 194-201.
MARGITTAI, É., ENYEDI, B., CSALA, M., GEISZT, M. & BÁNHEGYI, G. 2015. Composition of the redox environment of the endoplasmic reticulum and sources of hydrogen peroxide. *Free Radical Biology and Medicine,* 83**,** 331-340.
MARINIELLO, B., RONCONI, V., RILLI, S., BERNANTE, P., BOSCARO, M., MANTERO, F. & GIACCHETTI, G. 2006. Adipose tissue 11β-hydroxysteroid dehydrogenase type 1 expression in obesity and Cushing's syndrome. 155**,** 435.
MARTENS, C. R., DENMAN, B. A., MAZZO, M. R., ARMSTRONG, M. L., REISDORPH, N., MCQUEEN, M. B., CHONCHOL, M. & SEALS, D. R. 2018. Chronic nicotinamide riboside supplementation is well-tolerated and elevates NAD+ in healthy middle-aged and older adults. *Nature communications,* 9**,** 1-11.

MASSUDI, H., GRANT, R., BRAIDY, N., GUEST, J., FARNSWORTH, B. & GUILLEMIN, G. J. 2012. Age-associated changes in oxidative stress and NAD+ metabolism in human tissue.

MASUZAKI, H., PATERSON, J., SHINYAMA, H., MORTON, N. M., MULLINS, J. J., SECKL, J. R. & FLIER, J. S. 2001. A transgenic model of visceral obesity and the metabolic syndrome. *Science,* 294**,** 2166-2170.

MASUZAKI, H., YAMAMOTO, H., KENYON, C. J., ELMQUIST, J. K., MORTON, N. M., PATERSON, J. M., SHINYAMA, H., SHARP, M. G., FLEMING, S. & MULLINS, J. J. 2003. Transgenic amplification of glucocorticoid action in adipose tissue causes high blood pressure in mice. *The Journal of clinical investigation,* 112**,** 83-90.

MCCORMICK, K. L., WANG, X. & MICK, G. J. 2006. Evidence That the 11 β-hydroxysteroid dehydrogenase (11 β-HSD1) is regulated by pentose pathway flux: studies in rat adipocytes and microsomes. *Journal of Biological Chemistry,* 281**,** 341-347.

MELDOLESI, J. & POZZAN, T. 1998. The endoplasmic reticulum Ca2+ store: a view from the lumen. *Trends in biochemical sciences,* 23**,** 10-14.

MICHISHITA, E., PARK, J. Y., BURNESKIS, J. M., BARRETT, J. C. & HORIKAWA, I. 2005. Evolutionarily conserved and nonconserved cellular localizations and functions of human SIRT proteins. *Molecular biology of the cell,* 16**,** 4623-4635.

MOORE, Z., CHAKRABARTI, G., LUO, X., ALI, A., HU, Z., FATTAH, F., VEMIREDDY, R., DEBERARDINIS, R., BREKKEN, R. & BOOTHMAN, D. 2015. NAMPT inhibition sensitizes pancreatic adenocarcinoma cells to tumor-selective, PAR-independent metabolic catastrophe and cell death induced by β-lapachone. *Cell death & disease,* 6**,** e1599-e1599.

MORALES, J., LI, L., FATTAH, F. J., DONG, Y., BEY, E. A., PATEL, M., GAO, J. & BOOTHMAN, D. A. 2014. Review of poly (ADP-ribose) polymerase (PARP) mechanisms of action and rationale for targeting in cancer and other diseases. *Critical Reviews™ in Eukaryotic Gene Expression,* 24.

MORGAN, S. A., HASSAN-SMITH, Z. K. & LAVERY, G. G. 2016. MECHANISMS IN ENDOCRINOLOGY: Tissue-specific activation of cortisol in Cushing's syndrome. 175**,** R81.

MORGAN, S. A., MCCABE, E. L., GATHERCOLE, L. L., HASSAN-SMITH, Z. K., LARNER, D. P., BUJALSKA, I. J., STEWART, P. M., TOMLINSON, J. W. & LAVERY, G. G. 2014. 11beta-HSD1 is the major regulator of the tissue-specific effects of circulating glucocorticoid excess. *Proc Natl Acad Sci U S A,* 111**,** E2482-91.

MORGAN, S. A., SHERLOCK, M., GATHERCOLE, L. L., LAVERY, G. G., LENAGHAN, C., BUJALSKA, I. J., LABER, D., YU, A., CONVEY, G., MAYERS, R., HEGYI, K., SETHI, J. K., STEWART, P. M., SMITH, D. M. & TOMLINSON, J. W. 2009. 11β-Hydroxysteroid Dehydrogenase Type 1 Regulates Glucocorticoid-Induced Insulin Resistance in Skeletal Muscle. *Diabetes,* 58**,** 2506.

MORTON, N. M., HOLMES, M. C., FIEVET, C., STAELS, B., TAILLEUX, A., MULLINS, J. J. & SECKL, J. R. 2001. Improved lipid and lipoprotein profile, hepatic insulin sensitivity, and glucose tolerance in 11beta-hydroxysteroid dehydrogenase type 1 null mice. *J Biol Chem,* 276**,** 41293-300.

MORTON, N. M., PATERSON, J. M., MASUZAKI, H., HOLMES, M. C., STAELS, B., FIEVET, C., WALKER, B. R., FLIER, J. S., MULLINS, J. J. & SECKL, J. R. 2004.

Novel adipose tissue-mediated resistance to diet-induced visceral obesity in 11 beta-hydroxysteroid dehydrogenase type 1-deficient mice. *Diabetes,* 53**,** 931-8.
MUNCK, A. & NARAY-FEJES-TOTH, A. 1992. The ups and downs of glucocorticoid physiology. Permissive and suppressive effects revisited. *Mol Cell Endocrinol,* 90**,** C1-4.
NAKAHATA, Y., SAHAR, S., ASTARITA, G., KALUZOVA, M. & SASSONE-CORSI, P. 2009. Circadian control of the NAD+ salvage pathway by CLOCK-SIRT1. *Science,* 324**,** 654-657.
NAPOLITANO, A., VOICE, M. W., EDWARDS, C. R. W., SECKL, J. R. & CHAPMAN, K. E. 1998. 11β-hydroxysteroid dehydrogenase 1 in adipocytes: Expression is differentiation-dependent and hormonally regulated. *The Journal of Steroid Biochemistry and Molecular Biology,* 64**,** 251-260.
NIKIFOROV, A., DÖLLE, C., NIERE, M. & ZIEGLER, M. 2011. Pathways and subcellular compartmentation of NAD biosynthesis in human cells: from entry of extracellular precursors to mitochondrial NAD generation. *Journal of Biological Chemistry,* 286**,** 21767-21778.
NIKIFOROV, A., KULIKOVA, V. & ZIEGLER, M. 2015. The human NAD metabolome: Functions, metabolism and compartmentalization. *Critical Reviews in Biochemistry and Molecular Biology,* 50**,** 284-297.
NISHIZUKA, Y. & HAYAISHI, O. 1963. STUDIES ON THE BIOSYNTHESIS OF NICOTINAMIDE ADENINE DINUCLEOTIDE. I. ENZYMIC SYNTHESIS OF NIACIN RIBONUCLEOTIDES FROM 3-HYDROXYANTHRANILIC ACID IN MAMMALIAN TISSUES. *J Biol Chem,* 238**,** 3369-77.
O'BRIEN, J., WILSON, I., ORTON, T. & POGNAN, F. 2000. Investigation of the Alamar Blue (resazurin) fluorescent dye for the assessment of mammalian cell cytotoxicity. *Eur J Biochem,* 267**,** 5421-6.
OKABE, K., YAKU, K., TOBE, K. & NAKAGAWA, T. 2019. Implications of altered NAD metabolism in metabolic disorders. *Journal of Biomedical Science,* 26**,** 34.
OKAMOTO, H. 1999. Cyclic ADP-ribose-mediated insulin secretion and Reg, regenerating gene. *Journal of molecular medicine,* 77**,** 74-78.
ONYANGO, P., CELIC, I., MCCAFFERY, J. M., BOEKE, J. D. & FEINBERG, A. P. 2002. SIRT3, a human SIR2 homologue, is an NAD-dependent deacetylase localized to mitochondria. *Proceedings of the National Academy of Sciences,* 99**,** 13653-13658.
ÖZCAN, U., CAO, Q., YILMAZ, E., LEE, A.-H., IWAKOSHI, N. N., ÖZDELEN, E., TUNCMAN, G., GÖRGÜN, C., GLIMCHER, L. H. & HOTAMISLIGIL, G. S. 2004. Endoplasmic reticulum stress links obesity, insulin action, and type 2 diabetes. *Science,* 306**,** 457-461.
PALADE, G. E. 1956. The endoplasmic reticulum. *The Journal of biophysical and biochemical cytology,* 2**,** 85.
PARK, S. D., KIM, C. G. & KIM, M. G. 1983. Inhibitors of poly (ADP-ribose) polymerase enhance DNA strand breaks, excision repair, and sister chromatid exchanges induced by alkylating agents. *Environmental mutagenesis,* 5**,** 515-525.
PARKER, M. G. 1986. Mechanism of steroid hormone action. *Cancer Surv,* 5**,** 625-33.
PATERSON, J. M., MORTON, N. M., FIEVET, C., KENYON, C. J., HOLMES, M. C., STAELS, B., SECKL, J. R. & MULLINS, J. J. 2004. Metabolic syndrome without

obesity: hepatic overexpression of 11β-hydroxysteroid dehydrogenase type 1 in transgenic mice. *Proceedings of the National Academy of Sciences,* 101**,** 7088-7093.
PAULMYER-LACROIX, O., BOULLU, S., OLIVER, C., ALESSI, M. C. & GRINO, M. 2002. Expression of the mRNA coding for 11beta-hydroxysteroid dehydrogenase type 1 in adipose tissue from obese patients: an in situ hybridization study. *J Clin Endocrinol Metab,* 87**,** 2701-5.
PECKETT, A. J., WRIGHT, D. C. & RIDDELL, M. C. 2011. The effects of glucocorticoids on adipose tissue lipid metabolism. *Metabolism,* 60**,** 1500-1510.
PRONSATO, L., LA COLLA, A., RONDA, A. C., MILANESI, L., BOLAND, R. & VASCONSUELO, A. 2013. High passage numbers induce resistance to apoptosis in C2C12 muscle cells. *Biocell,* 37**,** 1-9.
QUARONA, V., ZACCARELLO, G., CHILLEMI, A., BRUNETTI, E., SINGH, V. K., FERRERO, E., FUNARO, A., HORENSTEIN, A. L. & MALAVASI, F. 2013. CD38 and CD157: a long journey from activation markers to multifunctional molecules. *Cytometry Part B: Clinical Cytometry,* 84**,** 207-217.
RABBITT, E. H., LAVERY, G. G., WALKER, E. A., COOPER, M. S., STEWART, P. M. & HEWISON, M. 2002. Prereceptor regulation of glucocorticoid action by 11β-hydroxysteroid dehydrogenase: a novel determinant of cell proliferation. *The FASEB Journal,* 16**,** 36-44.
RAJAKUMAR, K. 2000. Pellagra in the United States: a historical perspective. *Southern medical journal,* 93**,** 272-277.
RAJAMOHAN, S. B., PILLAI, V. B., GUPTA, M., SUNDARESAN, N. R., BIRUKOV, K. G., SAMANT, S., HOTTIGER, M. O. & GUPTA, M. P. 2009. SIRT1 promotes cell survival under stress by deacetylation-dependent deactivation of poly (ADP-ribose) polymerase 1. *Molecular and cellular biology,* 29**,** 4116-4129.
RAMAMOORTHY, S. & CIDLOWSKI, J. A. 2016. Corticosteroids: Mechanisms of Action in Health and Disease. *Rheum Dis Clin North Am,* 42**,** 15-31, vii.
RAMSEY, K. M., YOSHINO, J., BRACE, C. S., ABRASSART, D., KOBAYASHI, Y., MARCHEVA, B., HONG, H.-K., CHONG, J. L., BUHR, E. D. & LEE, C. 2009. Circadian clock feedback cycle through NAMPT-mediated NAD+ biosynthesis. *Science,* 324**,** 651-654.
RATAJCZAK, J., JOFFRAUD, M., TRAMMELL, S. A., RAS, R., CANELA, N., BOUTANT, M., KULKARNI, S. S., RODRIGUES, M., REDPATH, P. & MIGAUD, M. E. 2016. NRK1 controls nicotinamide mononucleotide and nicotinamide riboside metabolism in mammalian cells. *Nature communications,* 7**,** 1-12.
RECILLAS-TARGA, F. 2006. Multiple strategies for gene transfer, expression, knockdown, and chromatin influence in mammalian cell lines and transgenic animals. *Molecular Biotechnology,* 34**,** 337-354.
REVOLLO, J. R., KÖRNER, A., MILLS, K. F., SATOH, A., WANG, T., GARTEN, A., DASGUPTA, B., SASAKI, Y., WOLBERGER, C. & TOWNSEND, R. R. 2007. Nampt/PBEF/visfatin regulates insulin secretion in β cells as a systemic NAD biosynthetic enzyme. *Cell metabolism,* 6**,** 363-375.
RHEN, T. & CIDLOWSKI, J. A. 2005. Antiinflammatory action of glucocorticoids--new mechanisms for old drugs. *N Engl J Med,* 353**,** 1711-23.

RICKETTS, M. L., SHOESMITH, K. J., HEWISON, M., STRAIN, A., EGGO, M. C. & STEWART, P. M. 1998a. Regulation of 11 beta-hydroxysteroid dehydrogenase type 1 in primary cultures of rat and human hepatocytes. *J Endocrinol,* 156**,** 159-68.

RICKETTS, M. L., VERHAEG, J. M., BUJALSKA, I., HOWIE, A. J., RAINEY, W. E. & STEWART, P. M. 1998b. Immunohistochemical Localization of Type 1 11β-Hydroxysteroid Dehydrogenase in Human Tissues1. *The Journal of Clinical Endocrinology & Metabolism,* 83**,** 1325-1335.

RUGGIERI, S., ORSOMANDO, G., SORCI, L. & RAFFAELLI, N. 2015. Regulation of NAD biosynthetic enzymes modulates NAD-sensing processes to shape mammalian cell physiology under varying biological cues. *Biochim Biophys Acta,* 1854**,** 1138-49.

SATRÚSTEGUI, J., PARDO, B. & DEL ARCO, A. 2007. Mitochondrial transporters as novel targets for intracellular calcium signaling. *Physiological reviews,* 87**,** 29-67.

SAUVE, A. A., WOLBERGER, C., SCHRAMM, V. L. & BOEKE, J. D. 2006. The biochemistry of sirtuins. *Annu. Rev. Biochem.,* 75**,** 435-465.

SAVITZ, J. 2020. The kynurenine pathway: a finger in every pie. *Molecular psychiatry,* 25**,** 131-147.

SCHACKE, H., DOCKE, W. D. & ASADULLAH, K. 2002. Mechanisms involved in the side effects of glucocorticoids. *Pharmacol Ther,* 96**,** 23-43.

SCHULZ, T. A. & PRINZ, W. A. 2007. Sterol transport in yeast and the oxysterol binding protein homologue (OSH) family. *Biochimica et Biophysica Acta (BBA)-Molecular and Cell Biology of Lipids,* 1771**,** 769-780.

SCHUSTER, S., PENKE, M., GORSKI, T., GEBHARDT, R., WEISS, T. S., KIESS, W. & GARTEN, A. 2015. FK866-induced NAMPT inhibition activates AMPK and downregulates mTOR signaling in hepatocarcinoma cells. *Biochemical and biophysical research communications,* 458**,** 334-340.

SCHWARZ, D. S. & BLOWER, M. D. 2016. The endoplasmic reticulum: structure, function and response to cellular signaling. *Cell Mol Life Sci,* 73**,** 79-94.

SECKL, J. R. & WALKER, B. R. 2001. Minireview: 11β-hydroxysteroid dehydrogenase type 1—a tissue-specific amplifier of glucocorticoid action. *Endocrinology,* 142**,** 1371-1376.

SEFRIED, S., HÄRING, H.-U., WEIGERT, C. & ECKSTEIN, S. S. 2018. Suitability of hepatocyte cell lines HepG2, AML12 and THLE-2 for investigation of insulin signalling and hepatokine gene expression. *Open Biology,* 8**,** 180147.

SHI, B., XUE, M., WANG, Y., WANG, Y., LI, D., ZHAO, X. & LI, X. 2018. An improved method for increasing the efficiency of gene transfection and transduction. *International journal of physiology, pathophysiology and pharmacology,* 10**,** 95.

SIMPSON, J. C. & PEPPERKOK, R. 2006. The subcellular localization of the mammalian proteome comes a fraction closer. *Genome Biology,* 7**,** 1-3.

SMITH, A. G. & MUSCAT, G. E. 2005. Skeletal muscle and nuclear hormone receptors: implications for cardiovascular and metabolic disease. *The international journal of biochemistry & cell biology,* 37**,** 2047-2063.

SMITH, S. 2001. The world according to PARP. *Trends in Biochemical Sciences,* 26**,** 174-179.

STEFAN, C. J., MANFORD, A. G., BAIRD, D., YAMADA-HANFF, J., MAO, Y. & EMR, S. D. 2011. Osh proteins regulate phosphoinositide metabolism at ER-plasma membrane contact sites. *Cell,* 144**,** 389-401.

STRØMLAND, Ø., DIAB, J., FERRARIO, E., SVERKELI, L. J. & ZIEGLER, M. 2021. The balance between NAD+ biosynthesis and consumption in ageing. *Mechanisms of Ageing and Development,* 199**,** 111569.

TAN, B., DONG, S., SHEPARD, R. L., KAYS, L., ROTH, K. D., GEEGANAGE, S., KUO, M.-S. & ZHAO, G. 2015. Inhibition of nicotinamide phosphoribosyltransferase (NAMPT), an enzyme essential for NAD+ biosynthesis, leads to altered carbohydrate metabolism in cancer cells. *Journal of Biological Chemistry,* 290**,** 15812-15824.

TAN, B., YOUNG, D. A., LU, Z.-H., WANG, T., MEIER, T. I., SHEPARD, R. L., ROTH, K., ZHAI, Y., HUSS, K. & KUO, M.-S. 2013. Pharmacological inhibition of nicotinamide phosphoribosyltransferase (NAMPT), an enzyme essential for NAD+ biosynthesis, in human cancer cells: metabolic basis and potential clinical implications. *Journal of Biological Chemistry,* 288**,** 3500-3511.

TANNER, F. C., CARR, D. P., NABEL, G. J. & NABEL, E. G. 1997. Transfection of human endothelial cells. *Cardiovascular research,* 35**,** 522-528.

TANNIN, G. M., AGARWAL, A. K., MONDER, C., NEW, M. I. & WHITE, P. C. 1991. The human gene for 11 beta-hydroxysteroid dehydrogenase. Structure, tissue distribution, and chromosomal localization. *J Biol Chem,* 266**,** 16653-8.

TERAKATA, M., FUKUWATARI, T., SANO, M., NAKAO, N., SASAKI, R., FUKUOKA, S.-I. & SHIBATA, K. 2012. Establishment of true niacin deficiency in quinolinic acid phosphoribosyltransferase knockout mice. *The Journal of nutrition,* 142**,** 2148-2153.

TERAO, M., TANI, M., ITOI, S., YOSHIMURA, T., HAMASAKI, T., MUROTA, H. & KATAYAMA, I. 2014. 11β-Hydroxysteroid Dehydrogenase 1 Specific Inhibitor Increased Dermal Collagen Content and Promotes Fibroblast Proliferation. *PLOS ONE,* 9**,** e93051.

TOMLINSON, J. W., DRAPER, N., MACKIE, J., JOHNSON, A. P., HOLDER, G., WOOD, P. & STEWART, P. M. 2002. Absence of Cushingoid Phenotype in a Patient with Cushing's Disease due to Defective Cortisone to Cortisol Conversion. *The Journal of Clinical Endocrinology & Metabolism,* 87**,** 57-62.

TRAMMELL, S. A., SCHMIDT, M. S., WEIDEMANN, B. J., REDPATH, P., JAKSCH, F., DELLINGER, R. W., LI, Z., ABEL, E. D., MIGAUD, M. E. & BRENNER, C. 2016a. Nicotinamide riboside is uniquely and orally bioavailable in mice and humans. *Nature communications,* 7**,** 1-14.

TRAMMELL, S. A., WEIDEMANN, B. J., CHADDA, A., YOREK, M. S., HOLMES, A., COPPEY, L. J., OBROSOV, A., KARDON, R. H., YOREK, M. A. & BRENNER, C. 2016b. Nicotinamide riboside opposes type 2 diabetes and neuropathy in mice. *Scientific reports,* 6**,** 1-7.

TSUKANO, H., GOTOH, T., ENDO, M., MIYATA, K., TAZUME, H., KADOMATSU, T., YANO, M., IWAWAKI, T., KOHNO, K. & ARAKI, K. 2010. The endoplasmic reticulum stress-C/EBP homologous protein pathway-mediated apoptosis in macrophages contributes to the instability of atherosclerotic plaques. *Arteriosclerosis, thrombosis, and vascular biology,* 30**,** 1925-1932.

VAZIRI, H., DESSAIN, S. K., EATON, E. N., IMAI, S.-I., FRYE, R. A., PANDITA, T. K., GUARENTE, L. & WEINBERG, R. A. 2001. hSIR2SIRT1 functions as an NAD-dependent p53 deacetylase. *Cell,* 107**,** 149-159.

WANG, B., HASAN, M., ALVARADO, E., YUAN, H., WU, H. & CHEN, W. 2011. NAMPT overexpression in prostate cancer and its contribution to tumor cell survival and stress response. *Oncogene,* 30**,** 907-921.
WANG, F., NGUYEN, M., QIN, F. X. F. & TONG, Q. 2007. SIRT2 deacetylates FOXO3a in response to oxidative stress and caloric restriction. *Aging cell,* 6**,** 505-514.
WANG, R., JIAO, H., ZHAO, J., WANG, X. & LIN, H. 2016. Glucocorticoids Enhance Muscle Proteolysis through a Myostatin-Dependent Pathway at the Early Stage. *PLOS ONE,* 11**,** e0156225.
WARBURG, O., CHRISTIAN, W. & GRIESE, A. 1935. Hydrogen-transferring coenzyme, its composition and mode of action. *Biochem Z,* 282**,** 157-205.
WEST, M., ZUREK, N., HOENGER, A. & VOELTZ, G. K. 2011. A 3D analysis of yeast ER structure reveals how ER domains are organized by membrane curvature. *Journal of Cell Biology,* 193**,** 333-346.
WESTRATE, L., LEE, J., PRINZ, W. & VOELTZ, G. 2015. Form follows function: the importance of endoplasmic reticulum shape. *Annual review of biochemistry,* 84**,** 791-811.
WHORWOOD, C. B., DONOVAN, S. J., FLANAGAN, D., PHILLIPS, D. I. & BYRNE, C. D. 2002. Increased glucocorticoid receptor expression in human skeletal muscle cells may contribute to the pathogenesis of the metabolic syndrome. *Diabetes,* 51**,** 1066-75.
WOLFE, R. R. 2006. The underappreciated role of muscle in health and disease. *The American journal of clinical nutrition,* 84**,** 475-482.
WONG, C. Y., AL-SALAMI, H. & DASS, C. R. 2020. C2C12 cell model: its role in understanding of insulin resistance at the molecular level and pharmaceutical development at the preclinical stage. *J Pharm Pharmacol,* 72**,** 1667-1693.
WU, M. M., LLOPIS, J., ADAMS, S., MCCAFFERY, J. M., KULOMAA, M. S., MACHEN, T. E., MOORE, H. P. & TSIEN, R. Y. 2000. Organelle pH studies using targeted avidin and fluorescein-biotin. *Chem Biol,* 7**,** 197-209.
YAFFE, D. & SAXEL, O. 1977. Serial passaging and differentiation of myogenic cells isolated from dystrophic mouse muscle. *Nature,* 270**,** 725-727.
YOSHINO, J., MILLS, K. F., YOON, M. J. & IMAI, S.-I. 2011. Nicotinamide mononucleotide, a key NAD+ intermediate, treats the pathophysiology of diet-and age-induced diabetes in mice. *Cell metabolism,* 14**,** 528-536.
ZHANG, T., BERROCAL, J. G., YAO, J., DUMOND, M. E., KRISHNAKUMAR, R., RUHL, D. D., RYU, K. W., GAMBLE, M. J. & KRAUS, W. L. 2012. Regulation of poly (ADP-ribose) polymerase-1-dependent gene expression through promoter-directed recruitment of a nuclear NAD+ synthase. *Journal of Biological Chemistry,* 287**,** 12405-12416.
ZHONG, D., ZHANG, Y., ZENG, Y.-J., GAO, M., WU, G.-Z., HU, C.-J., HUANG, G. & HE, F.-T. 2013. MicroRNA-613 represses lipogenesis in HepG2 cells by downregulating LXRα. *Lipids in Health and Disease,* 12**,** 1-9.
ZHOU, C. C., YANG, X., HUA, X., LIU, J., FAN, M. B., LI, G. Q., SONG, J., XU, T. Y., LI, Z. Y. & GUAN, Y. F. 2016. Hepatic NAD+ deficiency as a therapeutic target for non-alcoholic fatty liver disease in ageing. *British journal of pharmacology,* 173**,** 2352-2368.
ZHU, Y., LIU, J., PARK, J., RAI, P. & ZHAI, R. G. 2019. Subcellular compartmentalization of NAD+ and its role in cancer: A sereNADe of metabolic melodies. *Pharmacology & therapeutics,* 200**,** 27-41.

Appendix A: TaqMan probes used for RT-PCR.

Gene	Product Number
Bip	Mm01135937_g1 Hs00358796_m1
Chop	Mm00517691_m1 Hs00607129_g1
G6PDH	Mm99999915_g1
H6PDH	Mm00557617m1 Hs00188728_m1
11β-HSD1	Mm00476182_m1 Hs01547870_m1